AD/A-007 254

ANALYSIS OF A RADAR RAIN RETURN AT FREQUENCIES OF 9.375, 35, 70, AND 95 GHz

N. C. Currie, et al

Georgia Institute of Technology

Prepared for:

Frankford Arsenal

1 February 1975

DISTRIBUTED BY:

NTIS

National Technical Information Service
U. S. DEPARTMENT OF COMMERCE

REPORT DOCUMENTATION PAGE

READ INSTRUCTIONS BEFORE COMPLETING FORM

1 REPORT NUMBER	2 GOVT ACCESSION NO
3 RECIPIENT'S CATALOG NUMBER	AD/A-007254
4 TITLE (and Subtitle)	5 TYPE OF REPORT & PERIOD COVERED
Analysis of Radar Rain Return at Frequencies Of 9.375, 35, 70, and 95 GHz	Technical Report
	6 PERFORMING ORG. REPORT NUMBER: A-1485-TR-2
7 AUTHOR(s)	8 CONTRACT OR GRANT NUMBER(s)
N. C. Currie, F. B. Dyer, and R. D. Hayes	DAAA-25-73-C-0256
9 PERFORMING ORGANIZATION NAME AND ADDRESS Sensor Systems Division, Engineering Experiment Station, Georgia Institute of Technology Atlanta, Georgia 30332	10 PROGRAM ELEMENT, PROJECT, TASK AREA & WORK UNIT NUMBERS Mod. P-00003, P-00005
11 CONTROLLING OFFICE NAME AND ADDRESS Frankford Arsenal United States Army Philadelphia, Pennsylvania 19137	12 REPORT DATE 1 February 1975 13 NUMBER OF PAGES 103
14 MONITORING AGENCY NAME & ADDRESS (if different from Controlling Office)	15 SECURITY CLASS (of this report) Unclassified 15a. DECLASSIFICATION DOWNGRADING SCHEDULE

16 DISTRIBUTION STATEMENT (of this Report)

17 DISTRIBUTION STATEMENT (of the abstract entered in Block 20, if different from Report)

Reproduced by
NATIONAL TECHNICAL INFORMATION SERVICE
US Department of Commerce
Springfield VA 22151

18 SUPPLEMENTARY NOTES

Georgia Tech Project A-1485

19 KEY WORDS (Continue on reverse side if necessary and identify by block number)

Radar
Backscatter
Rain
Spectrum
Clutter
Drop-size

20 ABSTRACT (Continue on reverse side if necessary and identify by block number)

A series of measurements of radar backscatter from rain have been made at frequencies of 9.375, 35, 70, and 95 GHz. The geometry of the experiment and the equipment were chosen such as to provide data useful to the equipment designer in the choice of operating frequency for his particular mission. Amplitude statistics for both linear and circular polarization were obtained for rain rates between 1 mm/hr and 90 mm/hr. Non-coherent spectral measure-

20. Continued

ments and correlation properties were investigated in detail as functions of frequency and rain rate. Limited comparisons are made between theory and experimental results and certain properties of the results are discussed in relation to the phenomenology of rain return.

ENGINEERING EXPERIMENT STATION
Georgia Institute of Technology
Atlanta, Georgia

ANALYSIS OF RADAR RAIN RETURN AT FREQUENCIES OF 9.375, 35, 70, and 95 GHz

Technical Report 2
EES/GIT Project A-1485

by
N. C. Currie, F. B. Dyer, and R. D. Hayes

Prepared for

United States Army
Frankford Arsenal
Philadelphia, Pennsylvania 19137

under
Contract DAAA 25-73-C-0256

1 February 1975

ii

Contract DAAA-25-73-C-0256
Frankford Arsenal
United States Army
Philadelphia, Pennsylvania 19137

A-1485-TR-2
Engineering Experiment Station
Georgia Institute of Technology
Atlanta, Georgia 30332

ANALYSIS OF RADAR RAIN RETURN AT FREQUENCIES OF 9.375, 35, 70, and 95 GHz

by

N. C. Currie, F. B. Dyer and R. D. Hayes

ABSTRACT

A series of measurements of radar backscatter from rain have been made at frequencies of 9.375, 35, 70, and 95 GHz. The geometry of the experiment and the equipment were chosen such as to provide data useful to the equipment designer in the choice of operating frequency for his particular mission. Amplitude statistics for both linear and circular polarization were obtained for rain rates between 1 mm/hr and 90 mm/hr. Non-coherent spectral measurements and correlation properties were investigated in detail as functions of frequency and rain rate. Limited comparisons are made between theory and experimental results and certain properties of the results are discussed in relation to the phenomenology of rain return.

ic

TABLE OF CONTENTS

		Page
I.	INTRODUCTION	1
	A. Background	1
	B. Description of Radar Field Tests	2
	1. Radars	2
	2. Data Recording Equipment	3
	3. Calibration Procedure	6
	4. Radar Reference Targets	6
	5. Meteorological Instrumentation	9
	6. Measurement Procedure	11
II.	DATA ANALYSIS	13
	A. Data Analysis Techniques	13
	1. Data Reduction Facility	13
	2. Data Analysis Procedure	13
	a. Pulse Height Amplitude Distributions	15
	b. Frequency Spectra	15
	c. Auto- and Cross-Correlation Functions	18
	d. Rain Drop-Size Distributions	20
	B. Summary of Results	25
	1. Interpretation of Data	25
	2. Attenuation	27
	3. Average Return Amplitude	27
	4. Amplitude Fluctuations	31
	5. Power Density Spectrum	41
	6. Correlation Functions	48
III.	CONCLUSIONS AND RECOMMENDATIONS	59

Page

IV. REFERENCES 63

V. APPENDICES 65

A. Plotted Average Backscatter Data 67

B. Spectral Distributions for Selected Data Runs. 77

LIST OF FIGURES

		Page
1.	Exterior view of instrument van showing the antennas for the four radars.	5
2.	Interior of instrument van showing the data recording equipment.	5
3.	Block diagram of experimental equipment set-up for rain backscatter experiment.	7
4.	Field of view from radar van showing radar reference targets and rain instrumentation	8
5.	Close-up of 4 inch trihedral radar reference target illustrating deployment of rain tipping buckets.	8
6.	Close-up view of a rain tipping bucket with windshield	10
7.	Rain drop-size distribution spectrometer deployed near the 4 inch trihedral radar target.	10
8.	View of the Sensor Systems Division's PDP-8/F base data reduction facility.	14
9.	Time history of the recorded backscatter from rain; 9.375 GHz, 33 mm/hr rain rate, VV polarization	17
10.	Time history of the recorded backscatter from rain; 95 GHz, 33 mm/hr rain rate, VV polarization.	17
11.	Block diagram of the equipment setup used to process the rain drop-size tapes	22
12.	Least mean square fit to radar backscatter data, VV polarization.	29
13.	Least mean square fit to radar backscatter data, RC polarization.	30
14.	Probability density and cumulative distributions for backscatter from rain; 9.375 GHz, 5 mm/hr rain rate, VV polarization.	33
15.	Probability density and cumulative distributions for backscatter from rain; 35 GHz, 5 mm/hr rain rate, VV polarization.	34
16.	Probability density and cumulative distributions for backscatter from rain; 70 GHz, 5 mm/hr rain rate, VV polarization.	35

Page

17. Probability density and cumulative distributions for backscatter from rain; 95 GHz, 5 mm/hr rain rate, VV polarization. 36

18. Rain backscatter amplitude standard deviation versus rain rate for 9.375 GHz frequency, VV polarization 37

19. Rain backscatter amplitude standard deviation versus rain rate for 35 GHz frequency, VV polarization. 37

20. Rain backscatter amplitude standard deviation versus rain rate for 70 GHz frequency, VV polarization. 38

21. Rain backscatter amplitude standard deviation versus rain rate for 95 GHz frequency, VV polarization. 38

22. Rain backscatter amplitude standard deviation versus rain rate for 9.375 GHz frequency, RC polarization 39

23. Rain backscatter amplitude standard deviation versus rain rate for 35 GHz frequency, RC polarization. 39

24. Rain backscatter amplitude standard deviation versus rain rate for 70 GHz frequency, RC polarization. 40

25. Rain backscatter amplitude standard deviation versus rain rate for 95 GHz frequency, RC polarization. 40

26. Normalized frequency spectrum of rain return at 9.375 GHz, VV polarization. 42

27. Normalized frequency spectrum of rain return at 35 GHz, VV polarization. 43

28. Normalized frequency spectrum of rain return at 70 GHz, VV polarization. 44

29. Normalized frequency spectrum of rain return at 95 GHz, VV polarization. 45

30. Normalized frequency spectrum of rain return at 9.375 GHz, RC polarization 46

31. Normalized frequency spectrum of rain return at 95 GHz, RC polarization. 47

32. Decorrelation time versus rain rate and frequency for rain backscatter 49

33. Normalized auto-correlation function for rain backscatter; 9.375 GHz frequency, 9 mm/hr rain rate, VV polarization. 50

Page

34. Normalized auto-correlation function for rain backscatter; 95 GHz frequency, 9 mm/hr rain rate, VV polarization. 50

35. Rain drop-size distributions for four consecutive 30-second intervals with a light-to-moderate rain rate 52

36. Two rain drop-size distributions which resulted in different radar backscatter characteristics for a heavy rain rate. 54

37. Four rain drop-size distributions which resulted in different radar backscatter characteristics for a moderate rain rate.. 55

38. Four rain drop-size distributions which resulted in different radar backscatter characteristics for a light rain rate. 56

A1. Average radar backscatter cross-section per unit volume versus rain rate; 9.375 GHz, VV polarization. 68

A2. Average radar backscatter cross-section per unit volume versus rain rate; 35 GHz, VV polarization. 69

A3. Average radar backscatter cross-section per unit volume versus rain rate; 70 GHz, VV polarization 70

A4. Average radar backscatter cross-section per unit volume versus rain rate; 95 GHz, VV polarization 71

A5. Average radar backscatter cross-section per unit volume versus rain rate; 9.375 GHz, RC polarization. 72

A6. Average radar backscatter cross-section per unit volume versus rain rate; 35 GHz, RC polarization 73

A7. Average radar backscatter cross-section per unit volume versus rain rate; 70 GHz, RC polarization 74

A8. Average radar backscatter cross-section per unit volume versus rain rate; 95 GHz, RC polarization 75

B1. Amplitude of the frequency spectrum of a logarithmic reciever for rain backscatter; 5 mm/hr rain rate, 9.375 GHz frequency, and VV polarization 78

B2. Amplitude of the frequency spectrum of a logarithmic receiver for rain backscatter; 5 mm/hr rain rate, 35 GHz frequency, and VV polarization... 78

Page

B3. Amplitude of the frequency spectrum of a logarithmic receiver for rain backscatter; 5 mm/hr rain rate, 70 GHz frequency, and VV polarization. 79

B4. Amplitude of the frequency spectrum of a logarithmic receiver for rain backscatter; 5 mm/hr rain rate, 95 GHz frequency, and VV polarization. 79

B5. Amplitude of the frequency spectrum of a logarithmic receiver for rain backscatter; 23 mm/hr rain rate, 9.375 GHz frequency, and VV polarization 80

B6. Amplitude of the frequency spectrum of a logarithmic receiver for rain backscatter; 23 mm/hr rain rate, 35 GHz frequency, and VV polarization. 80

B7. Amplitude of the frequency spectrum of a logarithmic receiver for rain backscatter; 23 mm/hr rain rate, 70 GHz frequency, and VV polarization. 81

B8. Amplitude of the frequency spectrum of a logarithmic receiver for rain backscatter; 23 mm/hr rain rate, 95 GHz frequency, and VV polarization. 81

B9. Amplitude of the frequency spectrum of a logarithmic receiver for rain backscatter; 38 mm/hr rain rate, 9.375 GHz frequency, and VV polarization 82

B10. Amplitude of the frequency spectrum of a logarithmic receiver for rain backscatter; 38 mm/hr rain rate, 35 GHz frequency, and VV polarization. 82

B11. Amplitude of the frequency spectrum of a logarithmic receiver for rain backscatter; 38 mm/hr rain rate, 70 GHz frequency, and VV polarization. 83

B12. Amplitude of the frequency spectrum of a logarithmic receiver for rain backscatter; 38 mm/hr rain rate, 95 GHz frequency, and VV polarization. 83

B13. Amplitude of the frequency spectrum of a logarithmic receiver for rain backscatter; 70 mm/hr rain rate, 9.375 GHz frequency, and VV polarization. 84

B14. Amplitude of the frequency spectrum of a logarithmic receiver for rain backscatter; 70 mm/hr rain rate, 35 GHz frequency, and VV polarization. 84

B15. Amplitude of the frequency spectrum of a logarithmic receiver for rain backscatter; 70 mm/hr rain rate, 70 GHz frequency, and VV polarization. 85

Page

B16. Amplitude of the frequency spectrum of a logarithmic receiver for rain backscatter; 70 mm/hr rain rate, 95 GHz frequency, and VV polarization. 85

B17. Amplitude of the frequency spectrum of a logarithmic receiver for rain backscatter; 100 mm/hr rain rate, 9.375 GHz frequency, and VV polarization 86

B18. Amplitude of the frequency spectrum of a logarithmic receiver for rain backscatter; 100/mm/hr rain rate, 35 GHz frequency, and VV polarization. 86

B19. Amplitude of the frequency spectrum of a logarithmic receiver for rain backscatter; 100 mm/hr rain rate, 70 GHz frequency, and VV polarization. 87

B20. Amplitude of the frequency spectrum of a logarithmic receiver for rain backscatter; 100 mm/hr rain rate, 95 GHz frequency, and VV polarization. 87

B21. Amplitude of the frequency spectrum of a logarithmic receiver for rain backscatter; 3.1 mm/hr rain rate 9.375 GHz frequency, and RC polarization 88

B22. Amplitude of the frequency spectrum of a logarithmic receiver for rain backscatter; 3.1 mm/hr rain rate, 35 GHz frequency, and RC polarization. 88

B23. Amplitude of the frequency spectrum of a logarithmic receiver for rain backscatter; 3.1 mm/hr rain rate, 70 GHz frequency, and RC polarization. 89

B24. Amplitude of the frequency spectrum of a logarithmic receiver for rain backscatter; 3.1 mm/hr rain rate, 95 GHz frequency, and RC polarization. 89

B25 Amplitude of the frequency spectrum of a logarithmic receiver for rain backscatter; 32 mm/hr rain rate. 9.375 GHz frequency, and RC polarization 90

B26. Amplitude of the frequency spectrum of a logarithmic receiver for rain backscatter; 32 mm/hr rain rate, 35 GHz frequency, and RC polarization. 90

B27. Amplitude of the frequency spectrum of a logarithmic receiver for rain backscatter; 32 mm/hr rain rate, 70 GHz frequency, and RC polarization. 91

B28. Amplitude of the frequency spectrum of a logarithmic receiver for rain backscatter; 32 mm/hr rain rate, 95 GHz frequency, and RC polarization. 91

Page

B29. Amplitude of the frequency spectrum of a logarithmic receiver for rain backscatter; 91 mm/hr rain rate, 9.375 GHz frequency, and RC polarization. 92

B30. Amplitude of the frequency spectrum of a logarithmic receiver for rain backscatter; 91 mm/hr rain rate, 35 GHz frequency, and RC polarization. 92

B31. Amplitude of the frequency spectrum of a logarithmic receiver for rain backscatter; 91 mm/hr rain rate, 70 GHz frequency, and RC polarization 93

B32. Amplitude of the frequency spectrum of a logarithmic receiver for rain backscatter; 91 mm/hr rain rate, 95 GHz frequency, and RC polarization 93

LIST OF TABLES

		Page
Table 1.	Radar Parameters for Rain Experiment [3].	4
Table 2.	Attenuation Due to Rain	28

I. INTRODUCTION

This report summarizes the results of an analysis of measurements on the radar backscatter from rain at millimeter frequencies which was conducted at McCoy AFB, Florida, in August and September 1973 by the U. S. Army Ballistic Research Laboratories (BRL), Aberdeen, Md. Emphasis in the report is placed on those characteristics of the radar backscatter which could be determined from data recorded on magnetic tape, as opposed to a detailed description of the actual radar tests or analysis of photographic and video tape data which were also gathered. These parameters will be discussed elsewhere in a separate report to be published by BRL.

A. Background

Under Contract DAA25-73-C-0256 with the U. S. Army, Frankford Arsenal, the Engineering Experiment Station (EES) at Georgia Tech undertook to develop suitable mathematical models to allow computer simulation of fire-control radar systems in the millimeter region. As a first step in this program, a literature search was conducted to determine what data were available at millimeter frequencies on clutter and target characteristics which would affect system performance. A summary of these data and the empirical models which were developed were presented in Technical Report 1 on the contract [1].

The results of that study brought to light a number of deficiencies in the available data. It was determined that: (1) little or no data are available on the characteristics of ground clutter above 10 GHz, particularly below 10° grazing angle; (2) almost no data were available on the effects of atmospheric conditions such as precipitation in the millimeter region; and (3) there was a scarcity of data on the radar cross-section (RCS) properties of hard targets at these frequencies. EES then proposed to Frankford Arsenal a program of investigation to fill in these gaps in the available data to be followed by an analysis program aimed at tying the data results together in a unified model for millimeter radar systems.

Frankford Arsenal, in response to this proposal, undertook to fund studies of the backscatter from precipitation and from land clutter at millimeter frequencies.

Ballistic Research Laboratories was funded by Frankford to conduct an experiment on backscatter from rain at 10 GHz, 35 GHz, 70 GHz, and 95 GHz, and EES was tasked, in a modification to the original Army contract, to assist in the experiment planning and to act as on-site observers during the actual tests. In addition, under this program, EES constructed and delivered to BRL a range-gated boxcar sampler unit which would allow recording of backscatter data on magnetic tape during the tests. The services and activities performed were detailed in a letter report at the end of the field tests [2].

After the termination of the radar field tests on rain backscatter, Frankford Arsenal provided additional funds to EES for the purpose of reducing and analyzing the data contained on the magnetic tapes recorded during the tests. The goals of this analysis program were to (1) determine average backscatter parameters in terms of rain rate and drop-size distributions as a supplement and cross check to the results, obtained by BRL and (2) determine spectral auto-correlation and other properties of the backscatter which were not obtained during the initial analysis which used primarily photographic methods. This report summarizes the results of the magnetic tape analysis program.

B. Description of Radar Field Tests [3]

The radar field tests were conducted at McCoy Air Force Base, Orlando, Florida, during August and September 1973. This site was selected because of the afternoon rains that occur almost daily in this area during the summer months. During the tests, it rained 25 times, the rainfall rates varying from light drizzles up to very heavy rainfalls of 150 mm/hr.

For this experiment, an instrument van containing the four radars and the data recording equipment was positioned at one end of a large field, and the radar targets and rain instrumentation were placed near the other end. Data were taken whenever a rain cell passed through the region around the targets.

1. Radars

Four radars were used during the rain experiments with operating frequencies of 9.375 GHz, 35 GHz, 70 GHz, and 95 GHz. The basic radar

parameters are given in Table 1 [3]. Logarithmic receivers were provided for all of the radars, and 0 to 50-dB variable waveguide attenuators were installed in the rf paths to the receivers for calibration purposes.

Parabolic reflector antennas with Cassegrain feeds provided pencil beams for all the radars. Vertical, right circular, and left circular polarizations were available. The antennas were attached to mounts, which could be manually positioned in azimuth and elevation, and boresighted telescopes were provided for each mount. The radars and antennas were housed in an air-conditioned instrument van with a 1/8-inch thick Polycast window along one side to serve as a radome. Figure 1 gives an exterior view of the instrument van showing the antennas. The antennas, as shown left to right, are for the 9.375 GHz, 35 GHz, 70 GHz, and 95 GHz radars respectively.

2. Data Recording Equipment

During the tests, data were recorded on the rain backscatter in several ways in order to obtain as much information as possible. The received signals from each radar were displayed on an A-scope and polaroid photographs were made at regular intervals. In addition, video recordings were made on the A-scope displays, changing the video displayed at 10-second intervals. Finally the videos from the four radars were sampled by a four-channel, range-gated boxcar unit which stretched the return from a narrow gate so as to allow recording on low-bandwidth devices such as a strip chart recorder and an FM magnetic tape recorder.

In order to allow simultaneous data taking, all of the radar modulators were synchronized to a common trigger source. To accomplish this, the 1600-Hz prf from the 95-GHz radar timer was used to trigger the 9.375-GHz and 70-GHz radars directly, and was doubled to 3200 Hz to trigger the 35-GHz radar. Also, the four range gates in the boxcar sampler were slaved together and controlled by a single range delay adjustment, so that simultaneous data could be recorded at a given range at all four frequencies.

Figure 2 gives a view of the inside of the instrumentation van showing the A-scopes, videc monitor, boxcar sampler, FM magnetic tape recorder,

Table 1.

RADAR PARAMETERS FOR RAIN EXPERIMENT [3]

Frequency (GHz)	9.375	35	70	95
Radar Type	AN/TPS-25	AN/APQ-137	Assembled at BRL[1]	Constructed at NADC[2]
Peak Power (W)	40	20	10	8
Antenna Diameter (m)	1.83	0.92	0.92	0.92
Antenna Beamwidth (Deg)	1.2	0.68	0.34	0.24
IF Bandwidth (MHz)	4	6	14	20
Pulse Width (nsec)	700	200	85	80
prf (Hz)	1600	3200	1600	1600
Noise Figure (dB)	10	13.4	18	28
4-inch Reference Corner RCS(dBsm)	-3.67	+8.45	+12.04	+16.53
Rain Cell Volume at Radar Target (m^3)	5623	513	55	26

1. Assembled at BRL from components of the AN/MPS-29 radar originally developed for ECOM by EES.

2. Built by Naval Air Development Center, Warminster, Pa., Marvin Foral Project Engineer.

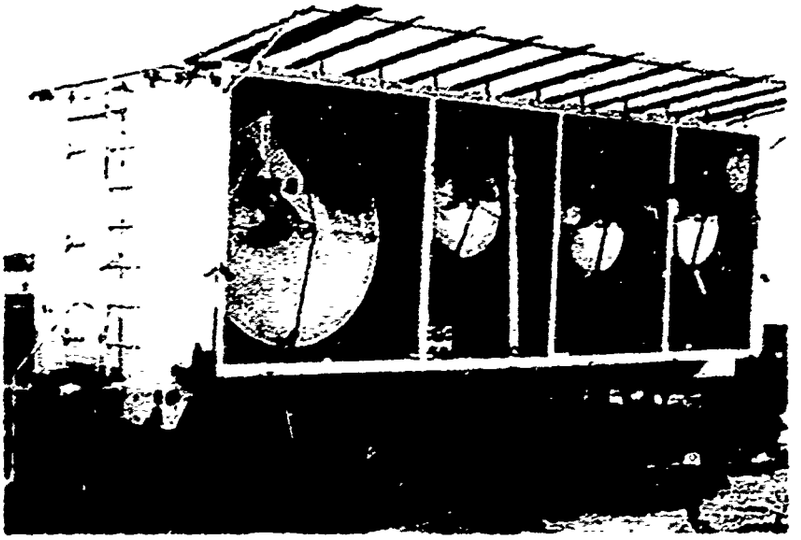

FIGURE 1. Exterior view of instrument van showing the antennas for the four radars.

FIGURE 2. Interior of instrument van showing the data recording equipment.

time-code generator, and strip chart recorder, while Figure 3 shows a block diagram of the data instrumentation setup.

The strip chart recorder served as a monitor on the radar performance, and was also used during the tests to record the bucket tips from the rain tipping buckets for later analysis. During the data reduction at a later time, the charts were particularly helpful in identifying data on the FM magnetic tapes, and in providing supplementary information in addition to the data sheets.

3. Calibration Procedure

The variable attenuators installed in the rf signal path of the radars were used to calibrate all the data. The procedure consisted of boresighting all four radars on to one of the calibrated radar targets (usually a 4-inch tricorner reflector) and recording the return from the target as the attenuators were varied from 0 to 50 dB in 5 dB steps. In the case of the 35 GHz radar, the receiver was saturated by the return from the corner, so that it is necessary to insert an extra 30 dB pad in series with the variable attenuator and repeat the above procedure. The calibrations were, of course, performed before and/or after a rain storm when no rain was falling in order to eliminate the effects of rain attenuation on the calibration. All the attenuators were calibrated against laboratory standards after the experiment.

4. Radar Reference Targets

A 4-inch trihedral corner reflector was mounted on a 32-foot-high fiberglass mast in the field in front of the radars at a range of 1478 feet for use as a primary reference target. Figure 4 is a view of the field from the radar van, showing the reference targets and the rain instrumentation. The primary reference target was chosen to be large enough to provide sufficient return to overide ground clutter and backscatter from heavy rain, but not so large that the signal could not be attenuated down to the receiver noise level with available attenuators. The aluminum trihedral was accurately machined, and had a radar cross-section of 0.43, 7, 16, and 45 square meters at 9.375, 35, 70, and 95 GHz, respectively. The trihedral was calibrated against a 10-inch-diameter aluminum sphere suspended from a rope strung between two poles. Figure 5 shows a close-up

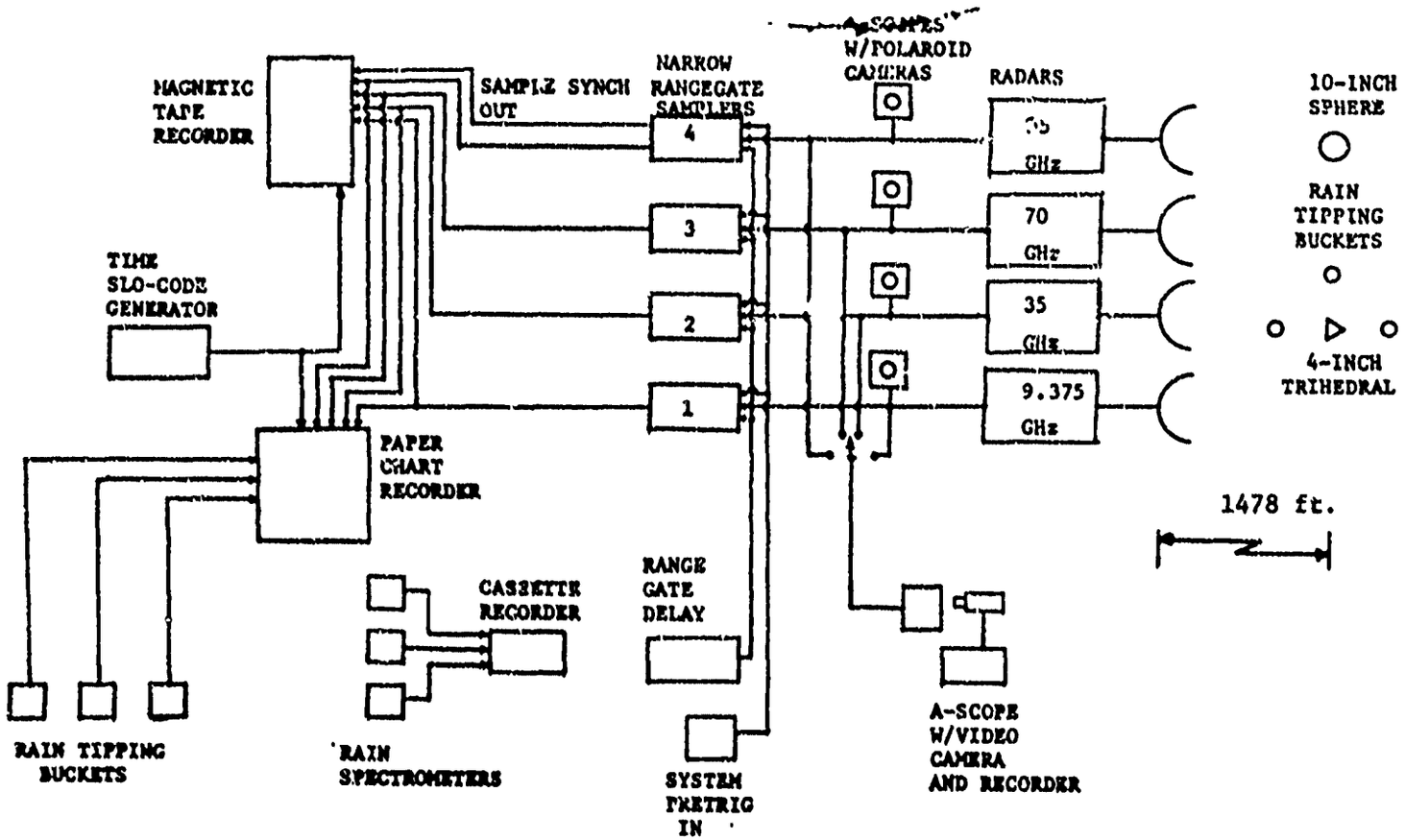

Figure 3. Block diagram of experimental equipment set-up for rain backscatter experiment.

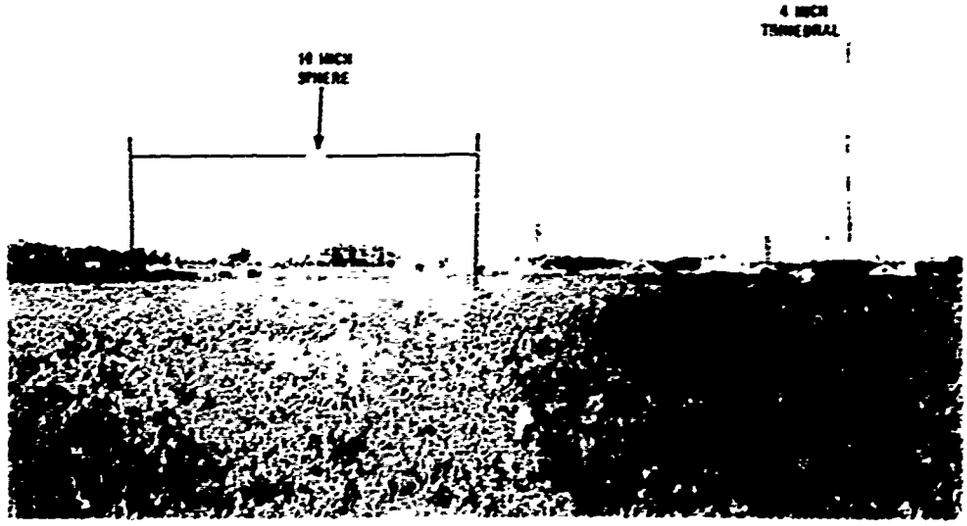

FIGURE 4. Field of view from radar van showing radar reference targets and rain instrumentation.

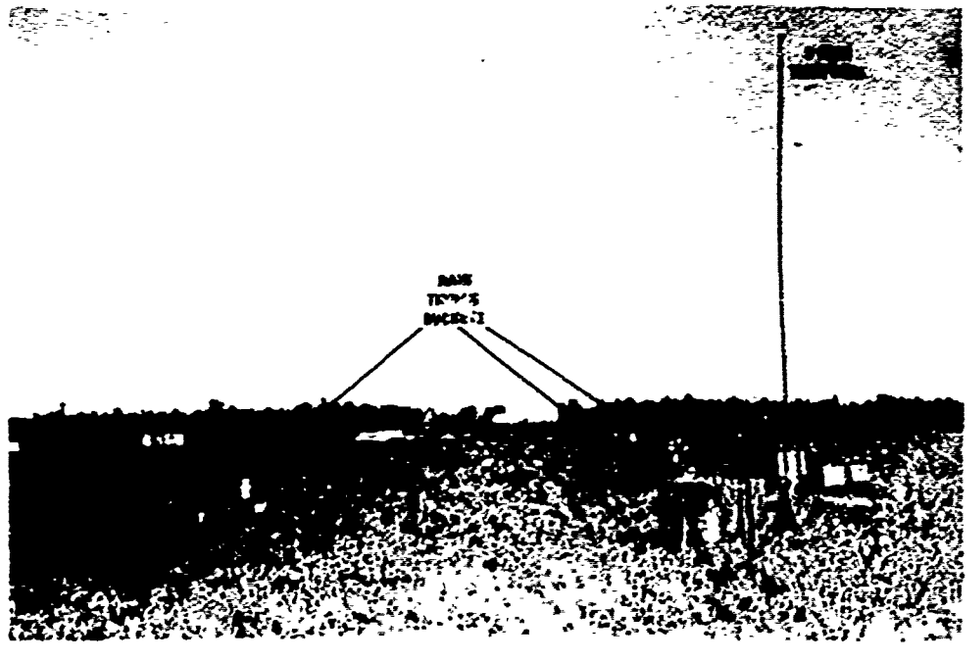

FIGURE 5. Close-up of 4 inch trihedral radar reference target illustrating deployment of rain tipping buckets.

of the trihedral in the field viewed from the radar van. The height of the reference trihedral was a compromise intended to be great enough to minimize ground clutter and multipath effects but not so great as to be unstable in orientation during a heavy rain and wind storm. The range of the reference target from the radars was determined by three criteria: (1) having the range as short as possible to maximize the elevation angle to the trihedral, thereby minimizing ground clutter, multipath, and vegetation interference (the latter was initially a problem with 6-foot high weeds in the field which had to be cut by hand); (2) having the range as great as possible to simulate long-range radar operation and still have measurable rain backscatter during all rainfall intensities; and (3) having the target beyond the near-field of the antennas. (Note: the near-field criterion was not achieved for the 95-GHz radar.) The target height of 32 feet and range of 1478 feet resulted in no discernible ground clutter at 35, 70, and 95 GHz at the target range; the ground clutter at 9.375 GHz was 45 dB down from the target return. Other refernce targets which were also used from time to time included a 6-inch tricorner and a 2-inch dihedral.

5. Meteorological Instrumentation

Meteorological conditions which were recorded during the tests include rainfall rate (from the tipping buckets), rainfall rate and drop-size distributions (from the rain spectrometers), temperature, atmospheric pressure, relative humidity, and wind speed and direction. The rain tipping buckets and spectrometers were located near the radar targets, while all other weather instrumentation was located at the radar van.

The basic measure of rainfall rate was obtained from the rain tipping buckets. Figure 6 gives a close-up view of a tipping bucket with windshield. (Two of the buckets had windshields and one did not.) A windshield consisted of a ring of hinged vanes intended to breakup cross winds. Each tipping bucket had a 7-inch diameter orifice and provided a switch closure for each .01 inch (0.254 mm) of rainfall. As previously mentioned, the switch closures from each bucket were recorded as pulses on the paper chart recorder. It has since been discovered that the accuracy of the tipping buckets in determining rain rate is in doubt below 10 mm/hr rain rates and above 60 mm/hr rain rates.

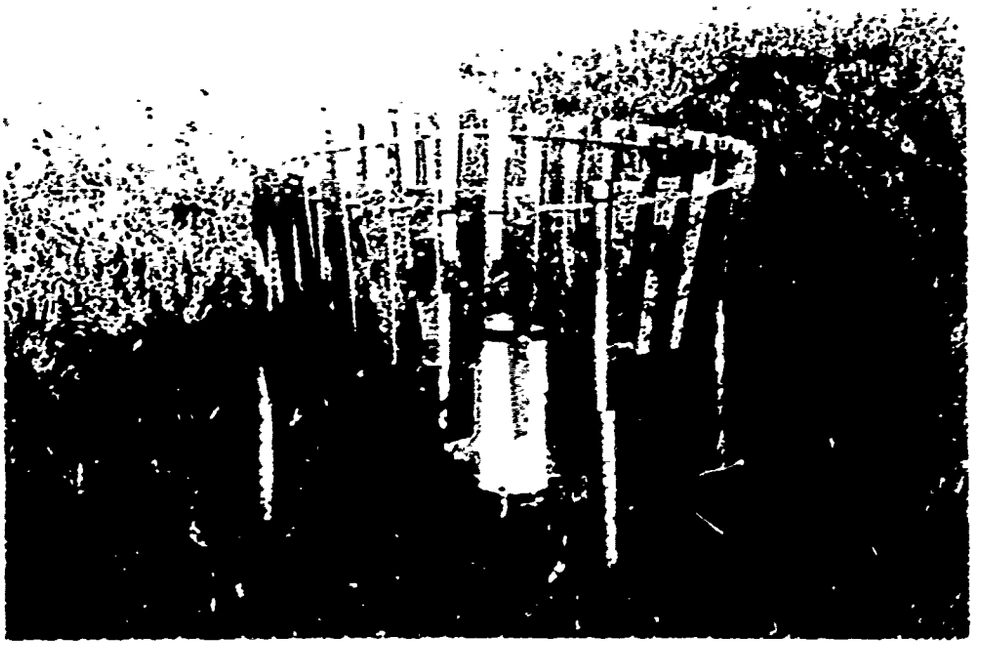

FIGURE 6. Close-up view of a rain tipping bucket with windshield.

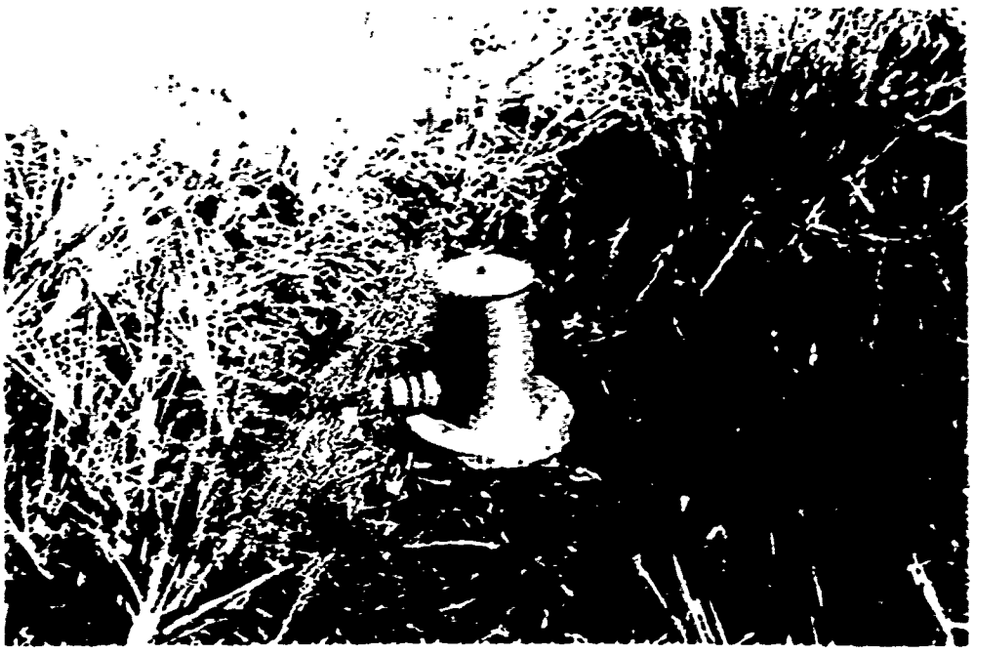

FIGURE 7. Rain drop-size distribution spectrometer deployed near the 4 inch trihedral radar target.

The rain drop-size spectrometers were located near the tipping buckets, and were intended to provide data on the rain particle sizes and to serve as a check on the rain rates indicated by the tipping buckets. Figure 7 gives a close-up view of one of the spectrometers. These units were furnished by the Illinois State Water Survey, Urbana, Illinois, and consisted of a piezoelectric sensor mounted under a plastic cylinder, 2-3/4 inches long. The sensor generated a voltage pulse for each raindrop that impacted on the top surface of the plastic cylinder, with an amplitude that was proportional to the drop size. The sensor also contained a preamplifier and an electronic switch so that a calibration signal could be introduced periodically.

A cassette tape recorder activated by the first raindrop to hit the spectrometer, was used to record the voltage pulses along with a time-code signal. A field calibration of the spectrometer was achieved by dropping a plastic bead from a known height onto the spectrometer and recording the resulting pulse. Correlation between the bead-drop calibration and water drop-size was done in a water drop tower test by the Illinois Water Survey Laboratory, who also reduced a portion of the drop-size tapes following the field operations. An important limitation of the spectrometers was their inability to measure drops below 0.5 mm diameter.

The other meteorological instruments were located at the instrument van, and readings such as temperature, barometric pressure, and wind speed and direction were made at intervals during a rain storm.

6. Measurement Procedure

The measurement procedure followed in taking rain backscatter data typically consisted of the following steps:

(1) At the onset of rain (which was usually detected by the 70 or 95 GHz radars well in advance of the tipping of the buckets), all the recording equipment was turned on.

(2) A-scope photographs were taken at intervals during the rain storm, as considered necessary to record the complete range of rain intensities being monitored via the bucket tips recorded on the paper chart recorder. Typically, A-scope photographs were taken at intervals of between one and five minutes. Photos were made for all three available polarizations during each interval.

(3) At 5- to 10-minute intervals the range gate controlling the pulse sampler boxcar was changed to different settings, thus providing a magnetic tape and paper chart record of the amplitude of the backscatter versus rain rate for different ranges.

(4) The output of each radar was switched sequentially at about 10-second intervals to the A-scope being recorded on video tape.

(5) Temperature, pressure, relative humidity, and wind speed and direction were measured at intervals during the rain storm.

(6) Calibration of all recorders was performed before and/or after the rain, the radars being boresighted on the reference target and the rf attenuation varied in 5-dB steps.

II. DATA ANALYSIS

A. Data Analysis Techniques

The data analysis performed under this contract consisted in reducing the data recorded on magnetic tapes during the field operations at McCoy AFB. Data from other sources, such as Polaroid photographs of A-scope displays, video recordings, and strip chart playouts, served to provide background information but were not analyzed directly.

1. Data-Reduction Facility

The PDP-8/F based data-reduction facility of the Sensor Systems Division of EES was used to process all the tapes which resulted from the McCoy AFB field tests. Figure 8 gives a view of the basic computer components. These include: (1) An analog signal-conditioner unit which provides variable gain and offset to allow the interface of varied types of signals to the data-reduction facility, (2) A Fabritek Series 1070 instrument computer which serves as an A/D and D/A interface, and also computes real-time pulse-height distributions and cross-correlation functions. The D/A output from the Fabritek computer can be displayed on a CRT display or be plotted on an x-y plotter. (3) A PDP-8/F computer which can exchange information directly with the Fabritek computer. (4) A teletype, and (5) a Sykes Compucorp Digital Cassette Recorder for program development and storage.

The PDP-8/F contains 12K of memory, of which 8K is magnetic core. An extended version of FOCAL$_{TM}$ has been developed for use with the PDP-8/F and is designated FOCAL/F [4]. This language is interactive and greatly facilitates program correction and modification. Also available is a machine language software package for calculating fast Fourier transforms (FFT), and a set of software commands for Fabritek control. These two machine language software packages along with the extended FOCAL$_{TM}$ software make this system a very powerful and flexible data-reduction tool.

2. Data Analysis Procedure

The types of results which can be obtained from the data facility include: (1) pulse-height amplitude distributions, (2) frequency spectra,

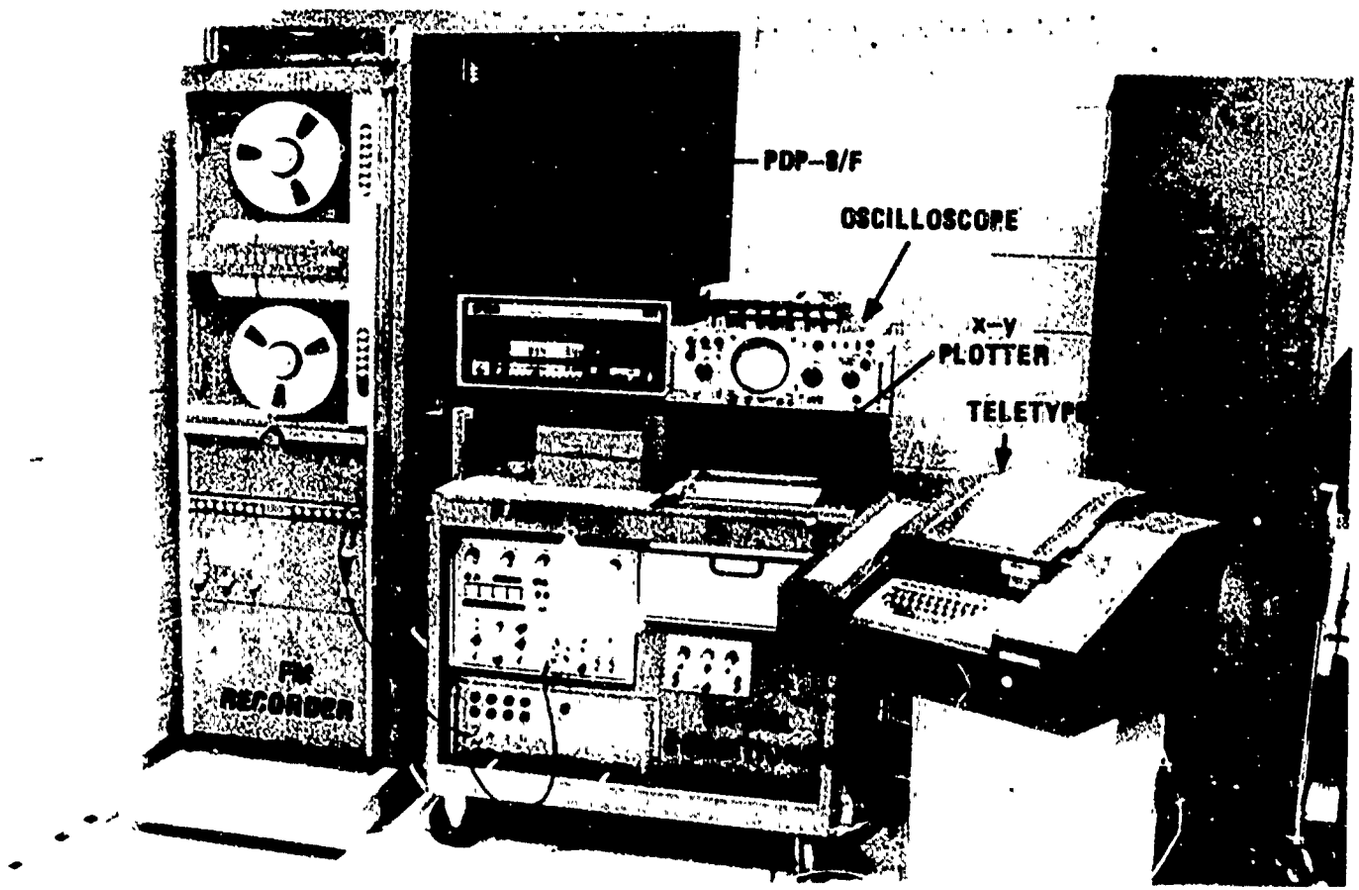

Figure 8. View of the Sensor Systems Division's PDP-8/F based data reduction facility.

and (3) auto- and cross-correlation functions. The methods for obtaining these three classes of results are sufficiently different as to require entirely different FOCAL$_{TM}$ programs for their calculation. Taken as a whole, these three results are considered to describe the recorded data.

a. Pulse-Height Amplitude Distributions

Pulse-height amplitude distributions calculated by the data facility are displayed in two forms: as probability density plots and as probability distribution functions. The probability density plots are generated from data time histories using a Fabritek Type SW-75 PHA plug-in as a preprocessor. This plug-in samples the input analog time history, A/D converts the samples, determines into which of 1024 amplitude bins the sample belongs, and increments a stored variable corresponding to the number of samples which have fallen in that amplitude window. When repeated a large number of times, this process generates an unnormalized density, which is then divided by the total number of samples to achieve a normalized probability density function.

The voltage amplitudes are calibrated by inputting a stepped calibration signal to the PHA program. The peak of the distribution for each voltage step in the calibration is then assigned the dB value corresponding to that calibration step. The PHA program in the PDP-8/F then does a cubic fit to the calibration and generates a table relating dB value and amplitude bin number. The cubic fit program was developed to "linearize" nonuniform calibration steps so that the output density functions can be plotted on a linear scale.

The probability distributions are calculated by a point-by-point numerical integration of the probability density functions. The functional values of these distributions are then multiplied by a nonlinear transfer function so that they can be plotted on probability paper.

The resultant probability distributions are useful in determining the median values of the distributions and also their shapes. In addition, for certain classes of functions, the average values can be determined from the distributions using a simple formula [5].

b. Frequency Spectra

The frequency spectra data-reduction program uses the fast Fourier transform subroutines available for the PDP-8/F to transform input time

histories to the frequency domain. The program has several options which allow the spectral data to be presented in several different forms including: (1) voltage amplitude in dB versus frequency, (2) normalized voltage amplitude in dB versus frequency, and (3) normalized power spectral density versus frequency.

The voltage amplitude program in the PDP-8/F computer processes an input time history which has been sampled, A/D converted, and stored by the Fabritek. The program computes the fast Fourier transform for that time history, and calculates the square root of the sum of the squares of the real and imaginary parts of each element in the transform. Since the time history represents the voltage out of a logarithmic receiver, the amplitude of the spectrum corresponding to the time history is measured in dB relative to a milliwatt (dBm). Thus, to calibrate the spectral amplitude in dB, a calibration is stored in memory which relates dB values to input voltage amplitudes, and each time history is converted to dB values as it is read in. Since the Fourier transform is a linear process, the spectrum amplitude will be proportional to dB if the time history is calibrated in dBm, and the proportionality constant is set equal to one in the program.

Figures 9 and 10 give typical time histories for 9.375 GHz and 95 GHz. The vertical scales are calibrated in units of dB relative to 1 m^2/m^3. (Received power can be related to cross-section per unit volume if the appropriate radar constants are known.) A time history is limited in duration to the number of Fabritek memory bits times the sample period. For this case, the sample rate equals the prf used in taking the data, so that a time history is given by: 1/1620 x 1024 = 0.632 seconds. To achieve the equivalent of a longer time history, the Fourier transforms of 8 adjacent time histories are averaged together.

In calculating the FFT, the dc term is set to zero because its amplitude is normally so much larger than the rest of the spectrum that dynamic range problems are encountered in the computer. Thus, the zero frequency point is zeroed in all the plots. However, this dc point can still be determined independently from the amplitude distributions.

A second method of displaying the log amplitude spectrum is to normalize the spectrum by dividing all the elements by the peak element value. The spectrum is then plotted as dB relative to the peak voltage

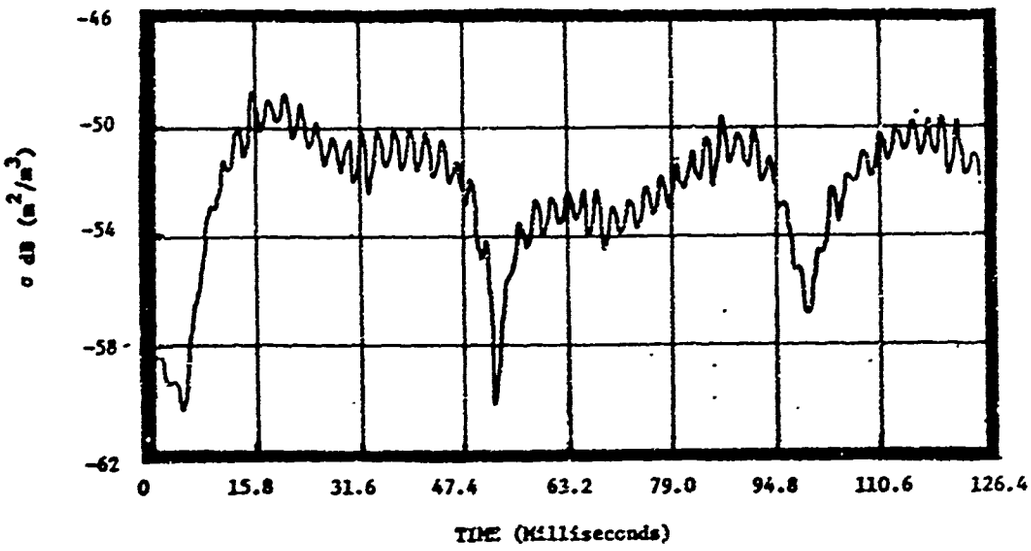

Figure 9. Time history of the recorded backscatter from rain; 9.375 GHz, 33 mm/hr rain rate, VV polarization.

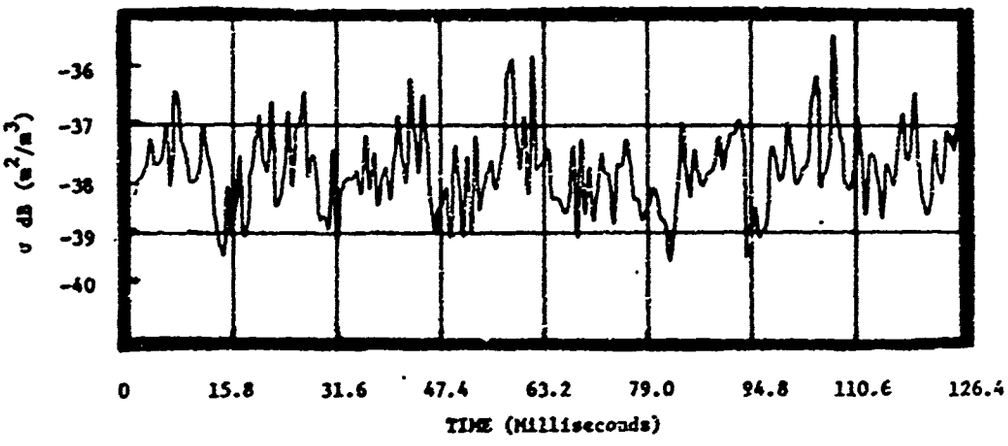

Figure 10. Time History of the recorded backscatter from rain; 95 GHz, 33 mm/hr rain rate, VV polarization.

amplitude, which is normally the lowest frequency point. This type of plot is very useful for comparing frequency rolloff characteristics of spectral plots with different amplitudes.

Although the data recorded on the magnetic tapes represents the voltage output from a logarithmic amplifier, it was deemed desirable to be able to plot an equivalent spectrum for a linear receiver. Therefore a modification was developed to the spectrum program which allowed the "delogging" of the input data prior to calculation of the Fourier transform. When normalized this program results in the calculation of the normalized power spectrum. For certain classes of functions, to which all of the data processed here belong, the power spectrum is equivilent to the power spectral density. The unnormalized calibrated power spectrum cannot be determined because the dc term is thrown away, as previously described.

Another program modification was developed to deal with both 60-Hz and 400-Hz interference signals in the recorded data. The 400-Hz (approximately) component was often so much larger than the backscatter data that the maximum allowed dynamic range for the computer variables was exceeded. To deal with this problem, the time history was passed through a six-pole Butterworth notch filter with a center frequency of 400 Hz prior to being A/D converted. An algorithm for the inverse of the amplitude versus frequency response of the filter was developed which, when multiplied by the spectrum of the filtered data, resulted in a spectrum equivalent to the unfiltered spectrum. The notch filter decreased the size of the 400-Hz component relative to the other spectral components, thus solving the dynamic range problem. The value of the 400-Hz component was then set to zero before the inverse filter algorithm was applied, yielding a net result of a spectrum equivalent to the unfiltered spectrum except for the absence of the 400-Hz component. The 400-Hz signal varied in frequency as seen in Appendix B.

C. Auto- and Cross-Correlation Functions

The auto-correlation functions and cross-correlations functions for input time histories are determined by two different methods in the data analysis. Auto-correlation functions are computed from the inverse transform of the magnitude of the Fourier transform squared in the PDP-8/F computer, while cross-correlation functions are measured using an SD-75 plug-in in the Fabritek computer. The SD-75 plug-in samples two separate

input signals, A/D converts them, and calculates partial products between samples as a function of time to generate the correlation function between the signals. This computation is given by

$$\phi_{AB}(n\Delta\tau) = \frac{1}{k} \sum_{i=1}^{k} A(t_i)\ B(t_i + n\Delta\tau);\ n = 0, 1, 2, \ldots, k-1$$

where, k = number of discrete points for which the correlation function is to be determined,

$k\Delta\tau$ = total sample length,

$A(t_i)$ = value of first sampled function at time t_i,

$B(t_i)$ = value of second sampled function at time t_i.

This method could have been used to generate auto-correlation functions by connecting the same signal to both plug-in inputs, but this was not done because of several limitations in the plug-in. These include: (1) There is no provision to calibrate the two input signals, making set-up and calibration of the auto-correlation function difficult. (2) Due to the limited memory available in the Fabritek, the lowest frequency that can be accurately measured is approximately one-tenth the total sampling period while the highest frequency is, from the sampling theorem, about one-half the sampling rate. Thus to measure the auto-correlation function of a signal with 800-Hz bandwidth, the sample rate would be 1600 Hz and the lowest frequency would be:

$$F_{low} = \frac{\text{Sample rate}}{\text{Total Memory}} = \frac{1600\ \text{Hz}}{1024\ \text{Memory bits}} = 1.56\ \text{Hz}.$$

(3) The finite computation time limits the sampling frequency since computations are performed in real time.

Utilizing the fast Fourier transform in the PDP-8/F to perform auto-correlation calculations solves the problems inherent in using the SD-75 plug-in in the Fabritek, except for the lower frequency limitation. Since the Fabritek memory is used to store the time histories, the same low-frequency limitations apply. However, a partial solution to this problem is to calculate the auto-correlation function using a lower sample rate

to pick-up lower frequencies at the expense of higher frequencies. A family of curves can thus be generated at different sampling rates which describe the auto-correlation function over any desired band of frequencies.

In the case of cross-correlation function computation, the FFT program in the PDP-8/F computer is not suitable, and the SD-75 plug-in in the Fabritek must be used even with its limitations. Calibration can be obtained with the plug-in by using signals with known correlation functions, such as, for example a sinewave or Gaussian noise, to calibrate the results from an unknown signal.

d. Rain Drop-Size Distributions

The rain drop-size distribution analysis was carried out as an addition to the initial rain data-reduction task because the drop-size distributions were thought to be the key to the problem of the large observed variations in backscatter for a constant rain rate. The Illinois Water Survey Group, which were originally contracted to analyze the drop-size tapes, were unable to do so due to the generally poor quality of the tapes. Because of the importance of the drop-size distributions to the backscatter question, EES proposed to attempt the analysis of the tapes as an additional task to the initial contract. The rain drop-size tapes were thus obtained from the Illinois Water Survey and processed to recover as much of the drop-size data as possible.

The drop-size spectrometers utilize a piezoelectric crystal to convert the impact of raindrops on the spectrometer heads to voltage pulses which are then recorded on a cassette recorder. The spectrometers are calibrated by dropping plastic beads of various diameters onto the sensor heads from a tower and recording the outputs. By this calibration technique, the Illinois Water Survey was able to determine that the relationship between drop diameter and the peak of the corresponding voltage pulse was approximately a linear function for these spectrometers. In order to account for changes in recorder gain and offset over a period of time, at the onset of each rain storm, a calibration signal was automatically recorded on the tape consisting of a 100-Hz square wave with an amplitude equal to the height of a voltage pulse corresponding to the impact of a 6-mm rain drop. In addition, time code was recorded on a second record channel, but unfortunately this feature did not function most of the time.

Figure 11 gives a block diagram of the equipment set-up used to analyze the drop-size data. The output of the data recorder was passed through a variable gain and offset amplifier to a peak detector. The peak detector was required because the output of the piezoelectric sensor exhibited an under-damped sin(x)/x type of response following the impact of a raindrop, whereas only the peak of the signal is of interest. The peak detector was triggered by a Tektronix 545A oscilloscope which served as a variable threshold trigger generator. When a rain drop impacted, the main sweep of the oscilloscope was triggered, which in turn triggered a pulse generator that enabled the peak detector for 250 μsec following the start of the Tektronix scope main-sweep. The Fabritek computer was used in the pulse-height analyzer mode (see discussion of the radar backscatter amplitude data reduction) to generate a density function consisting of the number of occurences versus drop-size (to the nearest 0.1 mm) during a given time interval (usually 30 seconds).

This distribution was then utilized to calculate both the rain rate and a normalized distribution function consisting of the number of drops, of a given diameter, that were contained in a cylinder above the sensor head of the drop-size spectrometer with a volume of 1 m^3. The rain rate can be expressed as follows:

$$R(mm/hr) = 3600\ H/T,$$

where H is the height of accumulated water over the sensor head in mm and T is the time in seconds.

H is equivalent to the volume of the water divided by the sensor head area (3848 mm^2). The volume is given by:

$$V = \frac{\pi}{6} \sum_{i=1}^{n} A_i D_i^3$$

where: A_i is the number of drops of a given diameter D_i ($\pm$ 0.05 mm) which strike the sensor head, and

D_n is the maximum drop diameter.

Combining the above factors yields:

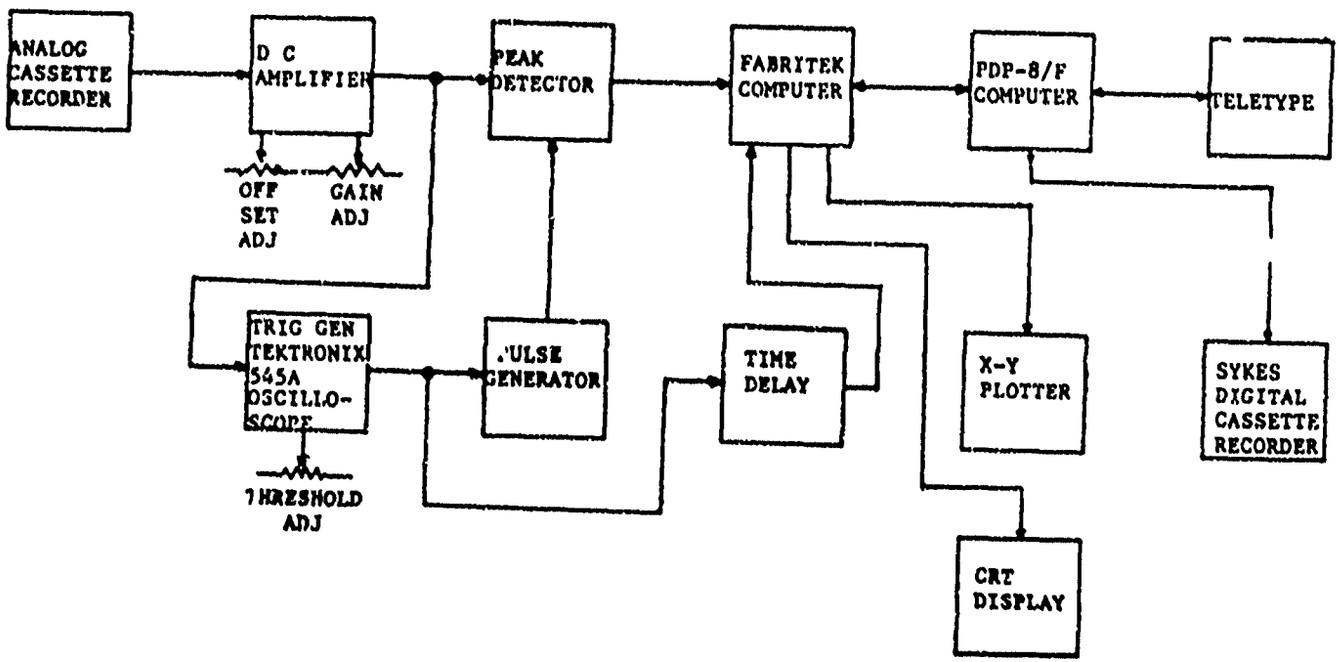

Figure 11. Block diagram of the equipment setup used to process the rain drop-size tapes.

$$R = \frac{0.49}{T} \sum_{i=1}^{n} A_i D_i^3$$

The volumetric distribution (number of drops in a cylindrical column above the sensor head with volume of one cubic meter) is related to the measured distribution over some time interval by:

$$N\ (vol.) = \frac{N_i D_i h}{T V_t}$$

where: N_i is the number of drops striking the sensor in time T with diameter D_i,

h is the height of a cylindrical column with the same diameter as the sensor head and a volume of 1 m^3 (260 meters for these sensors), and V_t is the terminal velocity of a drop diameter D_i.

The terminal velocities used to calculate the volumetric distributions were taken from Gunn and Kinzer [6].

A Focal program was written for the PDP-8/F computer to perform the above calculations, and to allow graphing of the rain rates and volumetric drop-size distributions on an X-Y plotter. The drop-size distributions were determined as closely as possible for the same time intervals as were analyzed radar backscatter data in order to determine any relationships.

A number of problems were encountered in the data reduction. The tape recorders used originally to record the data were not of adequate quality; due to poor frequency response, the calibrations on the tapes were often so distorted as to be unusable. Instead, the distributions were calibrated by comparing the calculated rain rates from the drop-size distributions to the tipping bucket records. Although this was a tedious process, it appeared to work quite well, as the match-up of rain rates between the spectrometers and the tipping buckets in general was quite good. The lack of time code on most of the tapes further complicated the process, but once again the tipping bucket records were used to determine times for the drop-size spectrometer tapes. In addition, high noise levels on the tapes prevented the detection of some of the small drops.

However, a number of distributions were obtained which correlated well in rates with the tipping buckets and appeared reasonable so as to allow some general determinations of the relationship between drop-size and radar backscatter characteristics to be made. These findings will be discussed in a later section.

3. Sources of Error in the Data

The analyzed backscatter data show large variability in both amplitude and spectral parameters when plotted as a function of rainfall rate. While this probably indicates that rainfall rate is not an adequate and sufficient parameter for backscatter characterization, there were some problems in the experiment and in the quality of the data on the tapes which could have affected the accuracy of the analyzed data.

There were two main problems with the way in which the experiments were structured. (1) The rain instrumentation was placed near the radar targets, while data on the backscatter, of necessity, had to be sampled at radar cells which did not include the radar targets. Since the rains seen during the field tests were often nonuniform, the rain rates and drop-sizes as measured by the rain instruments may not in general be the same as those in the radar cells being sampled. (2) The signal backscattered from rain is attenuated when propagating through a rain-filled volume. Because of the way the experiment was instrumented, there was no direct way to measure this attenuation for the data recorded on tape, so that an attenuation function had to be assumed from theoretical calculations. This fact, coupled with the problem that many of the measurements were made at ranges which were in the near field of the 70-GHz and 95-GHz antennas, could have contributed further to errors in the backscatter.

Several problems in the recorded data also could have caused errors in the analyzed data. Several of the tapes had no calibrations recorded on them, so that calibrations had to be used from tapes recorded on different days. Obviously, any changes in radar parameters such as transmitted power or reciever drift could result in calibration errors. Furthermore, the 35-GHz radar had an extremely nonlinear transfer-function, in terms of dB, which could have increased the errors in the data analysis. Normally the RMS error in processing the recorded data is about $\pm$ 0.5 dB, but could have been higher in this case. Also quite large 60-Hz and 400-Hz components were present in much of the data, requiring the use of notch

filters. This was particularly a problem in attempts to analyze the spectral shape of the data, since the notch filters distorted the spectrum. As explained previously, this problem was partially solved by the use of an algorithm in the PDP-8/F computer which multiplied the filtered spectrum by the filter inverse function after deletion of the 60-Hz or 400-Hz spikes.

It can therefore be seen that the spread in the data can be explained to some extent by the problems encountered in the data analysis. However, the data, in spite of the possible errors, does seem to be consistent enough to allow conclusions as to the mechanisms involved in the scattering, and to permit determination of worst-case conditions for backscatter amplitude and spectral width.

B. Summary of Results

1. Interpretation of Data

Periodic waves, such as radar signals, incident upon a material body can be described in terms of absorbed energy and scattered energy. The scattered wave is obtained by solving Maxwell's equations at the boundary of the body, where the geometrical description of the body thus dictates the coordinate system and the mathematical functions required for a solution. For the case of cylindrical and spherical objects, the Bessel functions and Legendre functions are required to describe the scattered waves. The variable parameter in these functions is the normalized particle diameter in units of wavelength.

When the argument of the Bessel function is small, i.e., if the radius of curvature is much smaller than the wavelength of the incident signal, then only the first term in the series representation of the Bessel function is used. The resulting solutions of Maxwell's equations take the same form as used by Rayleigh in describing scattering of light from small particles. An effective cross-section is defined in terms of the ratio of reflected power to incident power and the equation takes the form

$$\sigma = 4\pi r^2 \frac{S_{refl}}{S_{inc}} = 5|K|^2 \frac{D^6}{\lambda^4}$$

where K = function of material of the scattering object

D - diameter of the scattering object

λ = wavelength of incident radiation.

When the argument of the Bessel function is large, that is the radius of curvature is large relative to the wavelength, then Maxwell's equations reduce to the same form employed in geometrical optics. The resulting effective cross-section is independent of wavelength and takes the form

$$\sigma = \frac{\pi D^2}{4}$$

That region between the Rayleigh and Optical regions has generally been called the Mie Scattering region. The Bessel functions are used in detail and the typical decaying oscillating characteristic is evident [7]. For spherical objects, the three regions are generally described in terms of object diameter, D, and radar signal wavelength, λ, as

Rayleigh Scattering	$0 < \frac{\pi D}{\lambda} < 1$
Mie Scattering	$1 < \frac{\pi D}{\lambda} < 10$
Optical Scattering	$\frac{\pi D}{\lambda} > 10$

In the Mie Scattering region where the diameter of the object is comparable to the wavelength of the incident power, the effective backscatter changes in magnitude according to the Bessel function, having a decaying oscillatory response as the ratio of particle diameter to wavelength is varied.

Over the past 30 years, a number of attempts have been made by persons working in the fields of radar and meteorology to model rain and determine its scattering properties. Adjustments have been made in the models employed to account for such factors as the shape of rain drops (pure spheres, spheroids, or tear shaped); drop-size distribution; the dielectric constant (a function of temperature and frequency); frequency and polarization of the incident radiation; type and location of rain (such as thunder storms, frontal systems, over-water, in mountainous areas); and types of scattering mechanism.

A general relationship between the amount of water and the scattering properties has been developed. The usual presentation shows both

radar cross-section and attenuation to increase as rain rate increases. The exact values vary from one investigator to another, depending on the models employed.

Rain rate and drop-size distributions have a general relationship if measured over long time intervals and averaged over many minutes. However, it has been well documented that a wide variation in the total number of drops and in drop-size distribution will occur over intervals of a few seconds to a minute at a given rain rate [8].

2. Attenuation

Attenuation due to uncondensed gases, principally water vapor and oxygen, were not considered important during these tests since the range was so short. At 70 GHz, the highest attenuation for any of the frequencies used, the attenuation due to uncondensed gases is only a few tenths of a dB at worst.

However, attenuation caused by the water droplets themselves during rain storms is an important parameter. The data analyzed under this project were obtained from range-sampled signals and thus the signal strength is affected by the amount of path attenuation. During analysis, it was not possible to obtain values of attenuation since range samples were not recorded under constantly definable conditions. A search was made of the literature to obtain the most reasonable average value of attenuation caused by rain at the radar frequencies of interest.

Calculations made by J. de Bettencourt at Raytheon, [9] by Mueller and Sims at Illinois State Water Survey [10], and by Lin and Ishimaru at the University of Washington [11] appear to be the most reasonable as applied to this project. Table 2 contains the attenuation due to rain, as a function of rain rate and radar frequency, which have been used during the analysis efforts on this project.

3. Average Return Amplitude

The amount of backscatter per unit volume of radar resolution has been calculated and is presented in Figures 12 and 13 for two polarizations. These data could be compared with the many values presented in the literature and suggested by Richard and Kammerer [3], and L. D. Strom [12]. Basic experimental data used for the results presented in this report were collected by the same operators as those collecting dat. for Richard and

TABLE 2

Attenuation Due to Rain

f = 10 GHz	35 GHz	70 GHz	95 GHz
λ = 3.2 cm	0.86 cm	0.43 cm	0.32 cm
$\alpha = 0.00919R^{1.16}$	$0.273R^{0.985}$	$0.637R^{0.868}$	$1.6R^{0.64}$

R (mm/hr)	α (dB/Km)			
0	0	0	0	0
5	0.509	1.33	2.56	4.48
10	0.133	2.64	4.68	6.984
15	0.213	3.93	6.65	9.05
20	0.297	5.22	8.54	10.88
25	0.385	6.50	10.36	12.55
30	0.475	7.78	12.14	14.11
35	0.568	9.06	13.88	15.57
40	0.663	10.33	15.58	16.96
45	0.760	11.60	17.26	18.29
50	0.859	12.87	18.91	19.56
55	0.960	14.14	20.55	20.79
60	1.062	15.40	22.16	21.99
65	1.165	16.67	23.75	23.14
70	1.270	17.93	25.32	24.27
75	1.375	19.19	26.89	25.36
80	1.482	20.45	28.44	26.43
85	1.590	21.71	29.98	27.48
90	1.700	22.97	31.50	28.50
95	1.809	24.22	33.02	29.50
100	1.920	25.48	34.52	30.49

Mueller-Sims 1969 - Florida Rain

J. de Bettencourt 1973 Raytheon

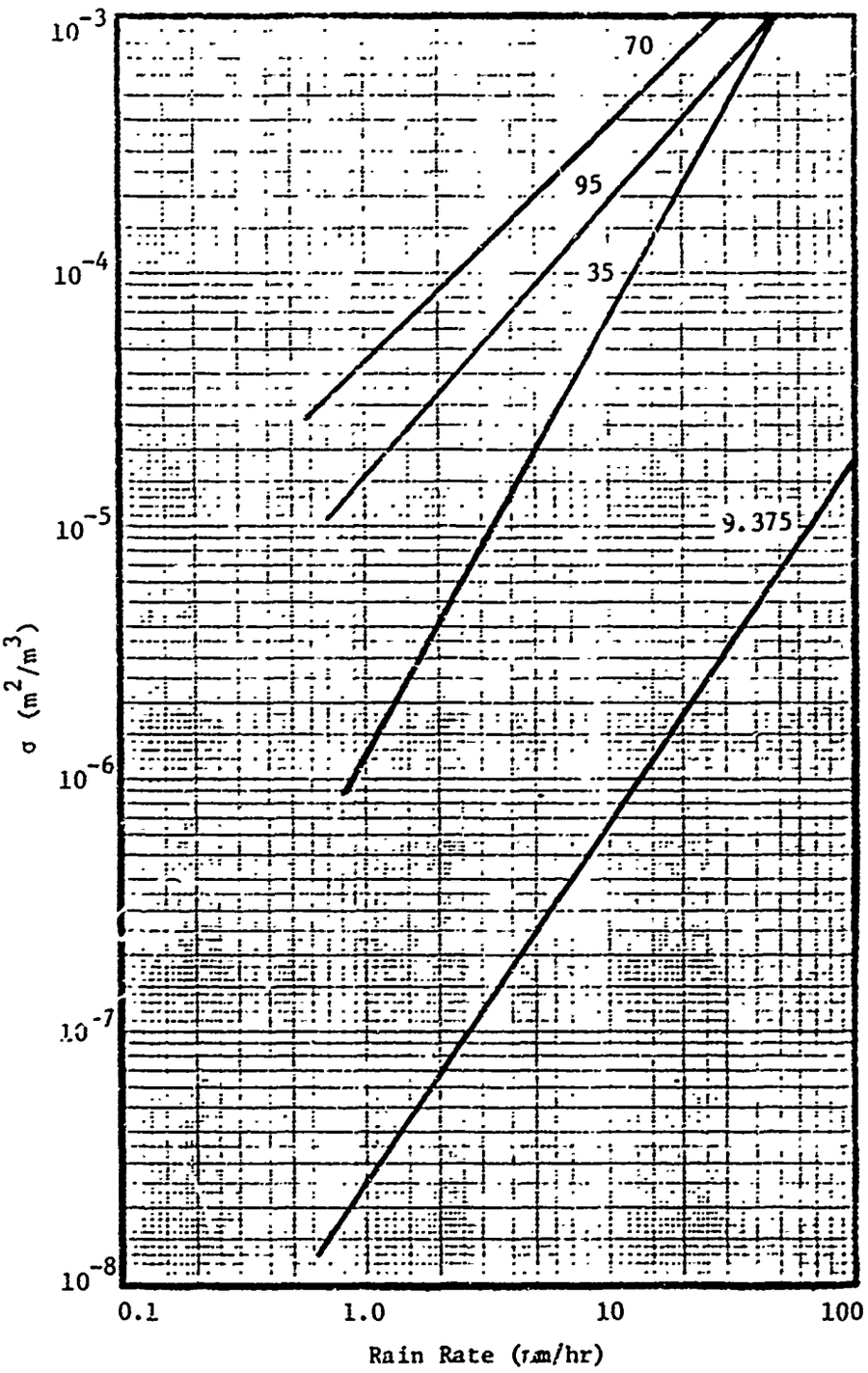

Figure 12. Least mean square fit to radar backscatter data, VV polarization.

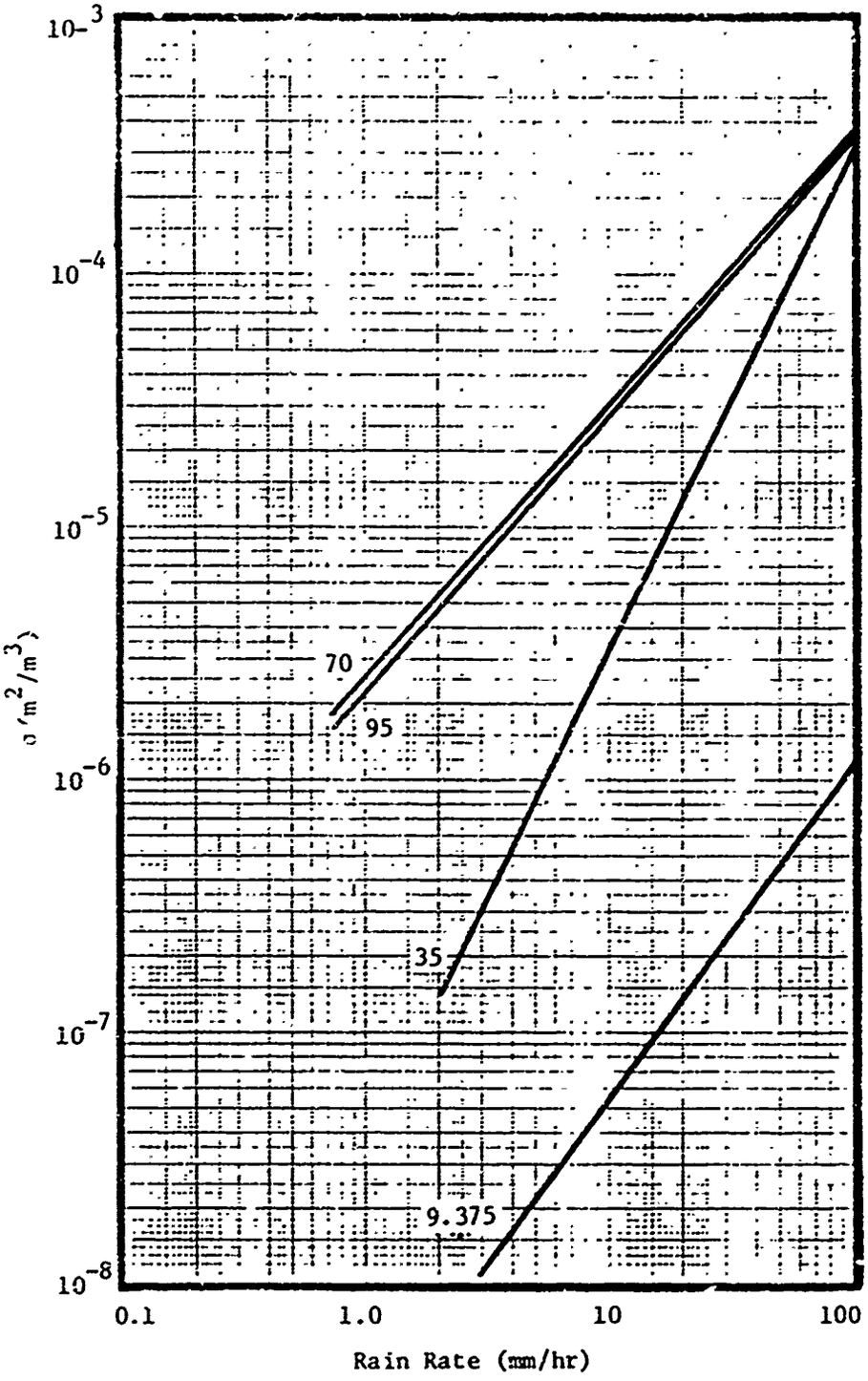

Figure 13. Least mean square fit to radar backscatter data, RC polarization.

Kammerer, as was discussed in a previous section.

Excellent agreement between data presented here and the previously reported data, both experimental and theoretical, exists at X-band. This is gratifying, since one of the primary reasons for having an X-band measurement system was to establish the data-base reference and validate the entire experiment. Good agreement between theory and experiment was expected since drop-size distributions show the maximum drop diameter to be less than 8 mm; thus, at X-band (λ = 32 mm) the scattering mechanism is Rayleigh.

On the average, the backscatter obtained at radar frequencies of 9.374 and 35 GHz are parallel to each other, which indicates that Rayleigh Scattering is the primary mechanism at both those frequencies However, it is noted that the backscatter, as a function of rain rate, becomes flatter at 70 and 95 GHz when compared to the lower frequencies. This might be expected since the radar wavelength is comparable to rain drop size and the mechanism is Mie Scattering. This same trend occurred for both vertical polarization and right circular polarization.

In general, circular polarization produced a lower backscatter than did linear polarization. Differences obtained during this investigation are smaller than reported previously. A fairly consistent 10 to 15 dB difference is reported here, whereas some investigators have reported circular returns 20 dB lower than linearly polarized returns.

An interesting result appeared in the averaged calculated backscatter produced on this phase of the program but not observed by other investigators. The backscatter at 95 GHz was lower than at 70 GHz for both linear and circular polarization. It is postualted that some forward scattering occurred at 95 GHz. This concept could be validated by measurements at 140 GHz, for which the transmitted signal would have a wavelength comparable to the rain drop size. If a resonant phenomenon is creating forward-scattering, the backscatter at 140 GHz should be even lower than at 95 GHz.

4. Amplitude Fluctuations

As discussed in a previous section, the radar signal was selected by a range gate sampler at selected ranges. The signal recorded on magnetic tape thus represents the return from a volume defined by the antenna beam

width and the transmitted pulse length. Considering all the various parameters of the four radar systems and the various ranges, the volumes spanned from 5 to 10,000 cubic meters.

From previously reported date [8] [10], the number of drops in a cubic meter varies as the rain rate increases. In general, for diameters around 0.3 mm, the concentration is 100 to 200 drops per cubic meter, almost independently of rain rate. However, as the rain rate increases, larger sized drops occur with maximum diameters up to 8 mm. As the rain rate increases from 4 mm/hr to 16 mm/hr, on the average the number of drops, greater than 0.5 mm in diameter will increase from a few drops to several hundred, and the mean diameter will increase from around 1.4 to 2.4 mm.

From the system parameters, the test area geometry, and previous rain data, it was anticipated that during light to moderate rain rates there should be a large number of scatterers and drops of sufficient size to produce measurable backscatter radar signals. This was indeed observed during the field data collection period. Analysis of the recorded data shows that the amplitude of the return signal fluctuates in a log-normal manner. In addition, analysis reveal that this log-normal characteristic exists at all rain rates from 1 mm/hr to 100 mm/hr and at all the operating frequencies from 9.375 Hz to 95 GHz. Examples of probability densities and cumulative distributions for the backscatter from rain are shown in Figures 14, 15, 16, and 17.

Calculation of the standard deviation and variance, from the log-normal distribution shows that for any of the radar systems, the standard deviation is independent of rain rate. This implies that from light rains to extremely heavy rains that there were a sufficient number of rain drops having a random location and distribution and without phase coherence within the rain cell resolution, so that the total signal reflected back to the radar was normally distributed. The probability plots obtained from right-circular and vertical polarization are both log-normal. The mean values for circular polarizations were, of course, consistantly lower than mean values for linear polarizations.

Standard deviations obtained from vertical polarizations are shown in Figures 18 through 21 and for circular polarization in Figures 21 through 25.

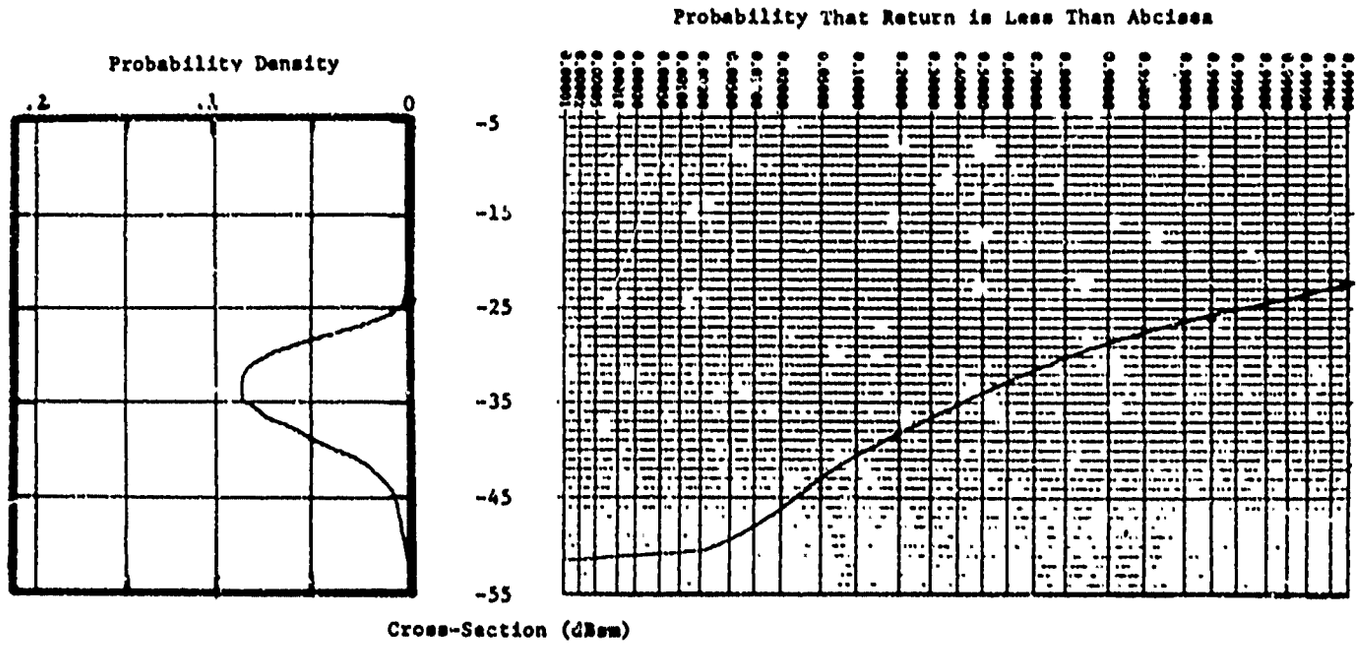

Figure 14. Probability density and cumulative distributions for backscatter from rain; 9.375 GHz, 5 mm/hr rain rate, VV polarization.

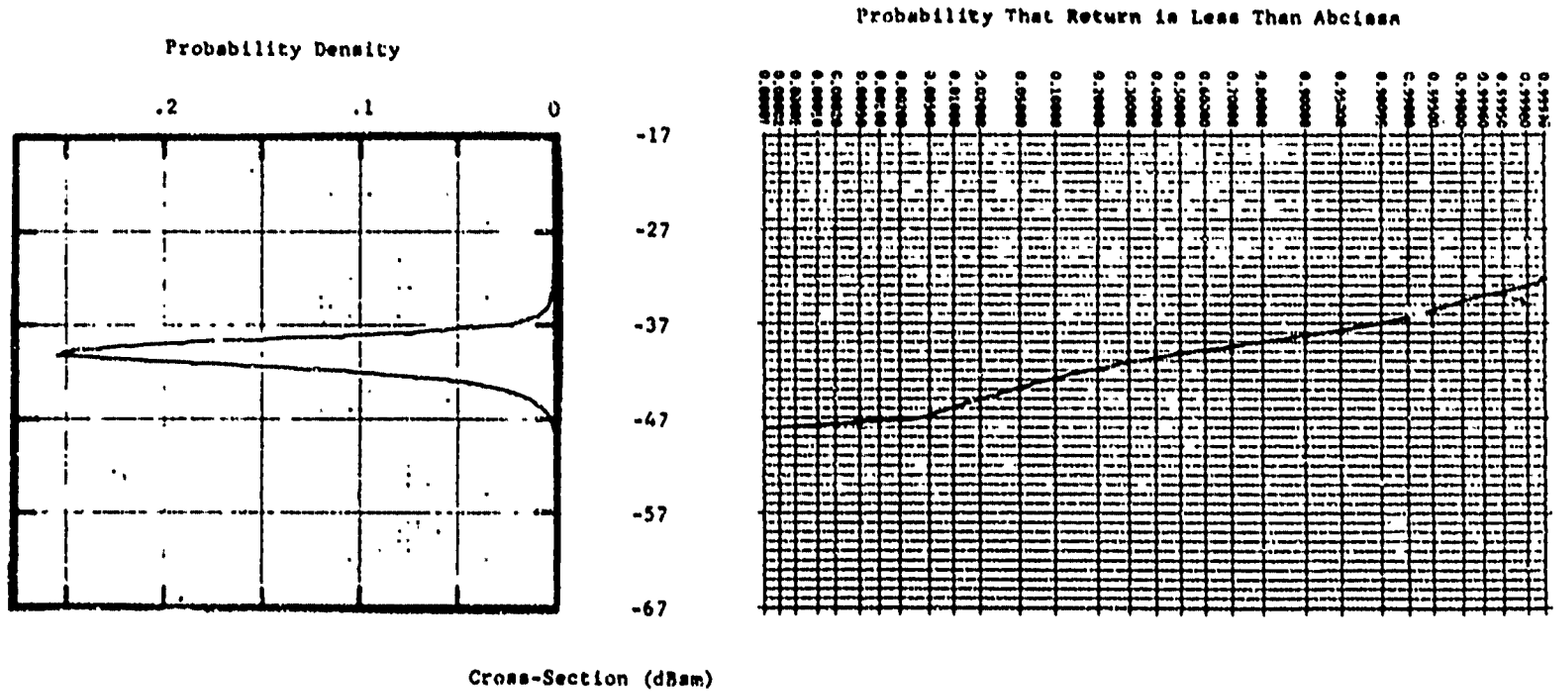

Figure 15. Probability density and cumulative distributions for backscatter from rain; 35 GHz, 5 mm/hr rain rate, VV polarization.

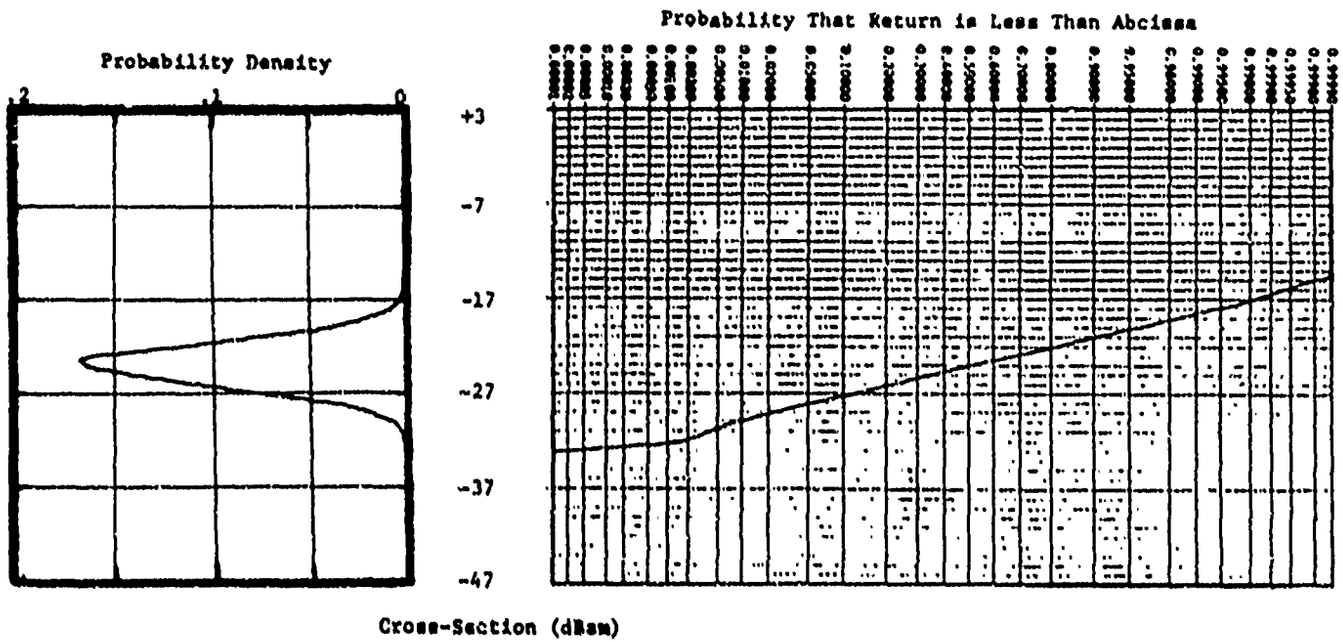

Figure 16. Probability density and cumulative distributions for backscatter from rain; 70 GHz, 5 mm/hr rain rate, VV polarization.

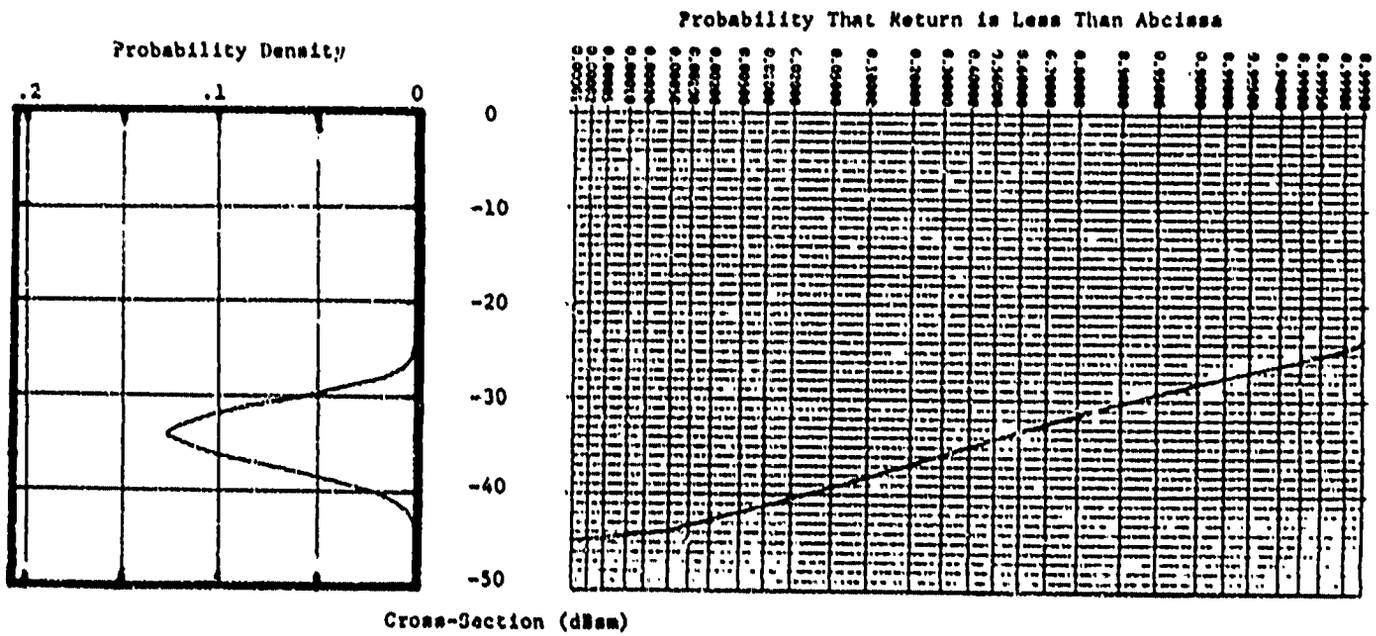

Figure 17. Probability density and cumulative distributions for backscatter from rain; 95 GHz, 5 mm/hr rain rate, VV polarization.

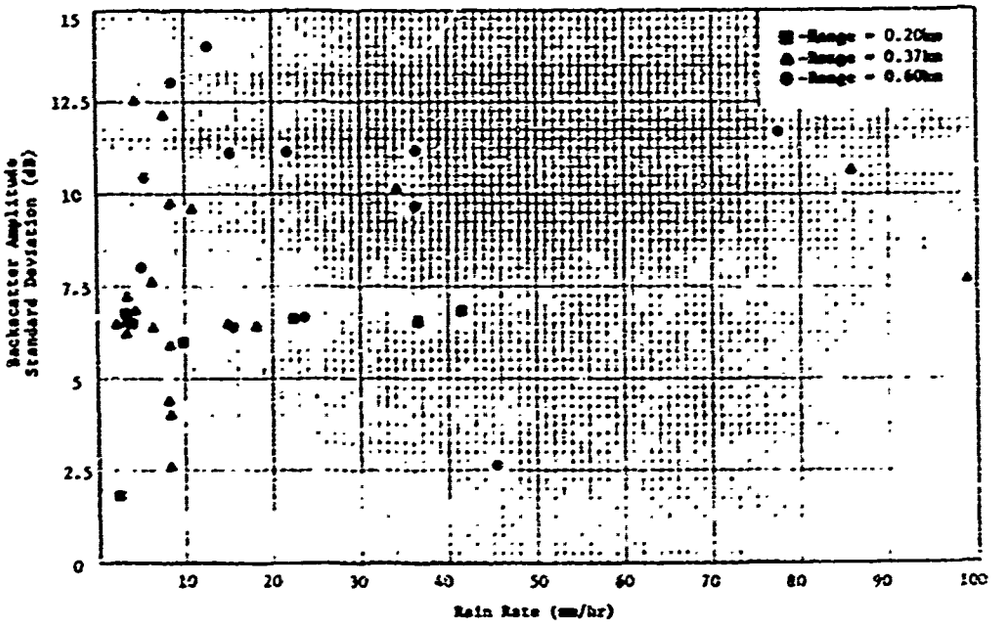

Figure 18. Rain backscatter amplitude standard deviation versus rain rate for 9.375 GHz frequency, VV polarization.

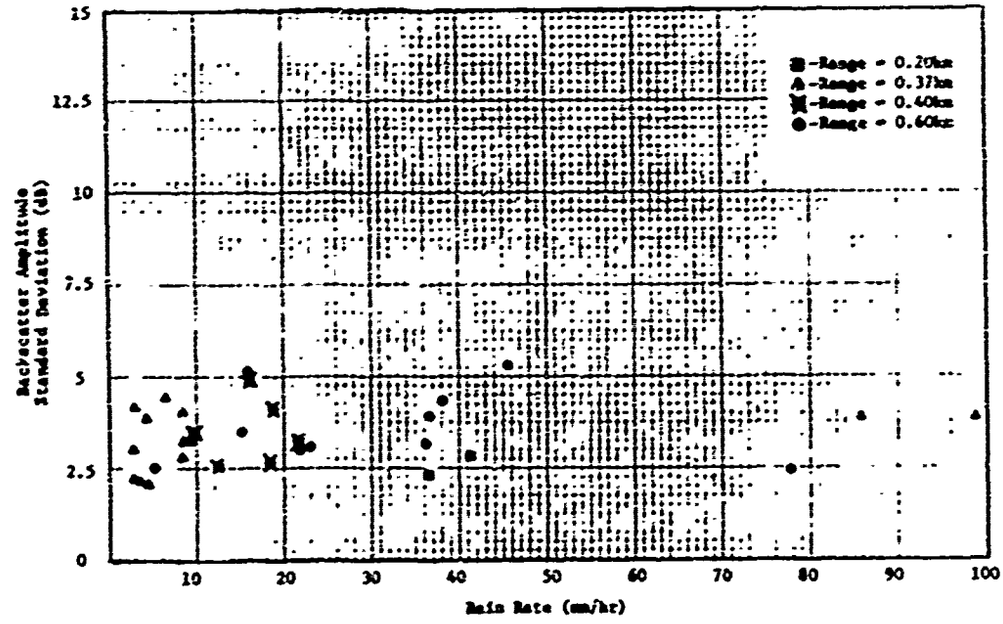

Figure 19. Rain backscatter amplitude standard deviation versus rain rate for 35 GHz frequency, VV polarization.

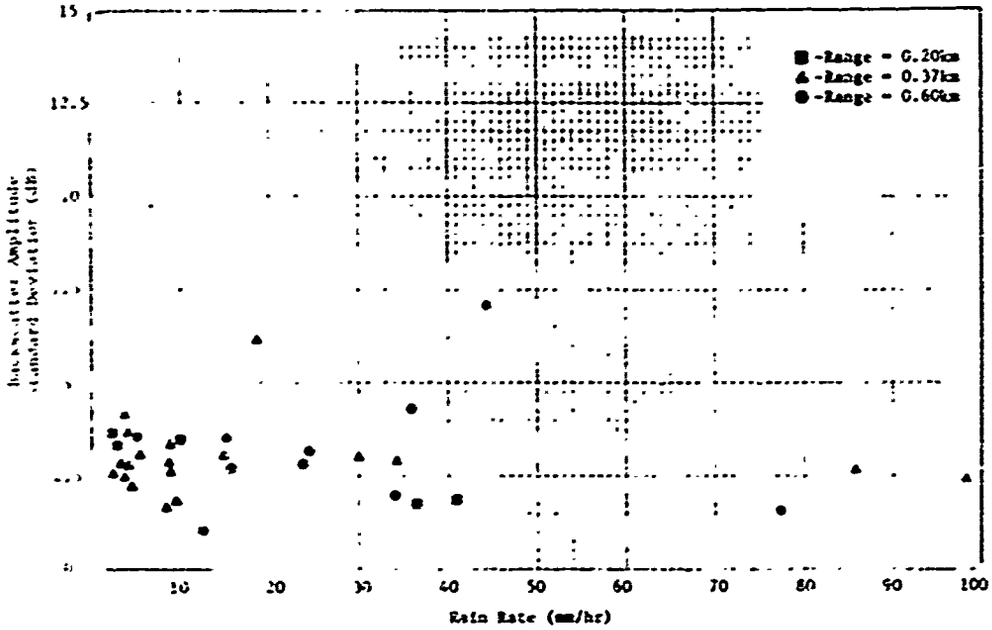

Figure 20. Rain backscatter amplitude standard deviation versus rain rate for 70 GHz frequency, VV polarization.

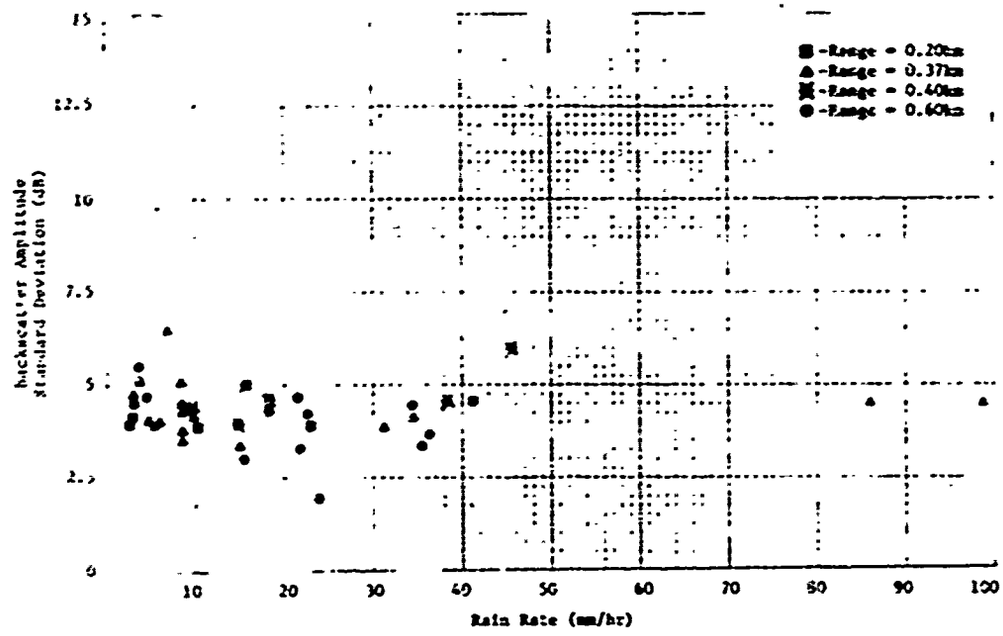

Figure 21. Rain backscatter amplitude standard deviation versus rain rate for 95 GHz frequency, VV polarization.

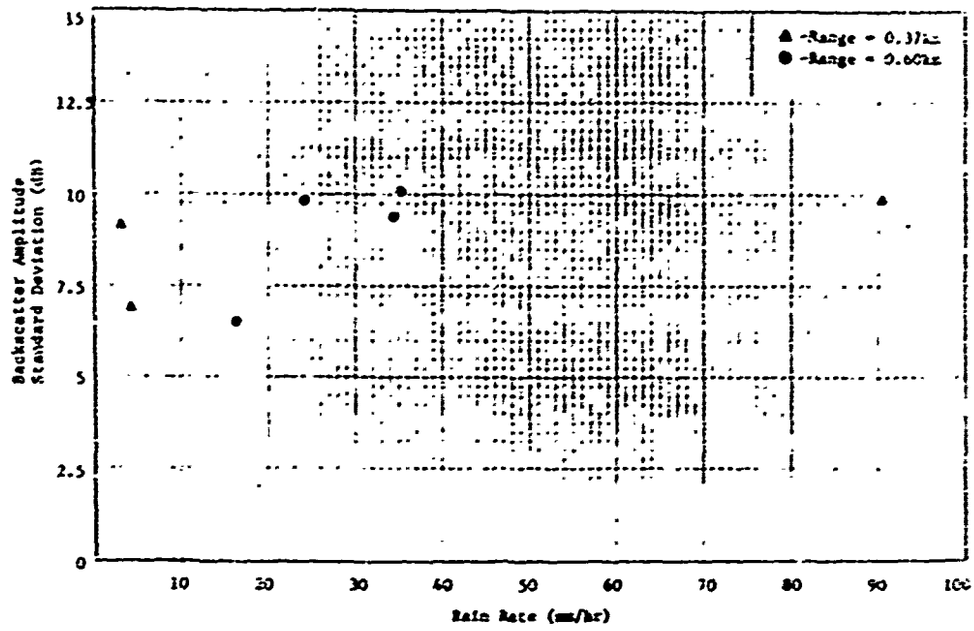

Figure 22. Rain backscatter amplitude standard deviation versus rain rate for 9.375 GHz frequency, RC polarization.

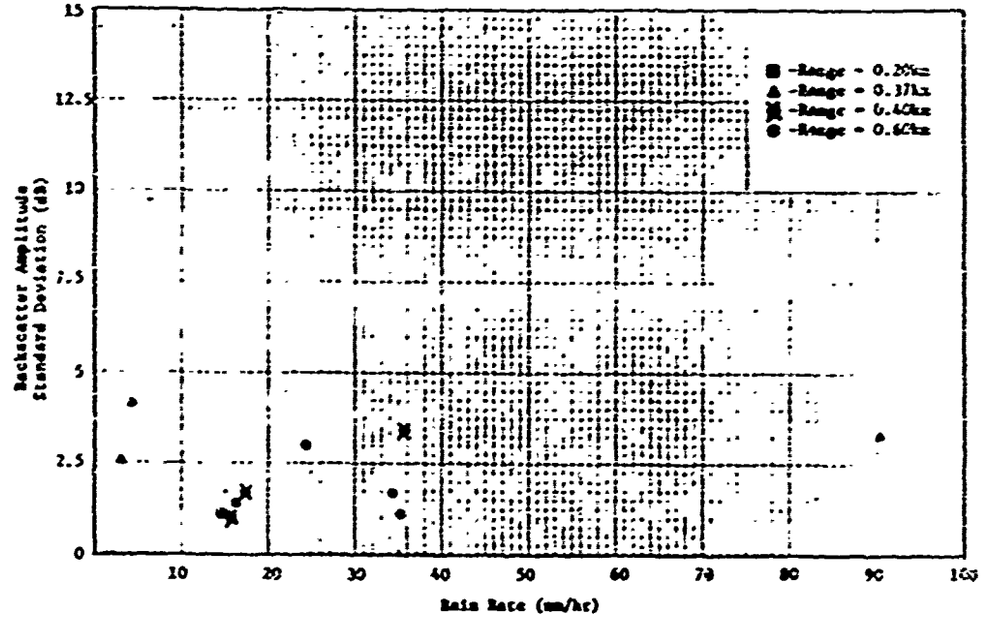

Figure 23. Rain backscatter amplitude standard deviation versus rain rate for 35 GHz frequency, RC polarization.

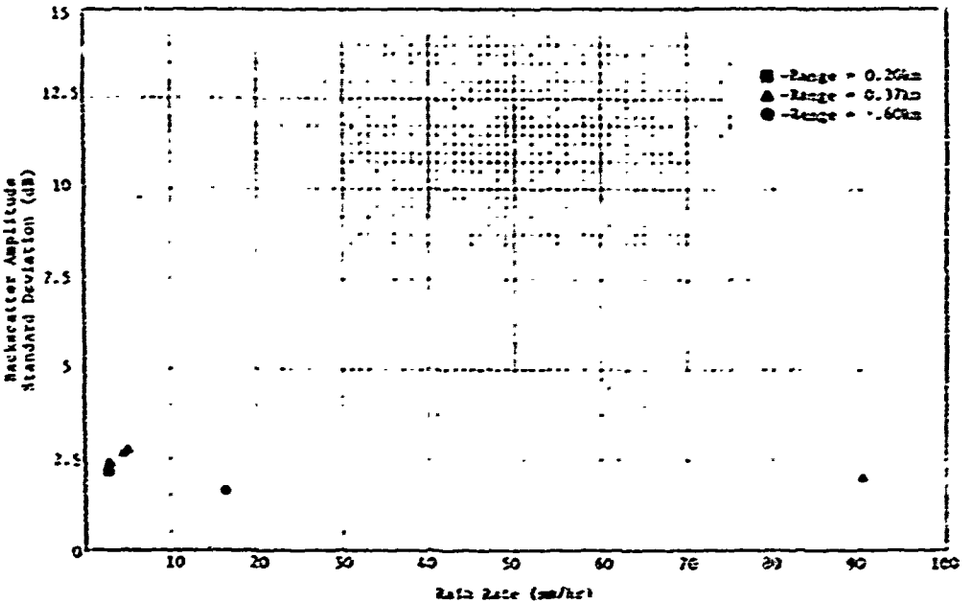

Figure 24. Rain backscatter amplitude standard deviation versus rain rate for 70 GHz frequency, RC polarization.

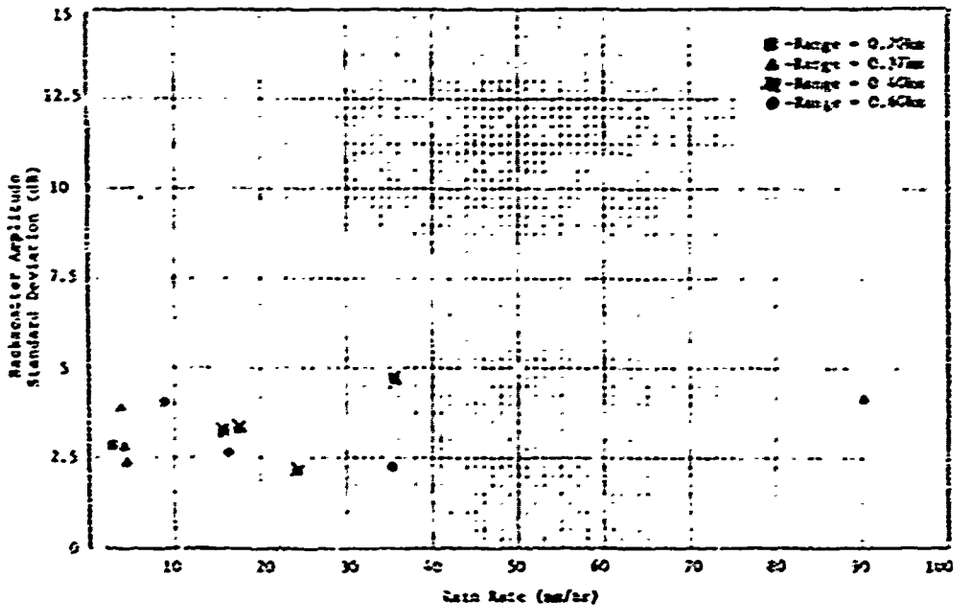

Figure 25. Rain backscatter amplitude standard deviation versus rain rate for 95 GHz frequency, RC polarization.

5. Power Density Spectrum

All the radars employed in these tests were incoherent systems. Thus, it was not possible to obtain the coherent Doppler frequency spectrum of the return signals from the rain clutter. However, it is possible to determine the frequency components without coherent phase relationship in the power spectrum. The equipment and data-processing techniques for obtaining the spectra are presented in a previous section of this report.

For the purpose of comparing data from this project to that obtained by previous investigators, it is important to note differences in the measurement radars employed. Three of the measurement radars used in this investigation employed log-if amplifiers; the 35-GHz (APQ-137) system uses a lin-log if amplifier. Previous investigators have used linear receiver systems. The analysis technique of using fast Fourier transforms to convert time-domain signals to frequency-domain signals requires that the signal be properly formated prior to computer processing.

Since many current radar systems are designed with logarithmic receivers, it was decided to process the data in the same form as they were recorded. This will allow system designers to use the final results directly. Thus, if a Doppler processor is used with log receivers, then the spectral width expected from rain backscatter will be as shown in Figures 26 through 29 for vertical polarization, and in Figures 30 through 31 for circular polarization.

The frequency bandwidth increases as rain rate increases, which is reasonable since having more particles allows more reflections and thus spreads out the spectrum in the frequency domain. It is also noted that as the radar frequency was increased, the spectrum width increased, but the amplitude of the spectrum decreased. This is consistant with the decrease in the standard deviation of the return when comparing X-band to 95 GHz signals. When observing the spectrum at a high rain rate (greater than 35 mm/hr) for the 70 and 95 GHz radars, the return appears almost as colored noise. It should be noted that the roll-off of the spectrum with frequency is not Gaussian, but rather is better fitted by a $1/(1 + (f/f_c)^3)$ response curve at 10 GHz (which is similar to the spectrum shape of the return from land clutter), and is more closely represented by a $1/(1 + f/f_c)^2)$ response at 35 GHz and higher. Thus,

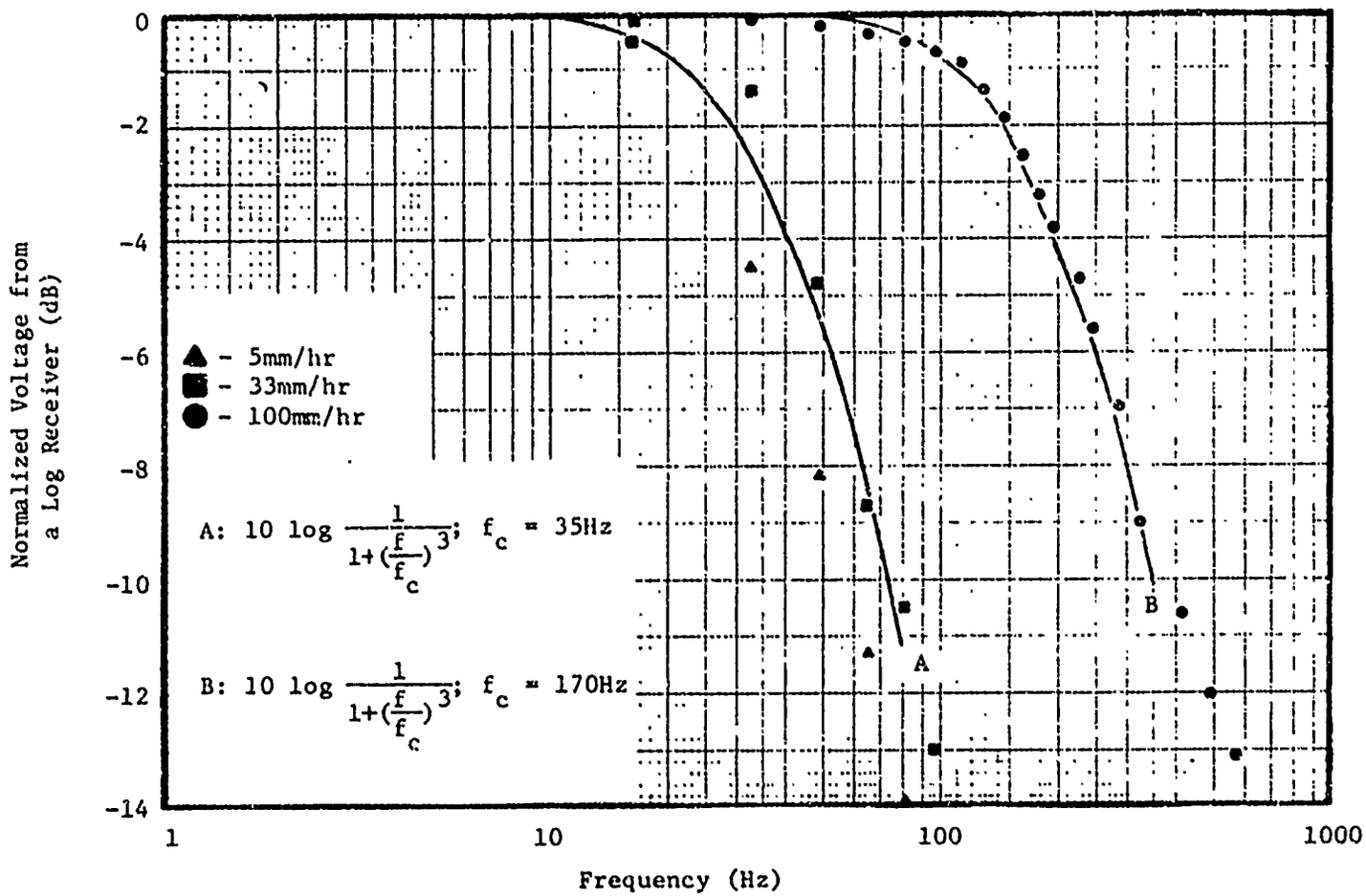

Figure 26. Normalized frequency spectrum of rain return at 9.375 GHz, VV polarization.

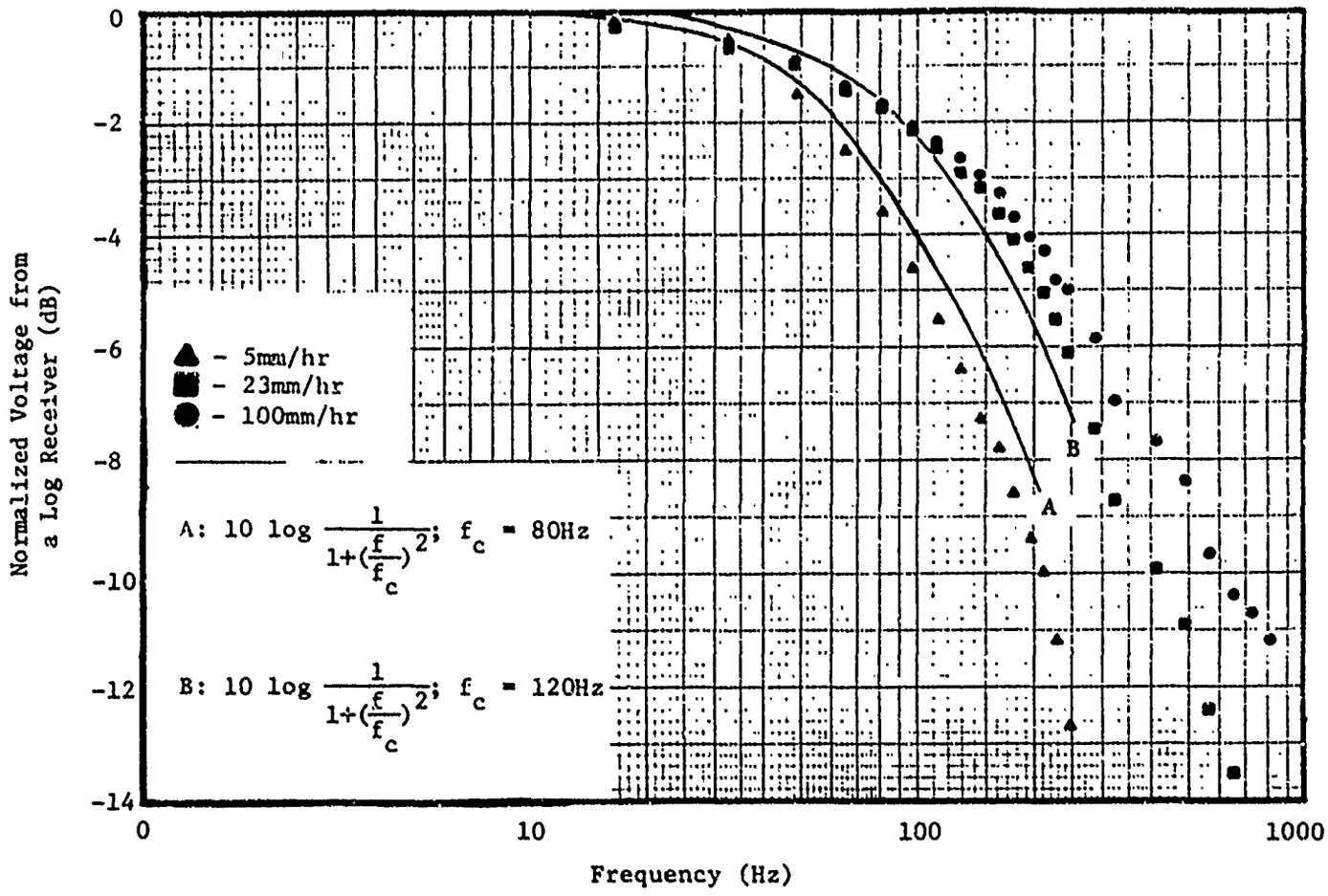

Figure 27. Normalized frequency spectrum of rain return at 35 GHz, VV polarization.

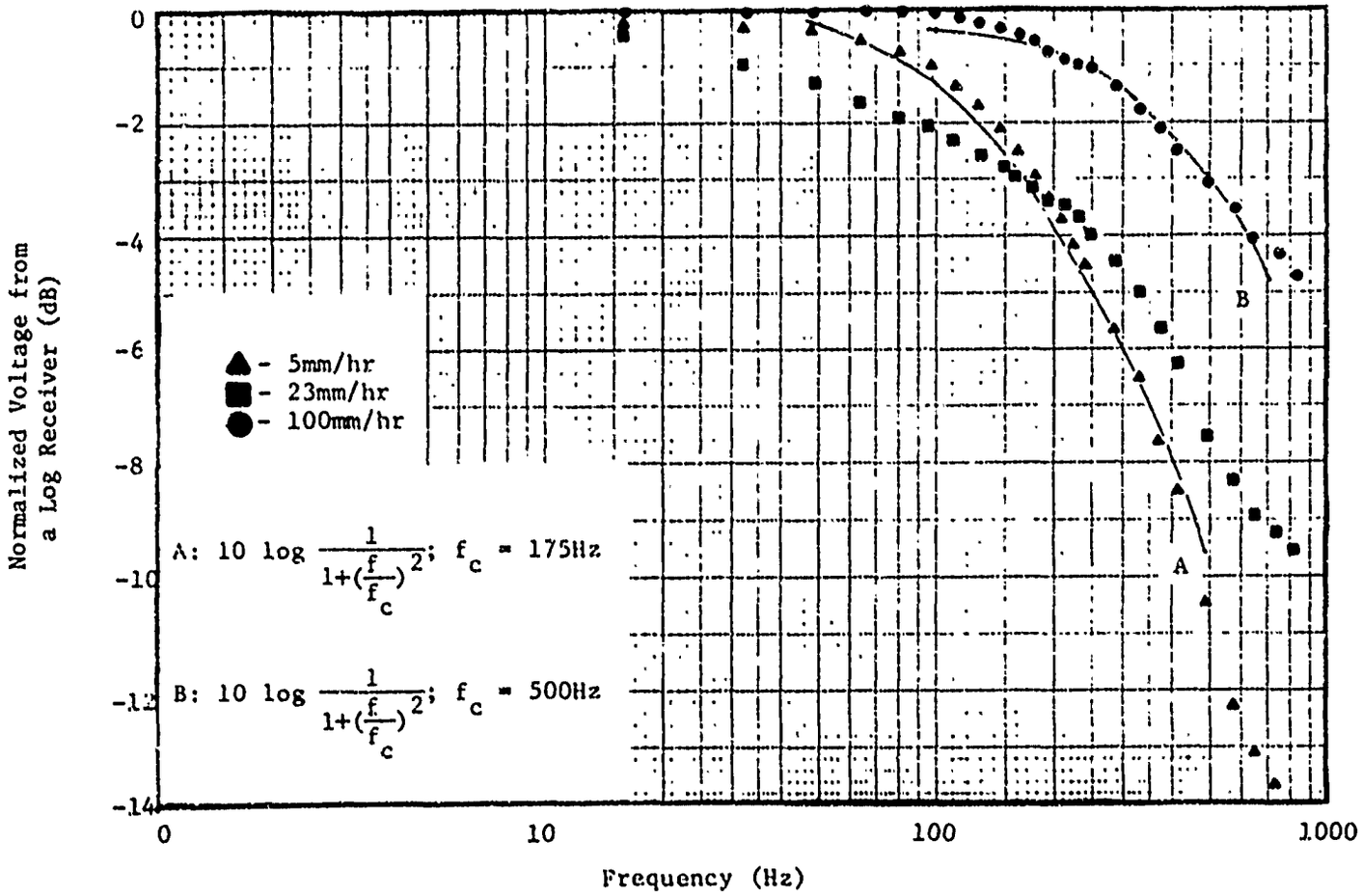

Figure 28. Normalized frequency spectrum of rain return at 70 GHz, VV polarization.

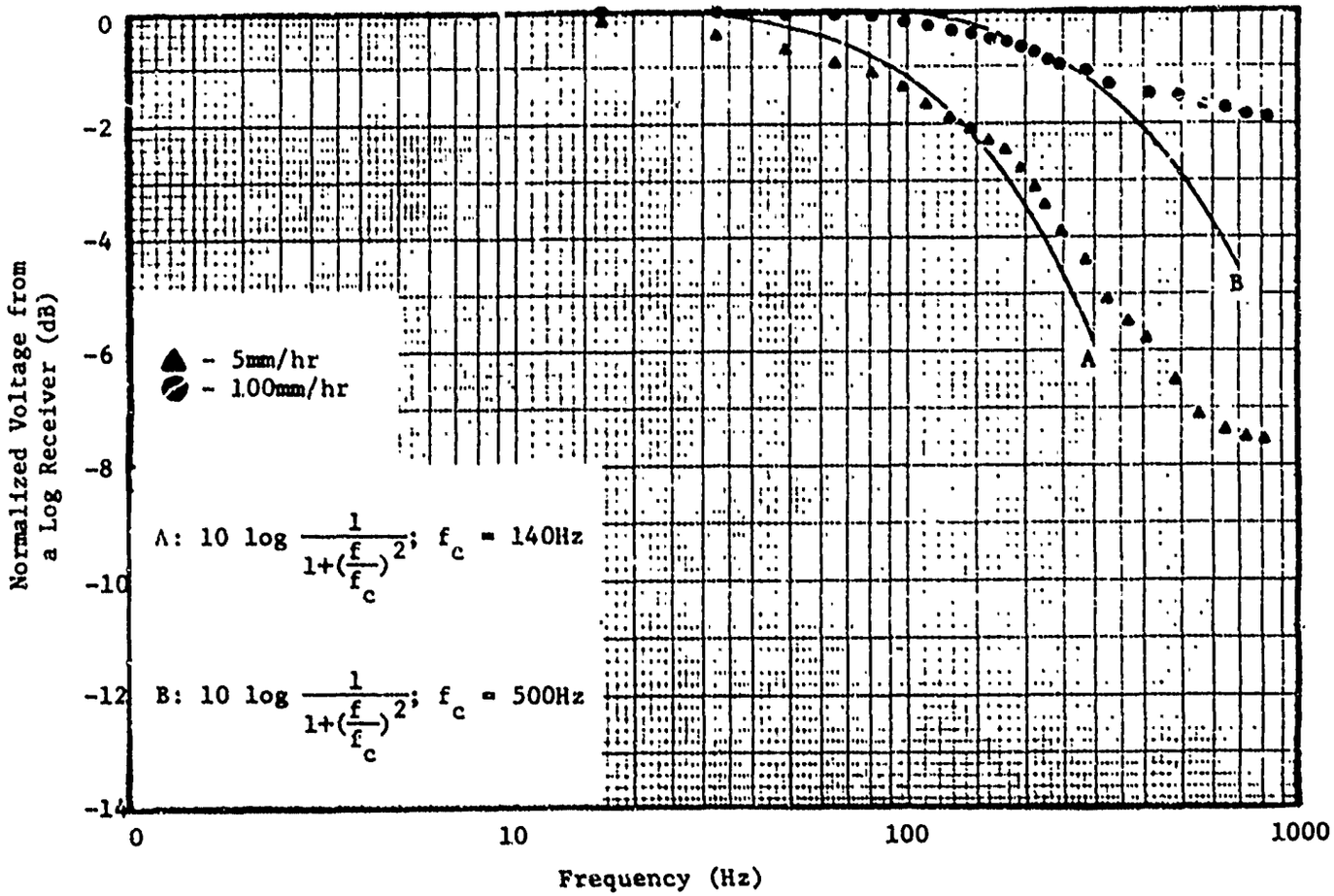

Figure 29. Normalized frequency spectrum of rain return at 95 GHz, VV polarization.

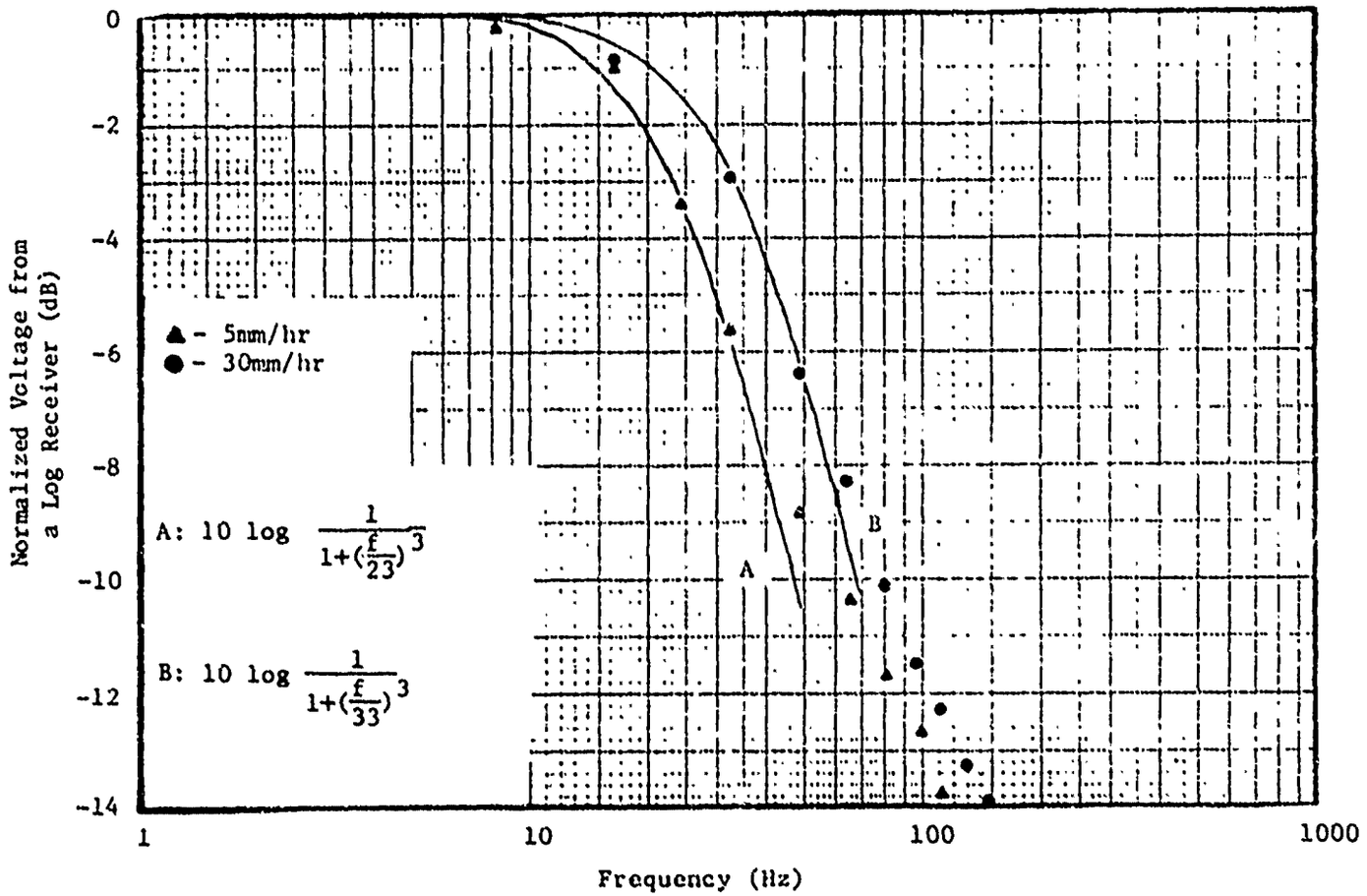

Figure 30. Normalized frequency spectrum of rain return at 9.375 GHz, RC polarization.

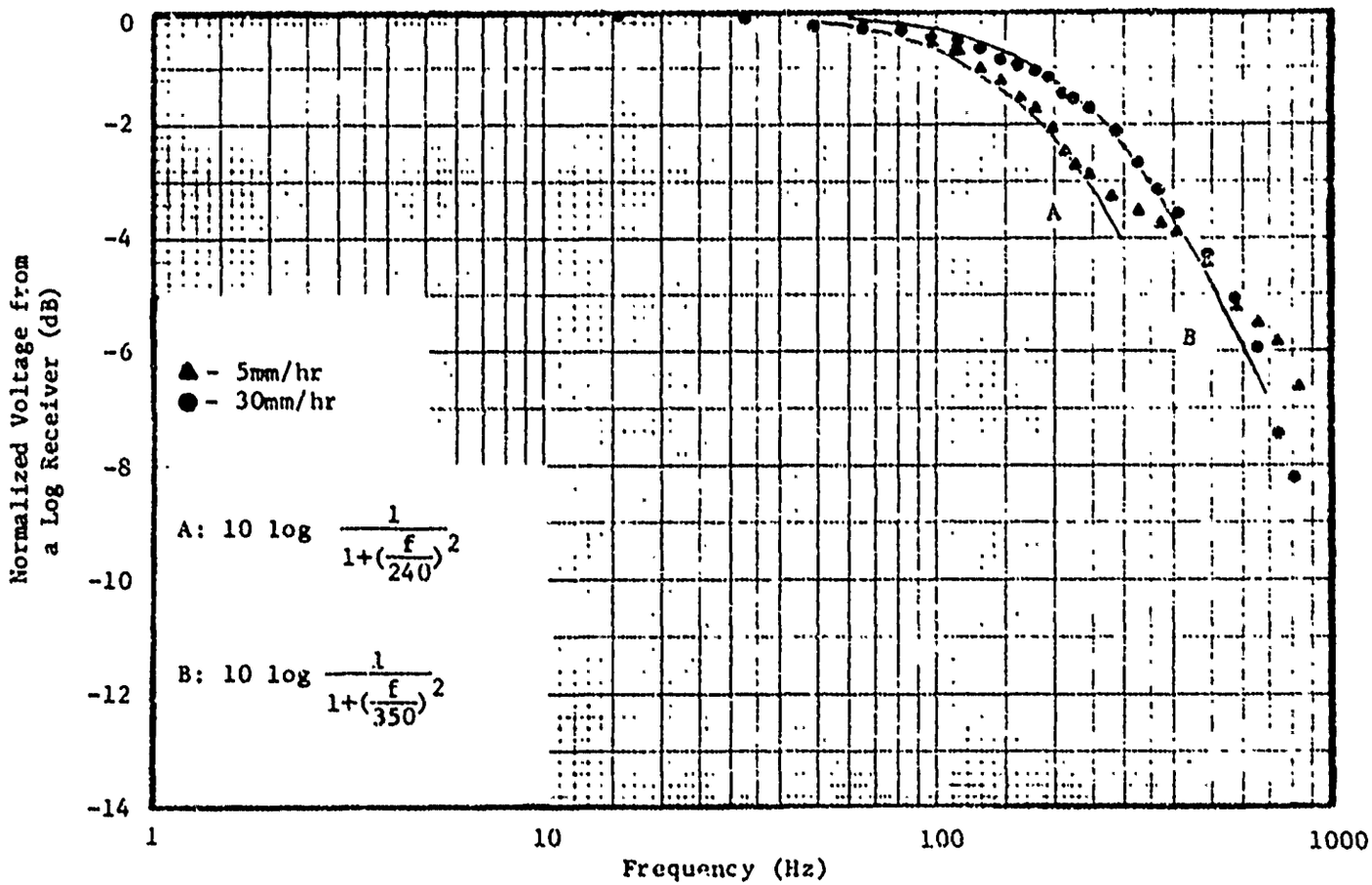

Figure 31. Normalized frequency spectrum of rain return at 95 GHz, RC polarization.

the assumption of a Gaussian shaped bandpass for rain clutter spectra for a radar system design could lead to serious errors in the calculated spectral bandwidth.

On a number of spectra, a second distribution appears removed from the low-frequency continous distribution. Application of the standard Doppler equation,

$$f = \frac{102 \times \text{velocity}}{\text{wavelength}}$$

reveals that the center frequency was produced by the movement of the total rain cell in a radial direction from the radars. For every case tested, the field logs indicate a wind speed and direction which would produce a Doppler frequency within 10% of that calculated. This accuracy was much higher than expected; however, it has been verified on enough occasions that one is led to believe that the data reduction process is accurate. (For an example of this type of spectrum, see Appendix b.)

6. Correlation Functions

Of concern to the designer of radars used in a space scanning mode, is the time required to obtain independent samples of radar returns. The auto-correlation function provides this basic information so that the radar backscatter data were processed to obtain the linear correlation functions. The results of this investigation are shown in Figure 32. Each point on this figure is the result of 8 data runs each lasting approximately 0.7 seconds. It is noticed that in general as the rain rate increases and/or the radar frequency is increased, the decorrelation time decreases. This is consistant with the observation that the power spectrum distribution becomes more noise like as the rain rate and/or the radar frequency is increased.

Values obtained from this investigation are consistant with those reported by Goldhirsh and Katz [13]. They reported that on the gross average one can expect decorrelation times as follows: S-band, 30 milliseconds; X-band 10 milliseconds; and K-band, 3 milliseconds. Examples of specific auto-correlation functions are shown in Figures 33 and 34.

Cross correlations functions were obtained between the signals from the four radar systems when operating at exactly the same time. Regardless of rain rate or transmitted polarization, the signals between the radars

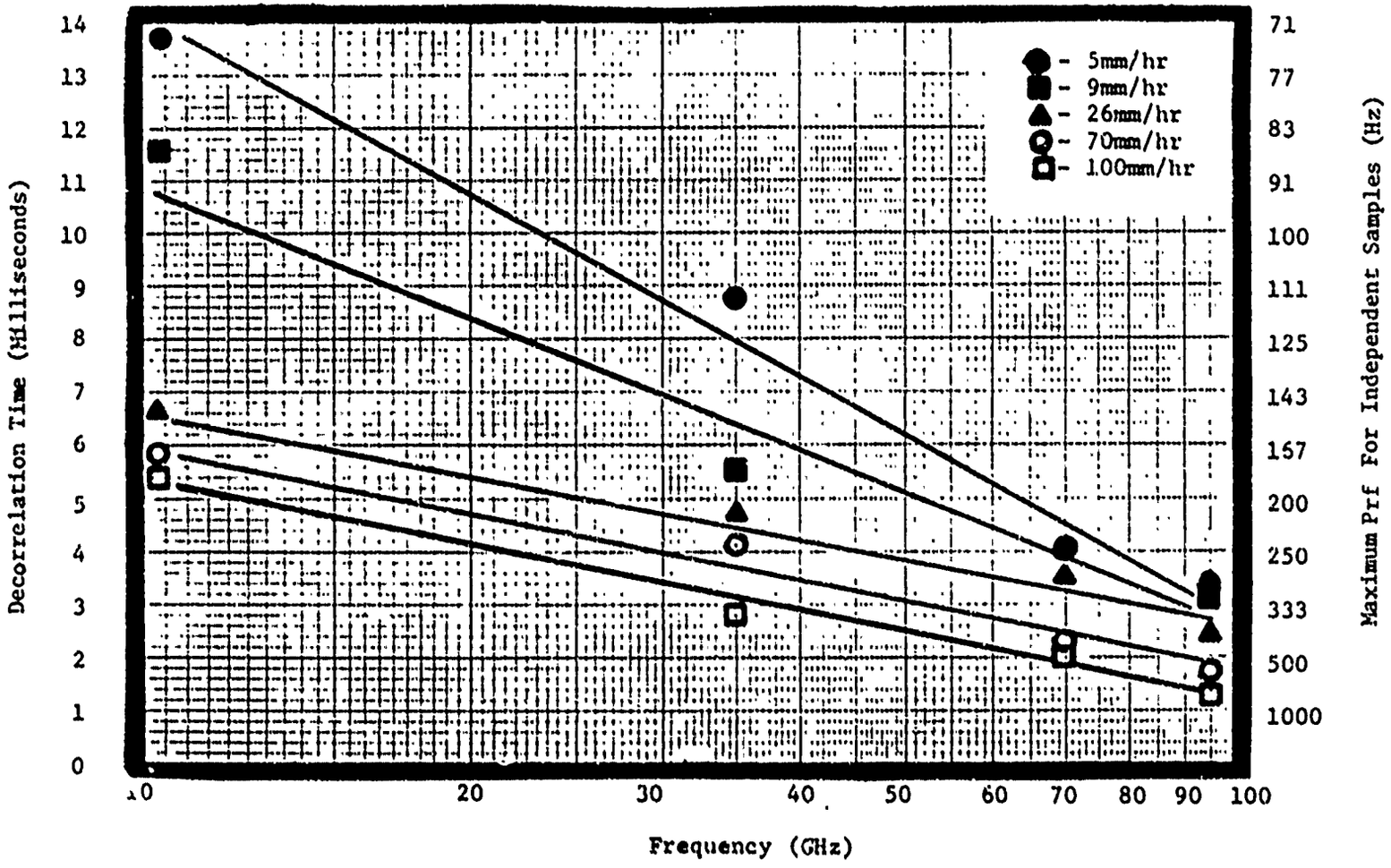

Figure 32. Decorrelation time versus rain rate and frequency for rain backscatter.

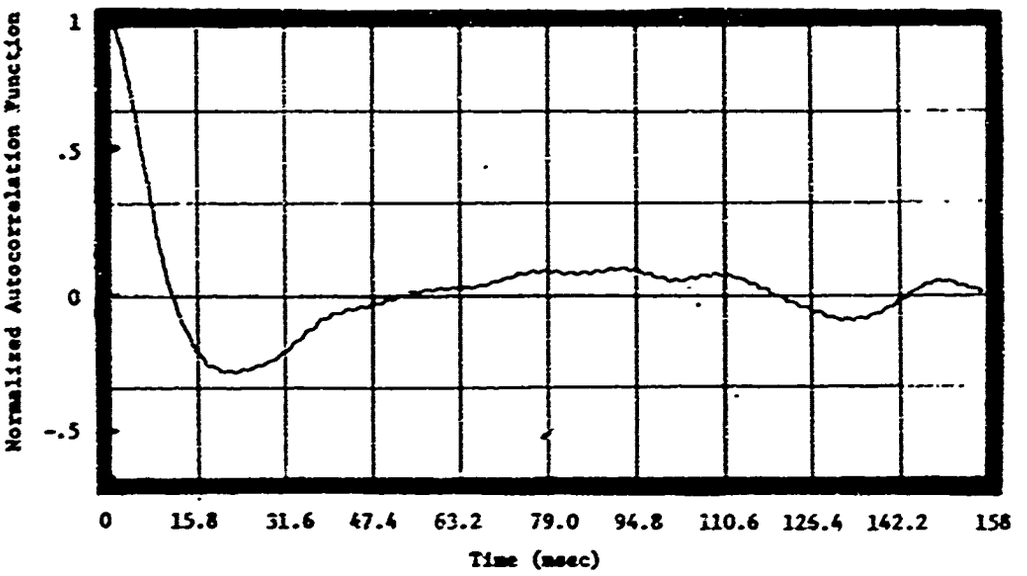

Figure 33. Normalized autocorrelation function for rain backscatter; 9.375 GHz frequency, 9 mm/hr rain rate, VV polarization.

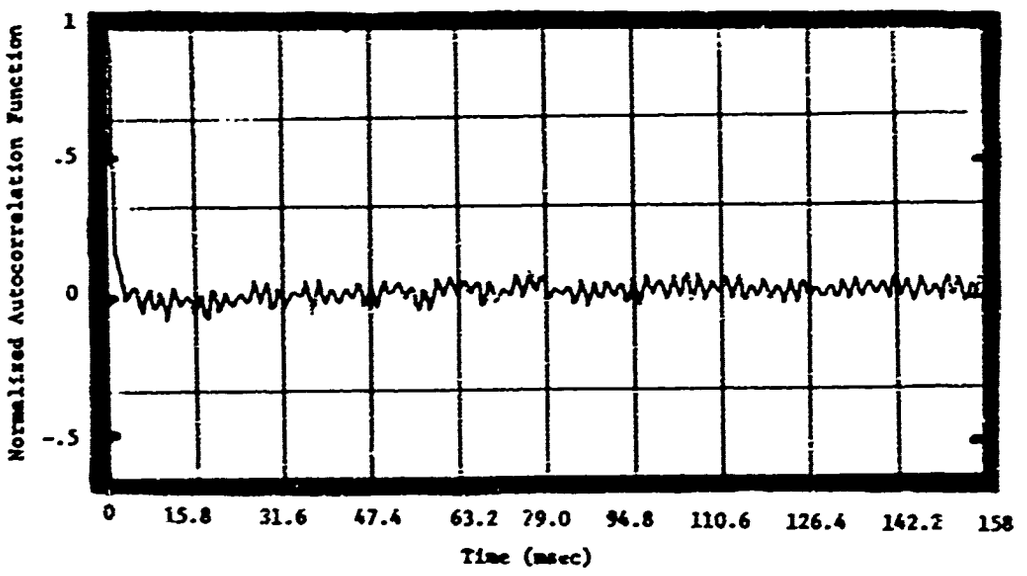

Figure 34. Normalized autocorrelation function for rain backscatter; 95 GHz frequency, 9 mm/hr rain rate, VV polarization.

were decorrelated at all times. Since the cross-correlation coefficients were always zero, no graphs are presented.

7. Drop-Size Distributions

The data from rain backscatter as a function of rain rate, as shown in Figures 12 and 13, were derived from rain tipping buckets. These devices are measurement units which average rain rate over a relatively long interval of time as compared to the observation period of a radar system. The buckets used during this experiment have a switch closure every .01 inch (0.254 mm) of water entering the bucket. Thus if the rain rate is 2.54 mm/hr, there will be 10 closures every hour, or one closure every 6 minutes while the radar data were evaluated for 30-second intervals. If good rain rate sampling were performed, then there should be two samples of the rain rate during the 30 second radar sample period. With the tipping buckets employed, this would require a minimum rain rate of 61 mm/hr. Obviously there is a conflict and the result is that a "gross-averaging" effect was involved whenever rain rate was related to any particular radar observation.

An example can be made by looking at Figure 35. There was a total lapsed time of 2 minutes, in which the radar returns were evaluated 4 times at 30-second intervals. The rain drop-size spectrometer data were also evaluated for four 30-second intervals, and the rain rates were calculated from the drop-size distributions. The tipping buckets indicated an average rain rate of 2.7 mm/hr, whereas the spectrometers show a dynamic change in rate varying from 4.5 mm/hr to 9.8 mm/hr, with an average of 7.25 mm/hr over this short 2-minute interval. The difference in average rain rate as determined by the tipping buckets compared to the spectrometers can be accounted for by the fact that the tipping bucket, at this rain rate, was averaging over 5 to 6 minute intervals. (This was the actual time between tips.)

In addition to rapidly changing rain rates, dynamic changes in drop-size distribution were also common. Since drop-size plays a major role in the magnitude of radar backscatter, this is a source of backscatter variance, as discussed earlier.

Due to a variety of equipment problems, not all radar data were recorded on magnetic tapes, and all that were recorded could not be analyzed. In addition, not all the rain spectrometers were functional

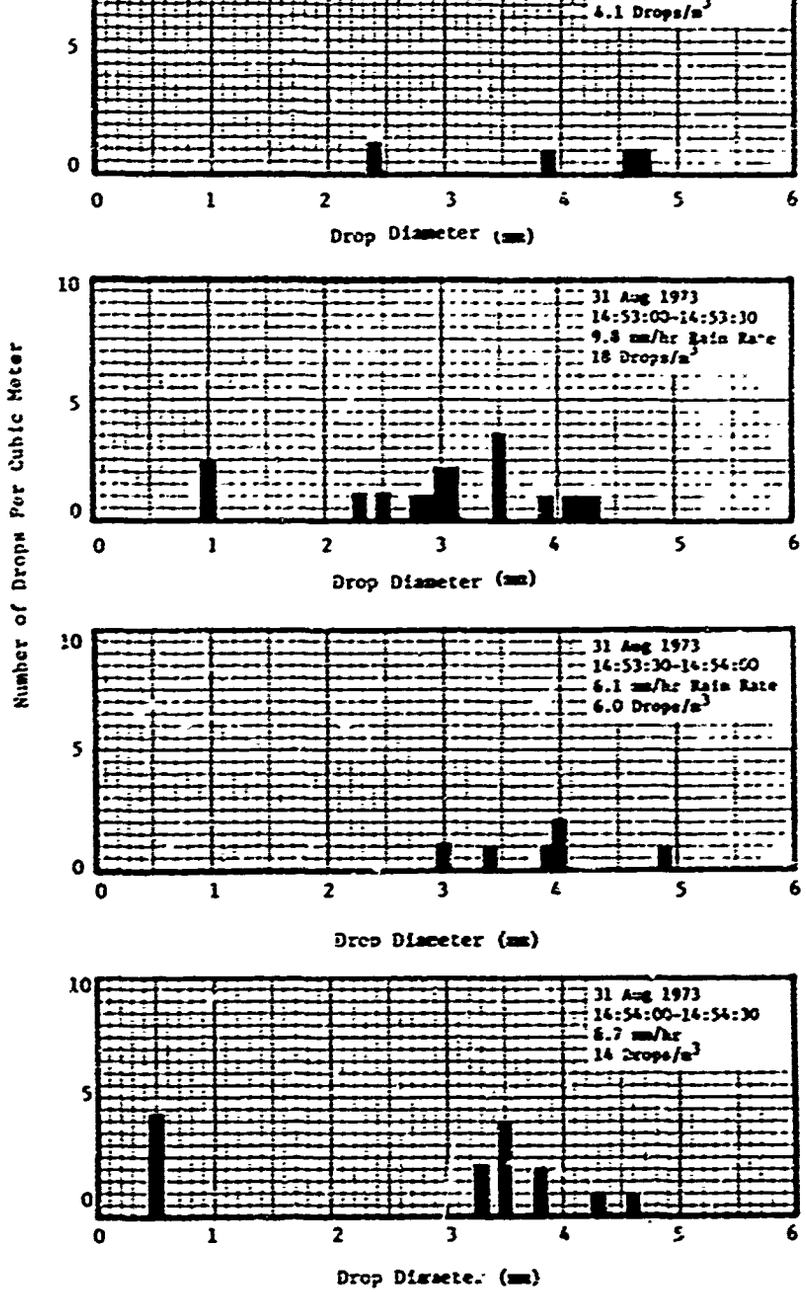

Figure 35. Rain drop-size distributions for four consecutive 30-second intervals with a light-to-moderate rain rate.

and spectrometer data are not available for all the periods corresponding to the collection of radar data. However, it was possible to obtain both radar data and rain spectrometer data at the same period for a limited amount of field recording time. Selected examples are presented to compare drop-size distributions and radar returns at three different rain-rates, namely 43-49 mm/hr, 8-10 mm/hr, and 2-5 mm/hr. At these rain rates, on different days, the radar returns differed by as much as 23 dB for the most extreme case.

First consider the heavy rain rate shown in Figure 36. For the rain distribution on 7 September, the radar returns at all frequencies were higher than those observed for the rain distribution obtained on 31 August. The amount of difference is a function of the radar frequency; the X-band returns in Figure 36-a are 100 times larger than in 36-b, but the 95-GHz returns are only two times larger.

Next consider the moderate rain rate case shown in Figure 37. The radar return on 30 August, (Figure 37-a), was always higher on the four radars than either that on 31 August, (Figures 37-b, 37-c) or that on 1 September (Figures 37-d). The greatest difference was between Figures 37-a and 37-d, with radar returns 200 times larger for Figure 37-a at X-band, and 30 times larger at 95 GHz. The uniform distribution of drops shown by Figure 37-c, even with a few large drops, did not produce the maximum radar return.

Drop-size distributions for selected low rain rates are shown in Figure 38. The largest radar returns occurred under drop size distributions shown in Figures 38-a and 38-b as compared to Figures 38-c and 38-d. The difference was about a factor of 10 at all frequencies.

From all the drop-size distributions considered, the maximum radar returns occured when there was a predominance of drops having diameters in the range of 2.5 to 3.5 mm. The same rain rate consisting of a few larger drops or many smaller drops apparently do not give as strong a radar return. It was also noted that the influence of drop-size distribution on return strength is greatest at X-band and decreases as frequency is increased. For the drop sizes measured during this experiment, all drops are Rayleigh scatterers at X-band, the largest drop being approximately $\lambda/5$. However at 95 GHz, the 3.2-mm diameter drop is equal to one wavelength, and resonance effects can be expected to occur.

(a)

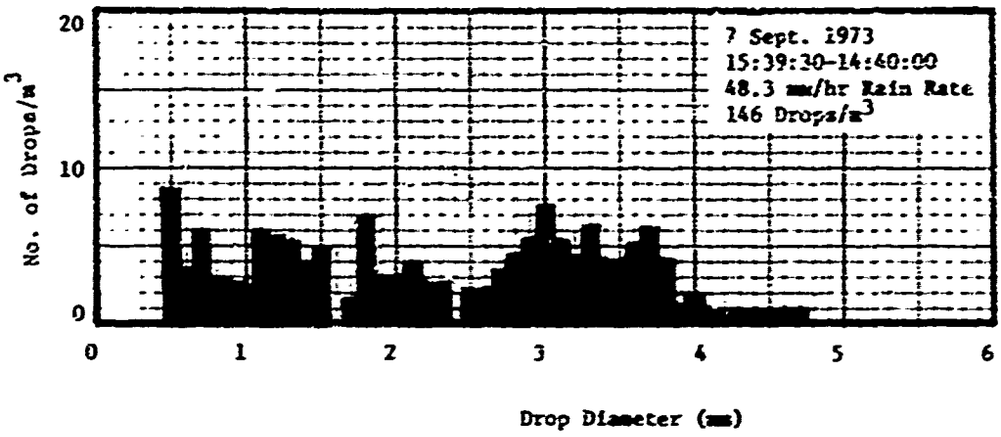

(b)

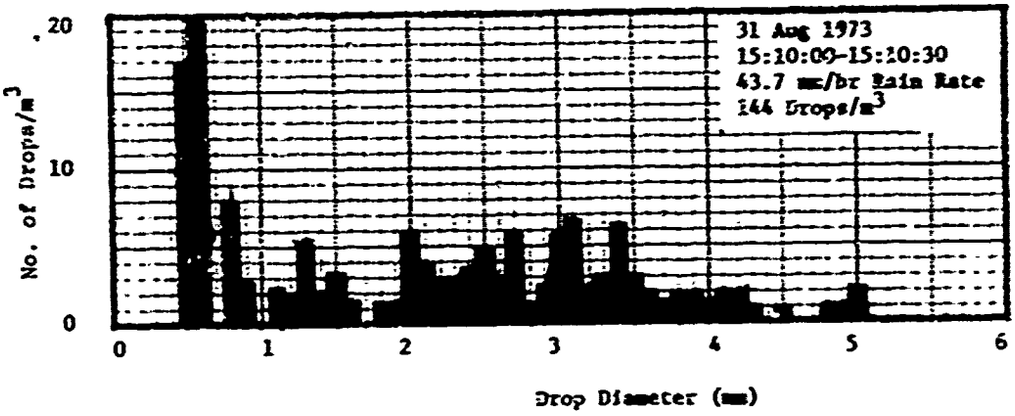

Figure 36. Two rain drop-size distributions which resulted in different radar backscatter characteristics for a heavy rain rate.

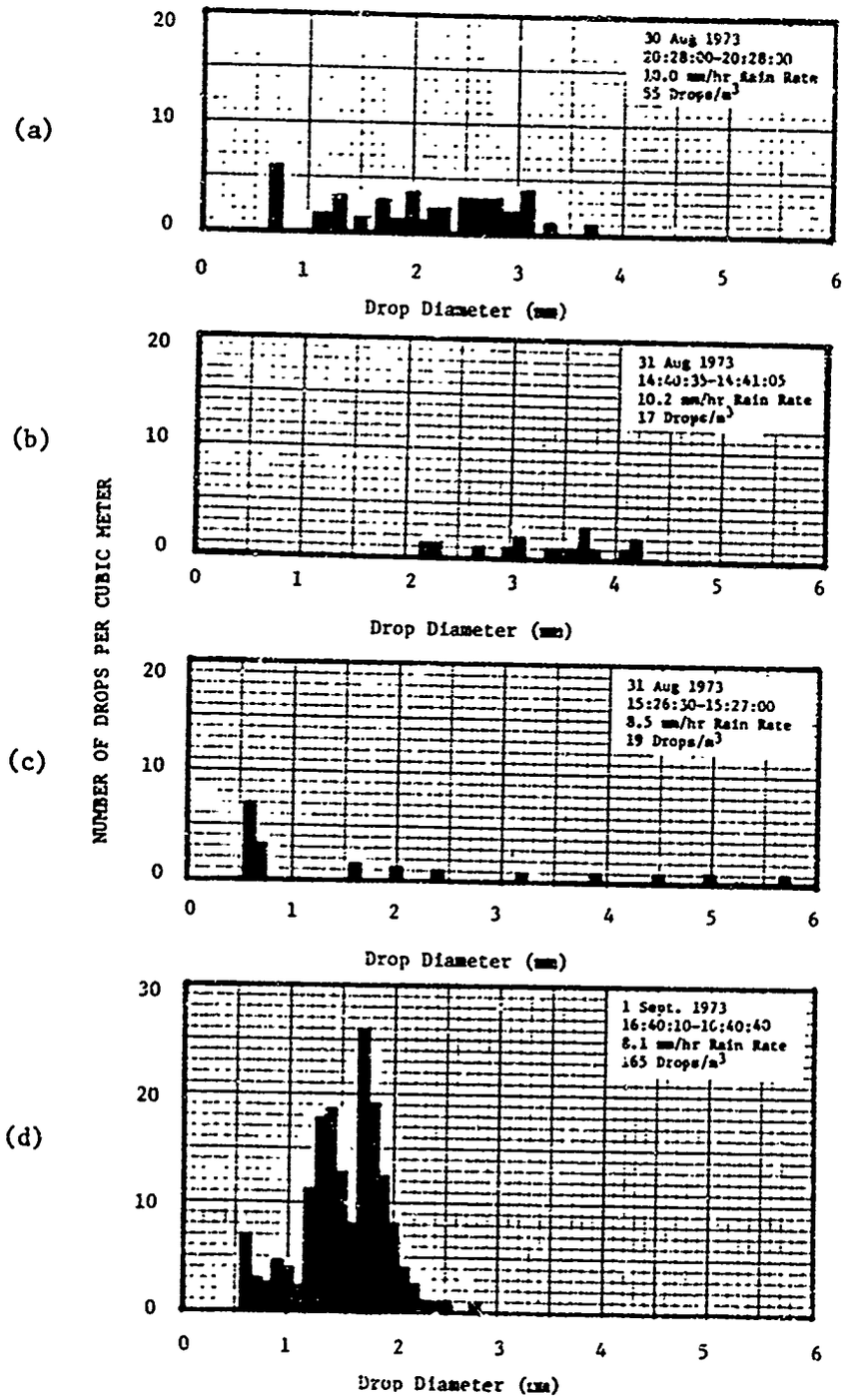

Figure 37. Four rain drop-size distributions which resulted in different radar backscatter characteristics for a moderate rain rate.

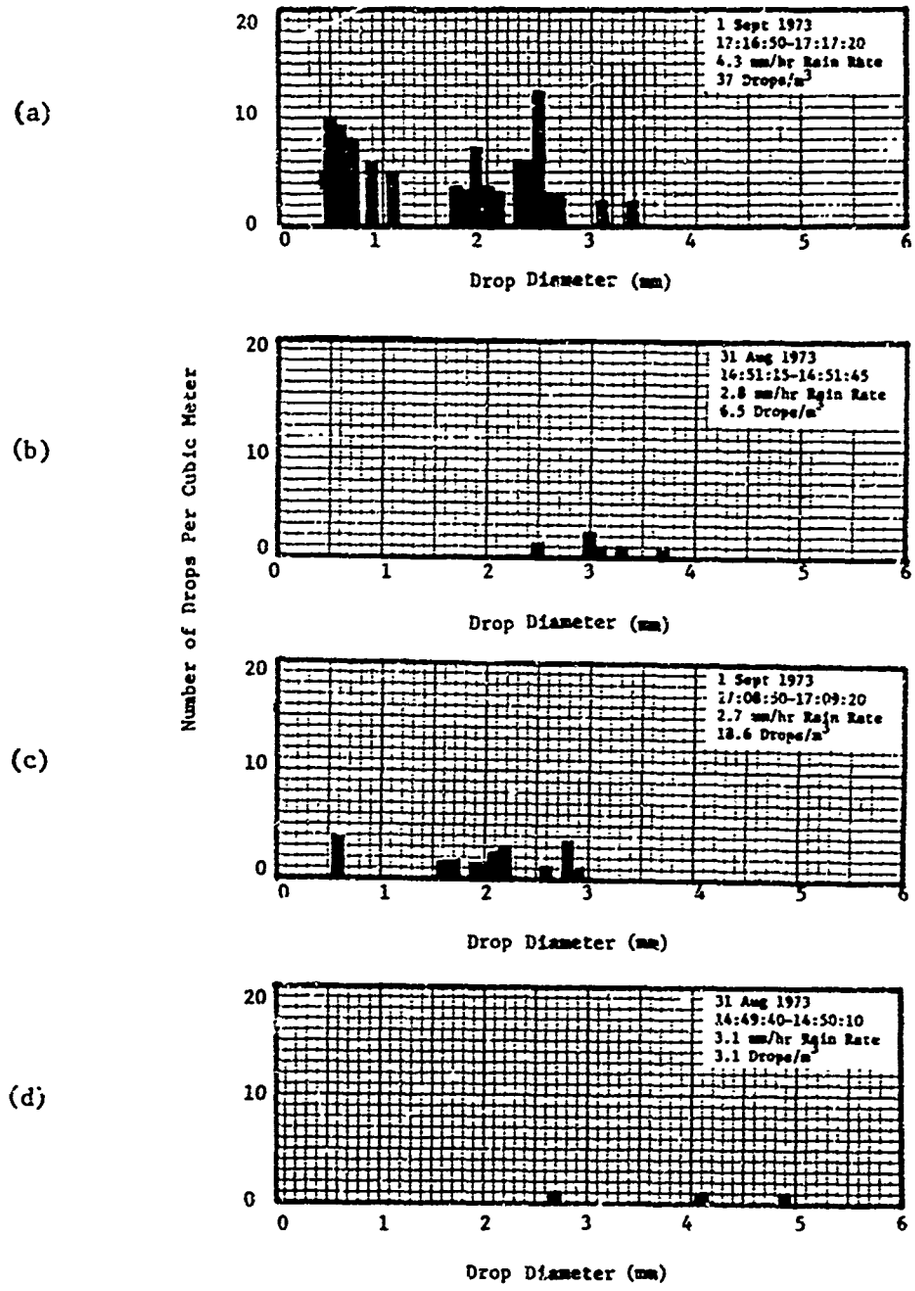

Figure 38. Four rain drop-size distributions which resulted in different radar backscatter characteristics for a light rain rate.

It has been observed that at low rain rates, the tipping buckets employed did not respond fast enough to present a real time measure of the rain rate. This affects not only the value of backscatter but also the path attenuation. Thus it is not unexpected that a wide spread in data points resulted at any given rain rate.

III. CONCLUSIONS AND RECOMMENDATIONS

This report summarizes results of a thorough analysis of data obtained during a series of measurements of radar backscatter from rain at frequencies of 9.375, 35, 70, and 95 GHz. The geometry of the experiment and the equipment used were chosen with the intent to provide data that would be useful to an equipment designer in specifying an optimum operating frequency for a given mission. It is believed that this goal has been achieved; however, a number of experimental difficulties were encountered which complicated the analysis, and which suggest that for future experiments in this area special care should be given to the choice and use of supporting instrumentation. A particularly important requirement exists for more extensive use of meterological instrumentation which is reliable and which can be readily calibrated. Not only is extensive rain rate and drop-size distribution measuring equipment required, but also other classes of instrumentation for measuring such parameters as wind speed, wind direction, and air temperature.

The emphasis of the measurements and subsequent analysis was directed toward investigating the amplitude and noncoherent frequency characteristics of the radar return. Limited checks of the attenuation characteristics of the path were attempted; however, since the measurements were not specifically designed to allow accurate determination of loss, only general agreement with published data was obtained. Because of limitations of the loss calculations based on the data reported here, detailed data from the literature have been used to determine the approprate attenuation values as described below. It is recommended that future experiments of this type be designed to address the question of path loss directly as one of the main objectives.

Rain rates occuring during the test program varied fro less than 1 mm/hr to more than 90 mm/hr. The average backscatter for linear polarization was observed to increase linearly (on a log-log plot), with increasing rain rate at all four frequencies. When circular polarization was used, the returns were consistently 10 to 15 dB less than when using linear polarization. The values obtained at X-band and K_a-band are accurately represented by theoretical calculations using Rayleigh scattering and drop-size distributions according to Laws and Parsons [14].

Preceding page blank

The backscatter values obtained at 70 and 95 GHz have a smaller slope than at 9.375 and 35 GHz. This is generally typical of the change expected when scattering is predominately in the Mie region. Since Mie scattering is extremely sensitive to the exact nature of the drop-size distribution, a number of actual distributions were checked and found to confirm both the general change in slope observed and the significant scatter of the average cross-section observed between runs. One anomaly noted here was that the backscatter at 95 GHz on the average was less than that at 70 GHz. It is suggested that this may result from a reasonance between drop-size and radar wavelength, thereby supporting the concept of enhanced forward scattering at these wavelengths. This hypothesis could not be checked here as the experiment did not provide the appropriate comparison data.

The rain storms observed during these measurements varied strongly in spatial and temporal nature, but were generally of relatively short duration. These characteristics were major contributors to the extreme variability of the drop-size distributions observed and thus, consequently, the variability of the backscatter. It is believed that the extreme variability of the storms observed made them represent essentially a "worse case" condition both from an experimental point of view and a radar systems design viewpoint.

Amplitude distributions of the backscatter were observed to be approximately log-normal at all frequencies and for rain rates between 2 and 60 mm/hr. For rain rates less than 1 mm/hr and greater than 60 mm/hr, the amplitude distributions were not consistently log-normal but were generally skewed. This may have been caused by having a low signal-to-noise ration, or, at the higher return levels, by system saturation; however, it is also possible that the skewness is a real phenomenon due to the observed behavior of the drop-size distributions at the extremes. In addition, the amplitude variance of the returns appeared to be independent, on the average, of rain rate, and to generally decrease with increasing frequency. The variance was generally less for circular polarization than for the linear polarization.

The noncoherent frequency spectral width was observed to increase with rain rate at each test frequency, and also to increase with frequency at a given rain rate. The spectrum amplitude was also observed to decrease with increasing frequency, approaching noiselike characteristics at 95 GHz.

The roll-off rate at the high-frequency end of the spectrum was observed to be much slower than Gaussian, being best described as quadratic in nature. The spectra at X-band were generally well described by a cubic function. No significant correlation (as obtained from the cross-correlation function) was discernible between the returns from the four radars when observed at the same time. The decorrelation time (as obtained from the auto-correlation function) became less with increasing rain rate and with increasing radar frequency. Values of the decorrelation time ranged from 14 milliseconds at 5 mm/hr rain at X-band to 1.4 milliseconds at 100 mm/hr rain at 95 GHz.

It is concluded that, while much new data are available to the designer as a result of this work, a number of important questions remain unanswered as to the impact of rain on system performance. Perhaps the hardest question to settle satisfactorily is still that of the comparative merits of a millimeter radar with other approaches (i.e. microwave or laser radar) in moderate rain and/or fog, for precision, short-range applications in situations where space or geometry limit the size of antenna. Examples of such situations include helicopter systems and most point-defense applications. Data reported here suggest that 95 GHz is very competitive in such applications. Experiments should be conducted which make the necessary comparisons between the competing approaches in rain, while giving adequate attention to the required meteorological conditions to resolve this question.

IV. REFERENCES

1. R. D. Hayes and F. B. Dyer, "Land Clutter Characteristics for Computer Modeling of Fire Control Radar Systems," Technical Report 1. on Contract DAAA 25-73-C-0256, Engineering Experiment Station, Georgia Institute of Technology, 15 May 1973.

2. F. B. Dyer, "Engineering Services in Support of Millimeter Rain Clutter Experiment," Final Letter Report on Contract DAAA 25-73-C-0256, Mod. P00002, Engineering Experiment Station, Georgia Institute of Technology, 25 October 1973.

3. V. W. Richards and J. E. Kammerer, "Millimeter Wave Rain Backscatter Measurements," 1973 Millimeter Waves Techniques Conference, Naval Electronics Laboratory Center, San Diego, California, 26 March 1973.

4. D. E. Wrege and D. S. Harmer, "FOCAL/F An Extended Version of 8-K FOCAL 69TM," School of Nuclear Engineering, Georgia Institute of Technology, 1 June 1972.

5. W. Rivers, "Low-Angle Radar Sea Return at 3-mm Wavelength," Final Technical Report on Contract N62269-70-C-0489, Engineering Experiment Station, Georgia Institute of Technology, 15 November 1970.

6. R. Gunn and G. D. Kinzer, "The Terminal Velocity of Fall For Water Droplets in Stagnant Air," Journal of Meteorology, August 1949, pp. 243-248.

7. M. I. Skolnik, Introduction to Radar Systems, McGraw-Hill Book Company, New York, 1962 p. 41.

8. G. D. Luke, "Penetrability of Haze, Fog, Clouds and Precipitation by Radiant Energy," The Center for Naval Analysis, Study No. 61, May 1968.

9. J. de Bettencourt, Raytheon, Private Communications with V. Richard, BRL, June 1972.

10. E. A. Mueller and A. L. Sims, "Relationships Between Reflectivity, Attenuation, and Rainfall Rate Derived from Drop Size Spectra," Illinois State Water Survey for ECOM Contract DA-28-043 AMC-02071(F), May 1969.

11. J. C. Lin and A. Ishimaru, "Propagation of Millimeter Waves in Rain," University of Washington, for AFCRL, COntract F19(628)-69-C-0123, May 1971.

12. L. D. Strom, "Applications for Millimeter Radar," Appendix C, Systems Planning Corp., for ARPA, Contract DNA001-73-C-0098, November 1973.

13. J. Goldhirsh and I. Katz, Private Communication, URSI Meeting 1974.

Preceding page blank

14. J. O. Laws and D. A. Parsons, "The Relationship of Rain Drop-size to Intensity," Transactions of the American Geophysics Union, 24th Annual Meeting, April 1943.

V. APPENDICES

APPENDIX A

Plotted Average Backscatter Data

This appendix contains the plotted values of average radar backscatter data versus rain rate which were used to calculate the least-squares functions presented in Figures 12 and 13. Each point represents approximately 30 seconds of data which were measured at one of four different ranges. The values have been normalized to remove dependence on range and system parameters, and thus have units of radar cross-section per unit volume (m^2/m^3). As has been previously noted, the data indicate that variations of greater than 10 dB in the magnitude of the backscatter can occur for a constant rain rate. As discussed in Section III-B-7, changes in the drop-size distribution constitute one important cause for such large variations in backscatter.

Preceding page blank

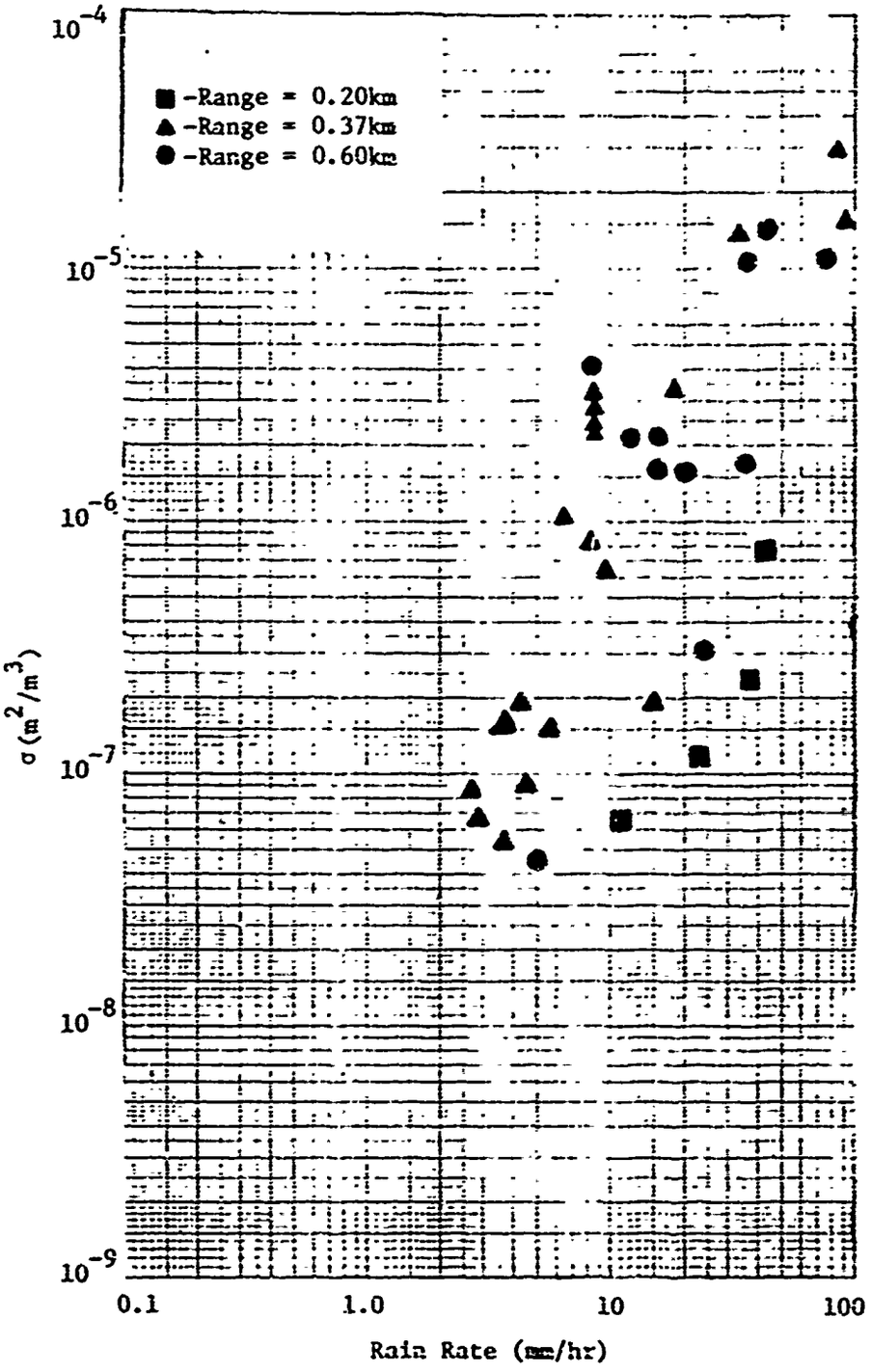

Figure A1. Average radar backscatter cross-section per unit volume versus rain rate; 9.375 GHz, VV polarization.

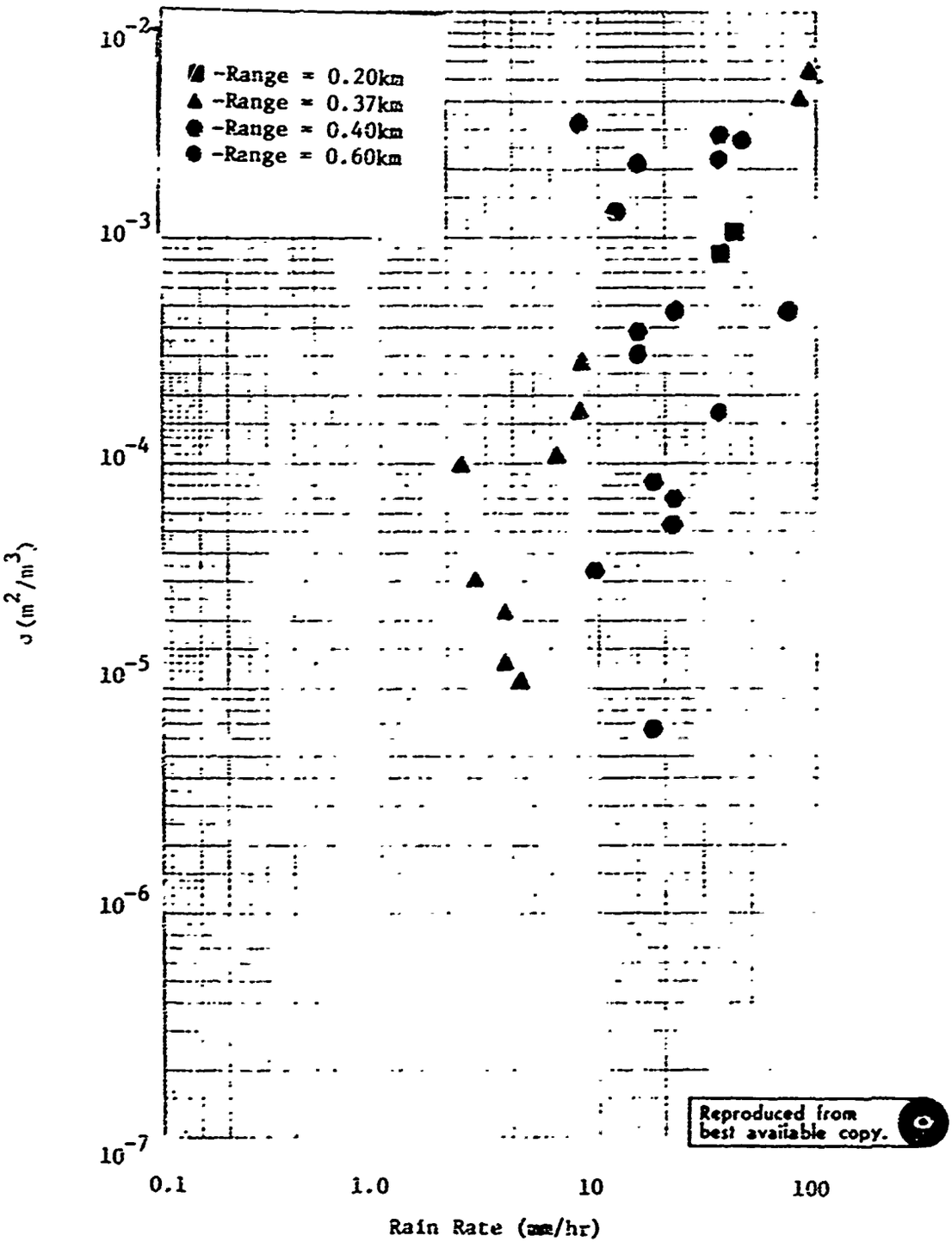

Figure A2. Average radar backscatter cross-section per unit volume versus rain rate; 35 GHz, VV polarization.

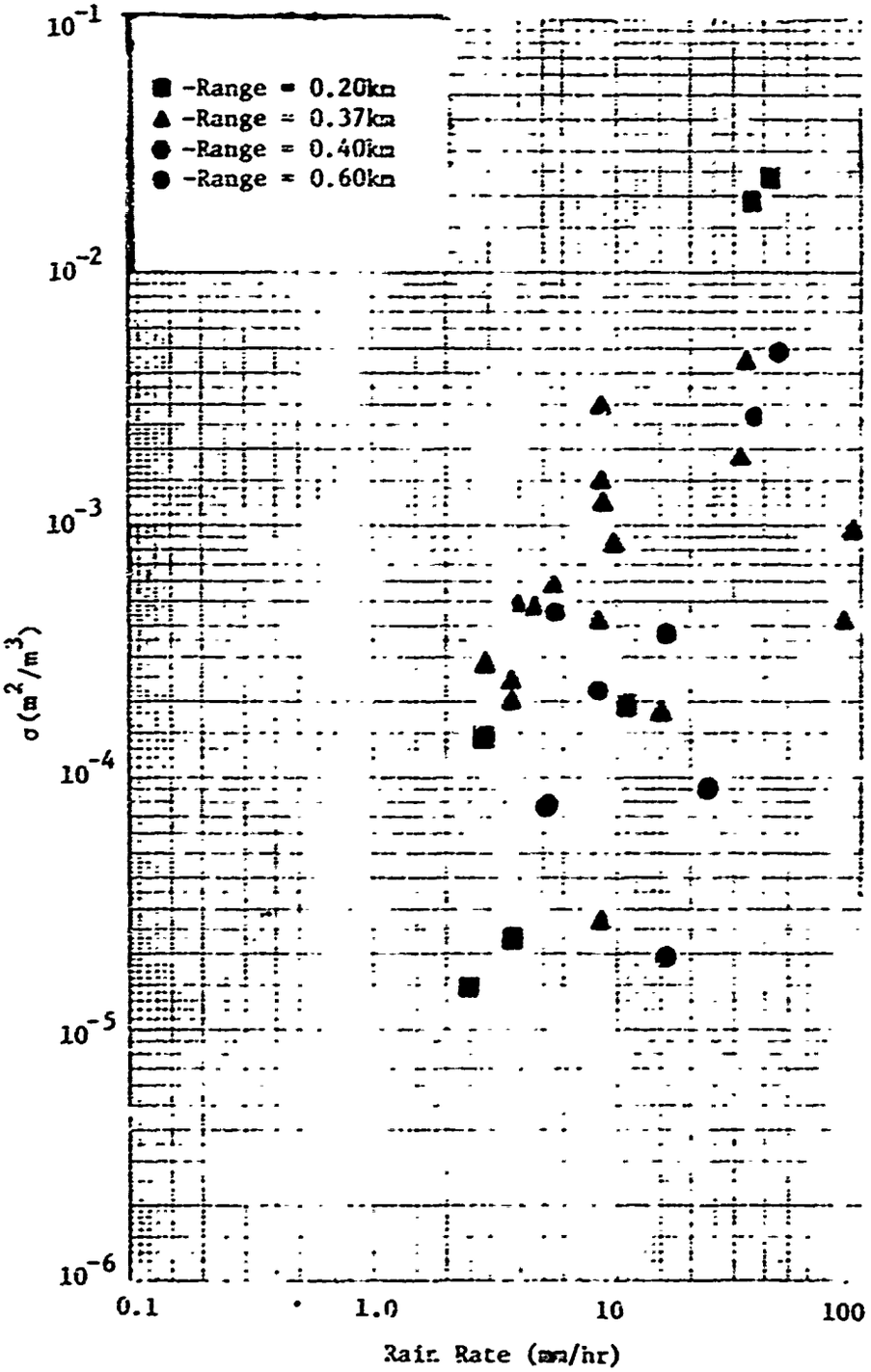

Figure A3. Average radar backscatter cross-section per unit volume versus rain rate; 70 GHz, VV polarization.

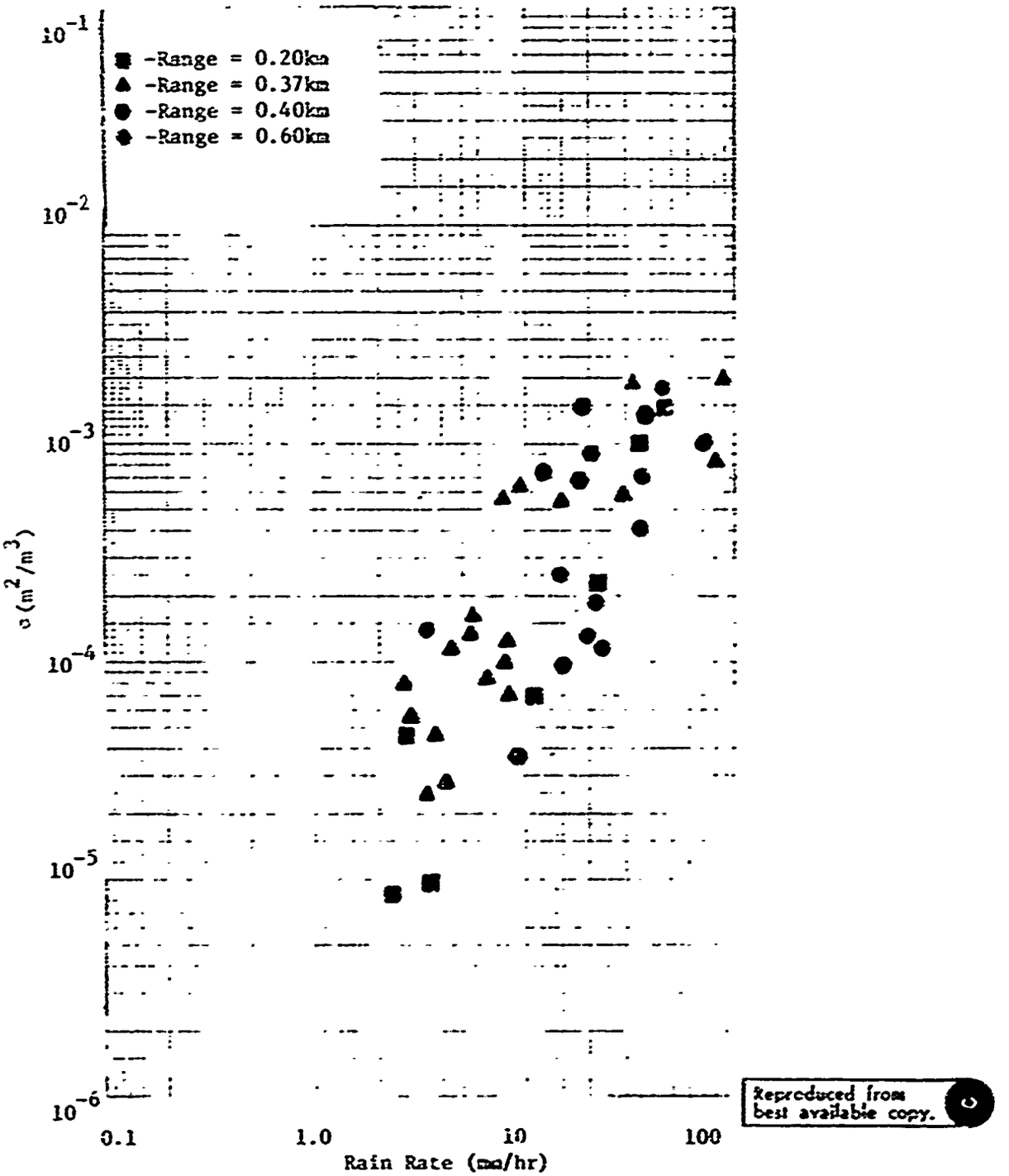

Figure A4. Average radar backscatter cross-section per unit volume versus rain rate; 95 GHz, VV polarization.

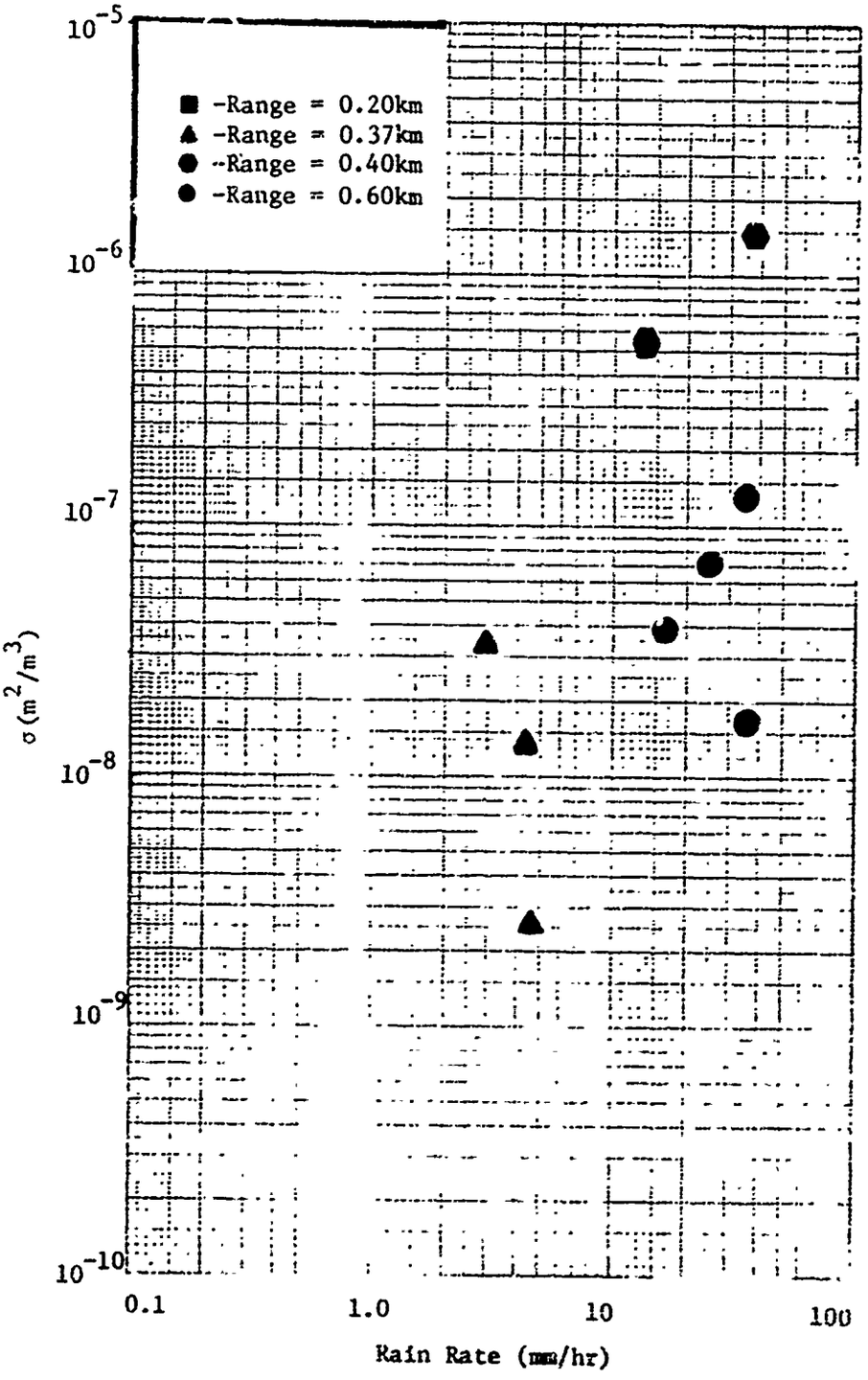

Figure A5. Average radar backscatter cross-section per unit volume versus rain rate; 9.375 GHz, RC polarization.

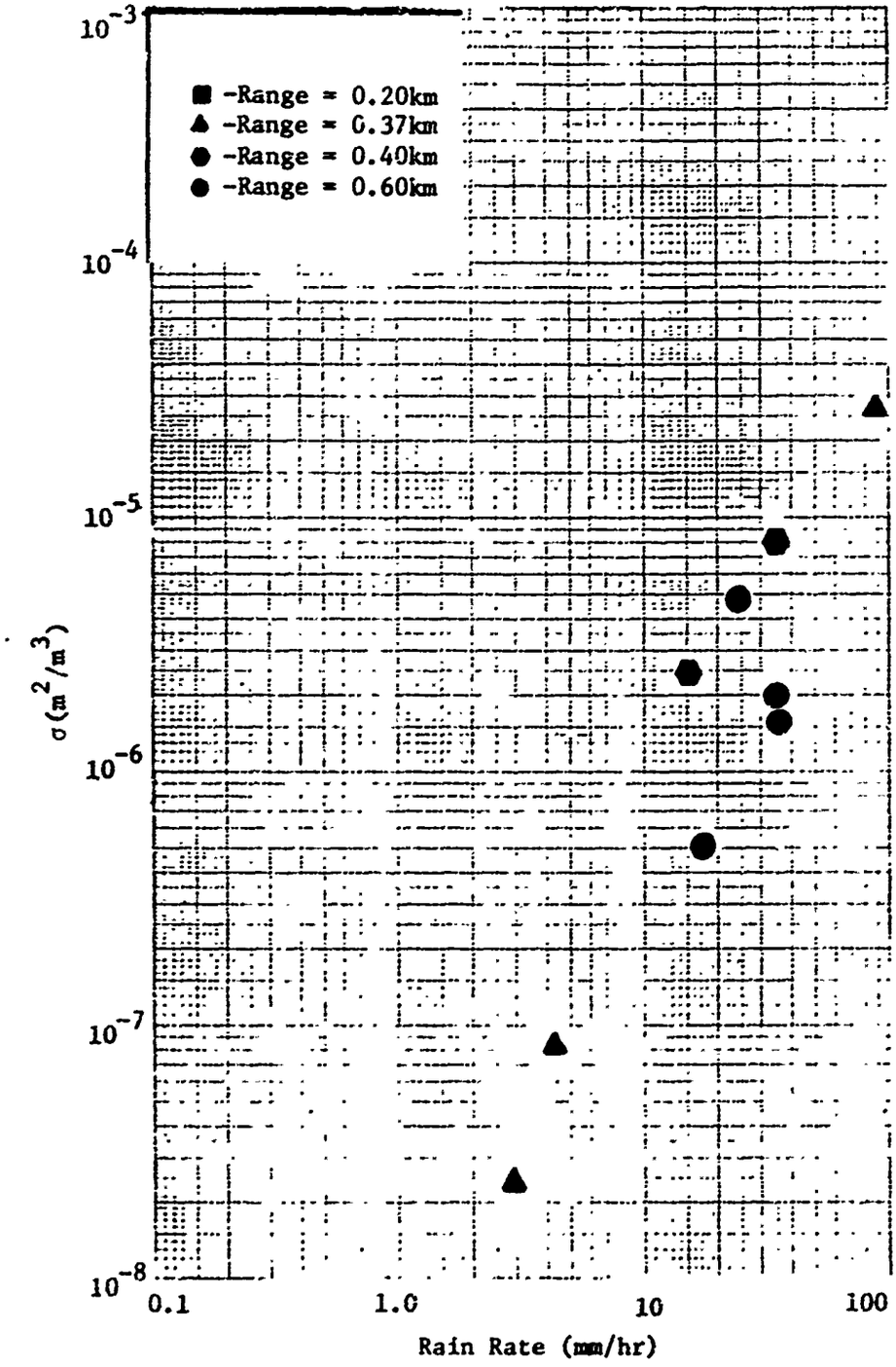

Figure A6. Average radar backscatter cross-section per unit volume versus rain rate; 35 GHz, RC polarization.

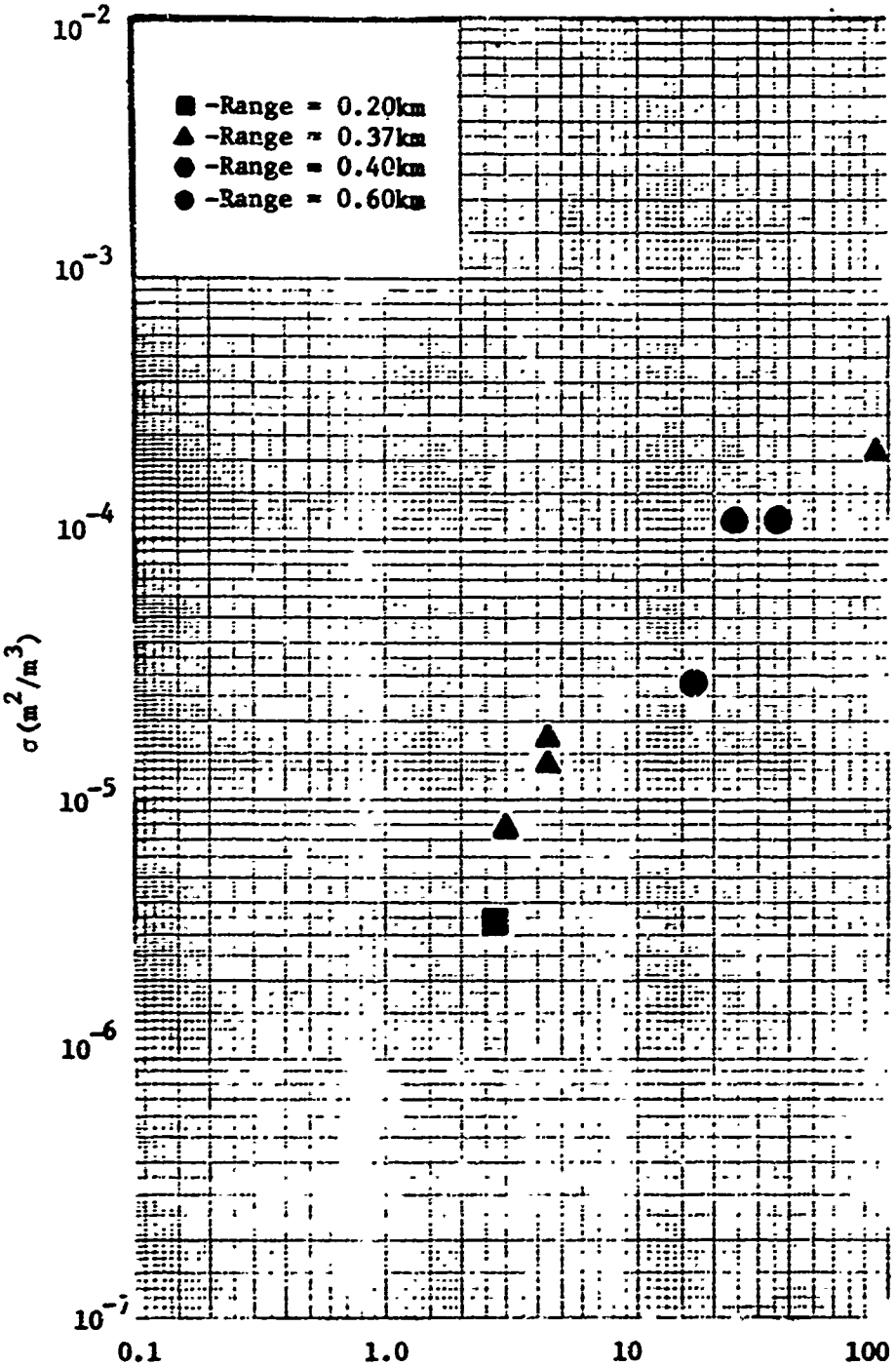

Figure A7. Average radar backscatter cross-section per unit volume versus rain rate; 70 GHz, RC polarization.

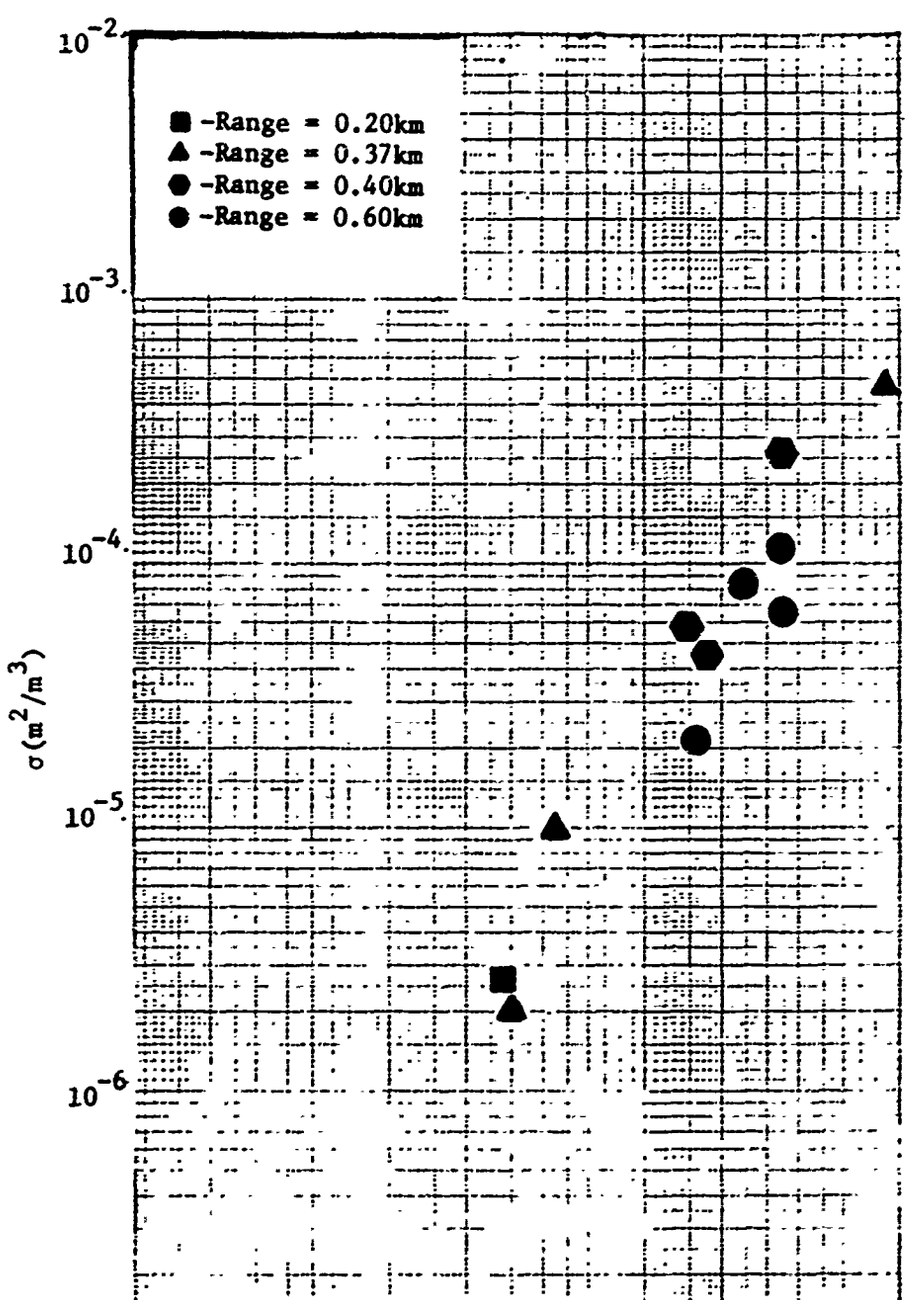

Figure A8. Average radar backscatter cross-section per unit volume versus rain rate; 95 GHz, RC polarization.

APPENDIX B

Spectral Distributions for Selected Data Runs

This appendix contains selected examples of spectral plots of the fluctuations of received backscatter from rain for frequencies of 9.375, 35, 70, and 95 GHz, rain rates of 5 to 100 mm/hr, and vertical and circular polarizations. Since all the radars utilized logarithmic receivers, the frequency spectra of their output voltages represent fluctuations about the mean values and thus have amplitudes calibrated in dB.

These examples illustrate the general trends observed for all the data, that is for increasing frequency and rain-rate, the peak spectral amplitude of the fluctuations decreases and the spectral width increases. In the limit, for 95 GHz frequency and 100 mm/hr rain-rate, the spectrum appears very noise-like with less than 1 dB of fluctuation and a very wide spectral width. The spectra also appear polarization-dependent in that, for circular polarization, in general the peak spectral amplitudes are lower and the spectral widths are greater than for vertical polarization.

Some of the data runs exhibit a second spectrum superimposed on the initial monotonic continuous spectrum of the rain. As discussed in the text (Section III-B-5) this phenomenon is caused by movement of the storm radially with respect to the radars. The center frequencies of the superimposed spectra can be related by the Doppler equation to the wind speed recorded in the field logs to within 10%, a close relationship. Figures B-5 and B-29 are examples of this type of spectral response.

Preceding page blank

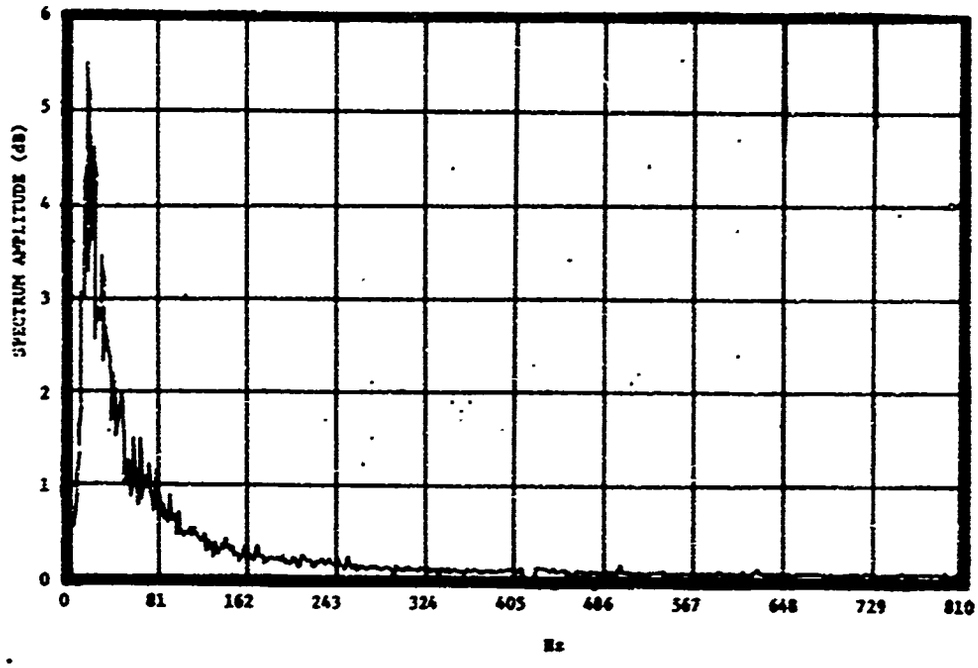

Figure B1. Amplitude of the frequency spectrum of a logarithmic receiver for rain backscatter; 5 mm/hr rain rate, 9.375 GHz frequency, and VV polarization.

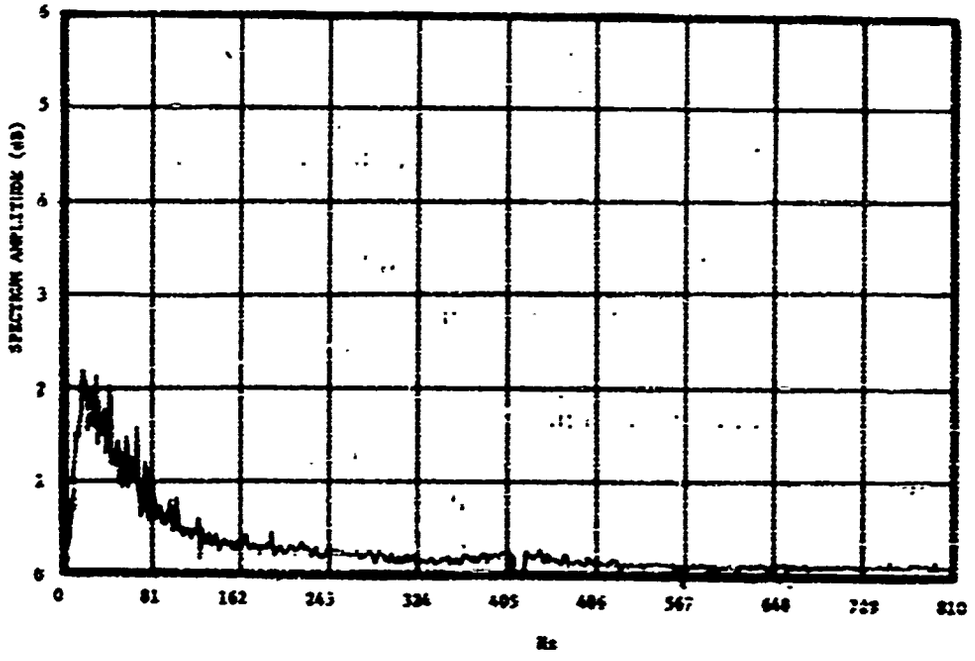

Figure B2. Amplitude of the frequency spectrum of a logarithmic receiver for rain backscatter; 5 mm/hr rain rate, 35 GHz frequency, and VV polarization.

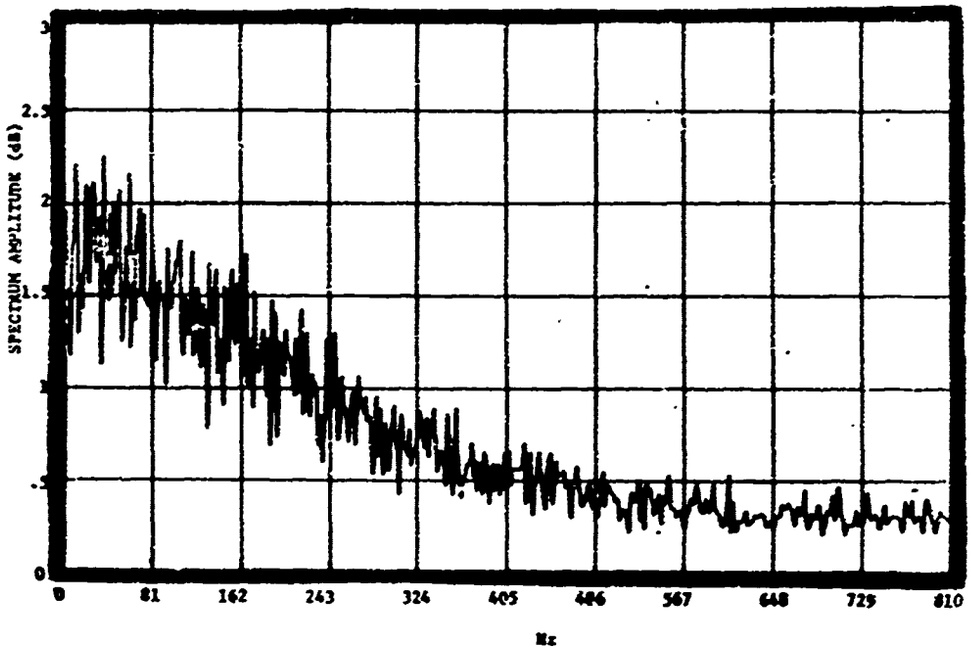

Figure B3. Amplitude of the frequency spectrum of a logarithmic receiver for rain backscatter; 5 mm/hr rain rate, 70 GHz frequency, and VV polarization.

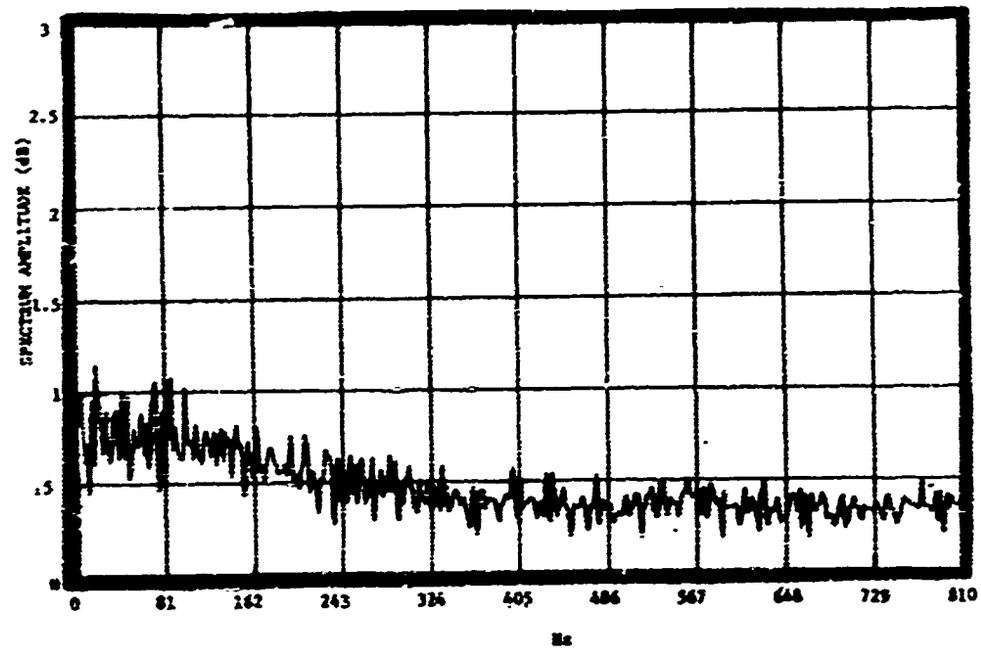

Figure B4. Amplitude of the frequency spectrum of a logarithmic receiver for rain backscatter; 5 mm/hr rain rate, 95 GHz frequency, and VV polarization.

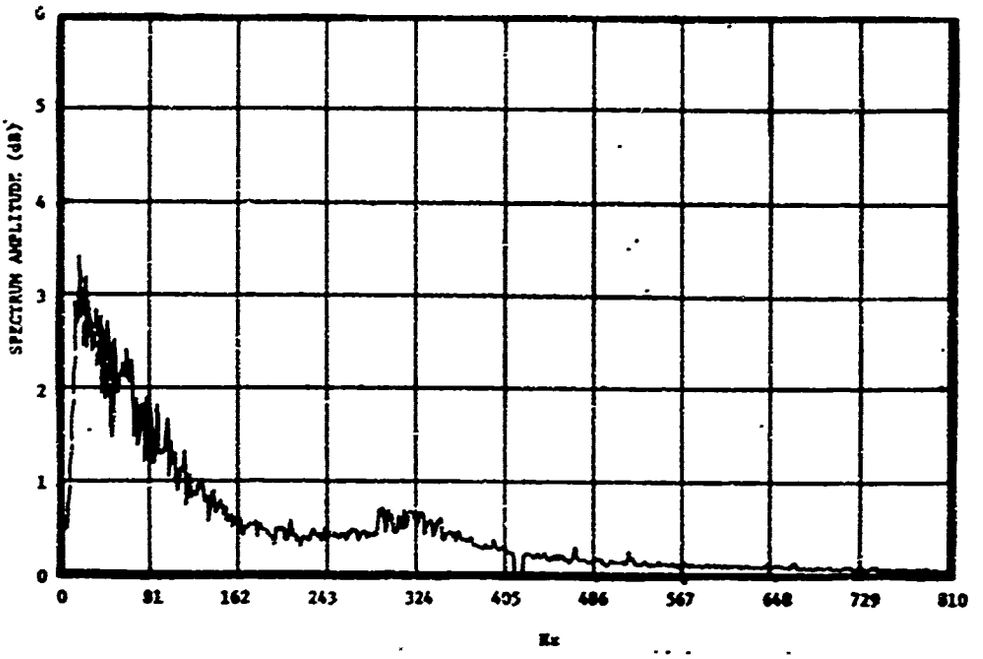

Figure B5. Amplitude of the frequency spectrum of a logarithmic receiver for rain backscatter; 23 mm/hr rain rate, 9.375 GHz frequency, and VV polarization.

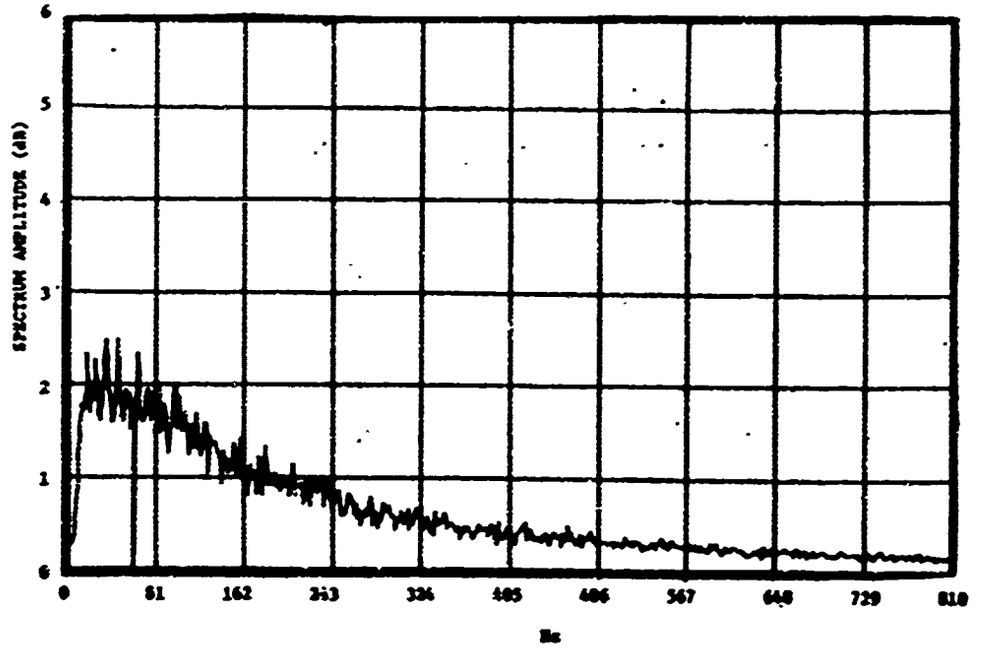

Figure B6. Amplitude of the frequency spectrum of a logarithmic receiver for rain backscatter; 23 mm/hr rain rate, 35 GHz frequency, and VV polarization.

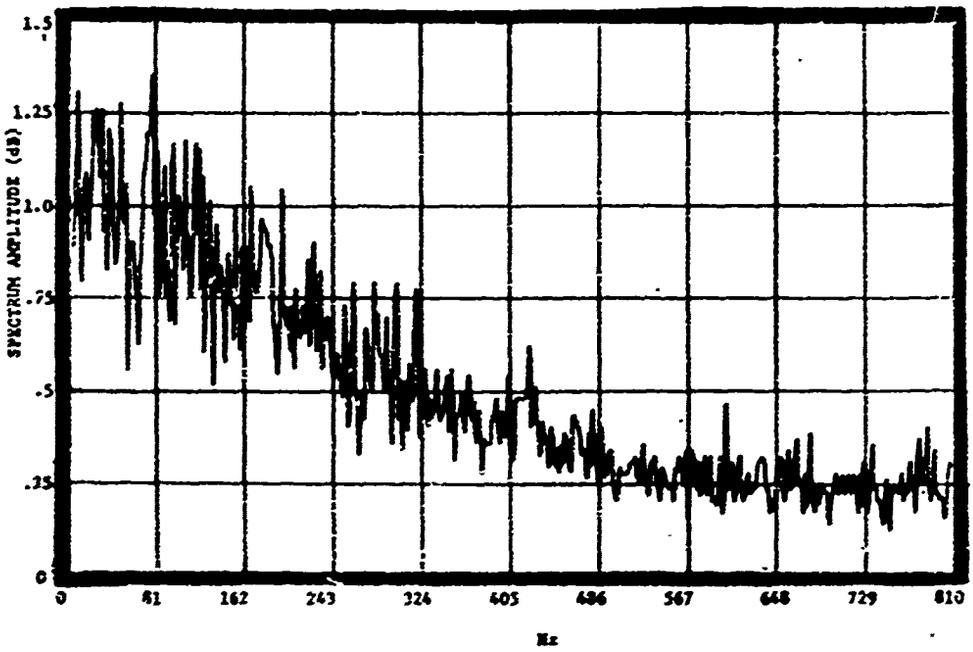

Figure B7. Amplitude of the frequency spectrum of a logarithmic receiver for rain backscatter; 23 mm/hr rain rate, 70 GHz frequency, and VV polarization.

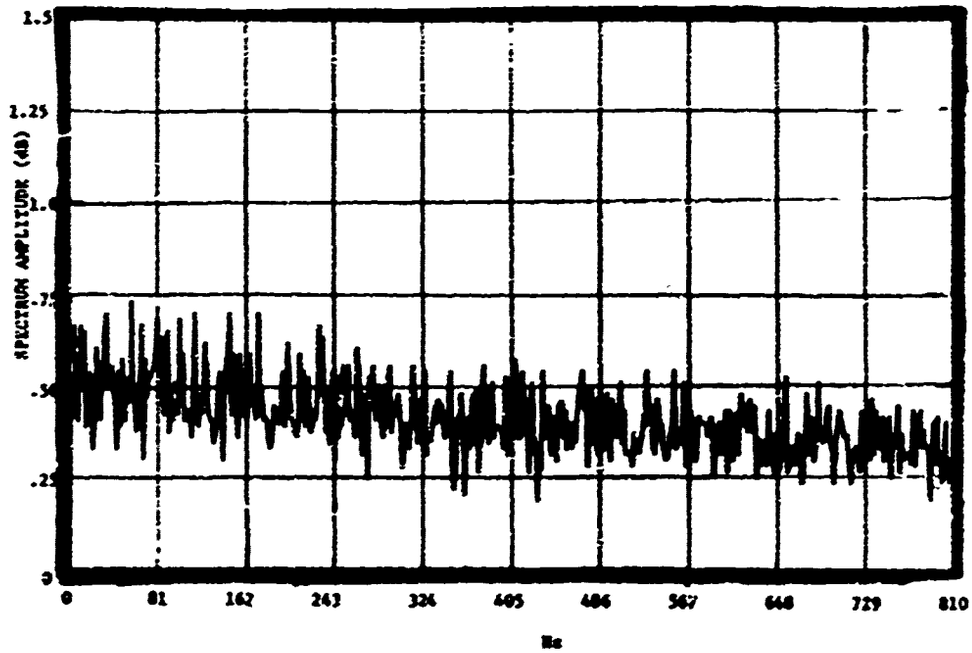

Figure B8. Amplitude of the frequency spectrum of a logarithmic receiver for rain backscatter; 23 mm/hr rain rate, 95 GHz frequency, and VV polarization.

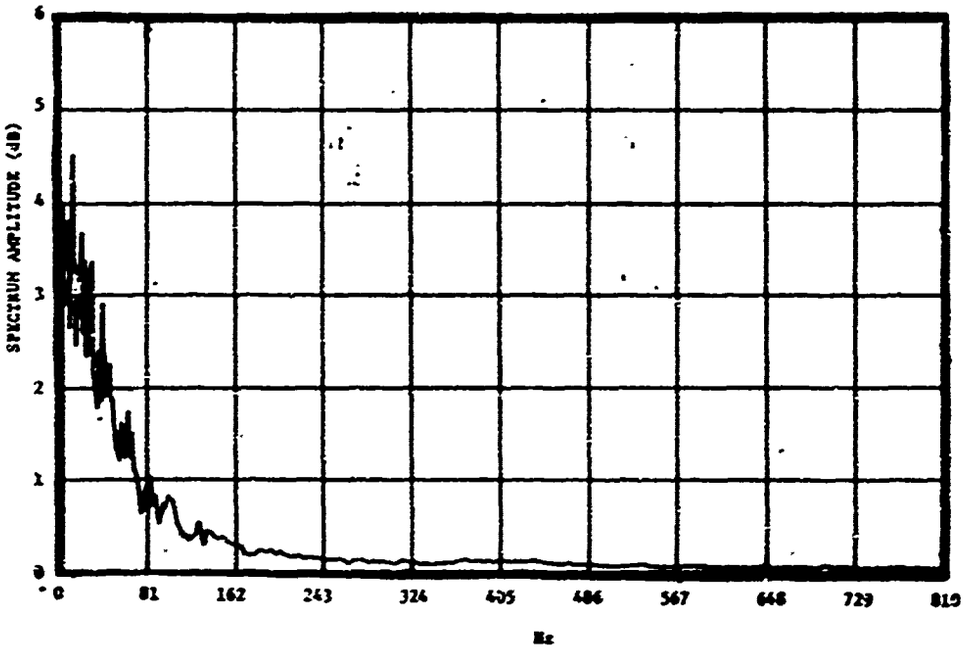

Figure B9. Amplitude of the frequency spectrum of a logarithmic receiver for rain backscatter; 38 mm/hr rain rate, 9.375 GHz frequency, and VV polarization.

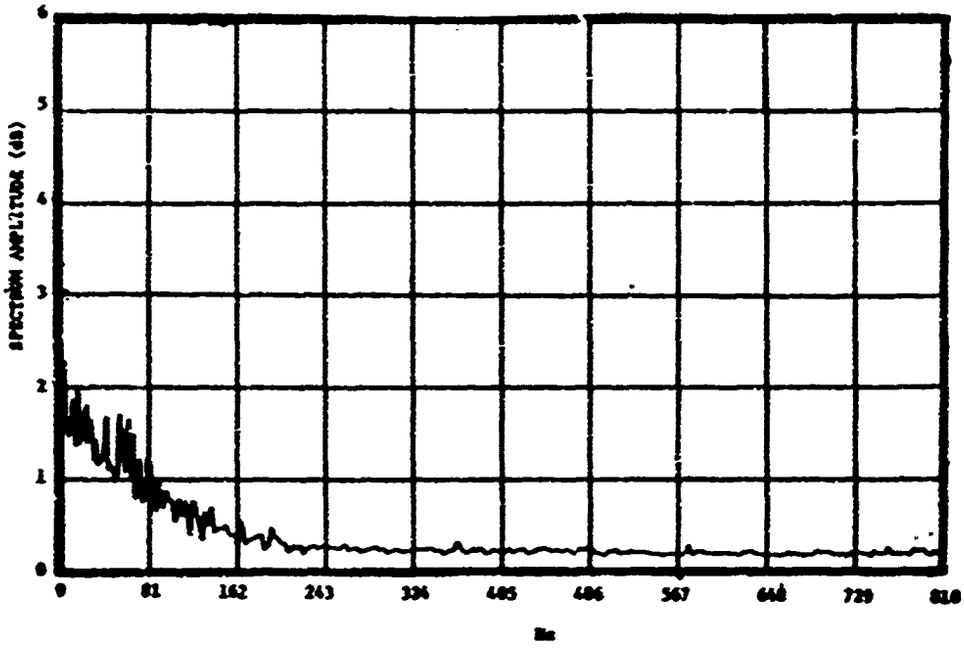

Figure B10. Amplitude of the frequency spectrum of a logarithmic receiver for rain backscatter; 38 mm/hr rain rate, 35 GHz frequency, and VV polarization.

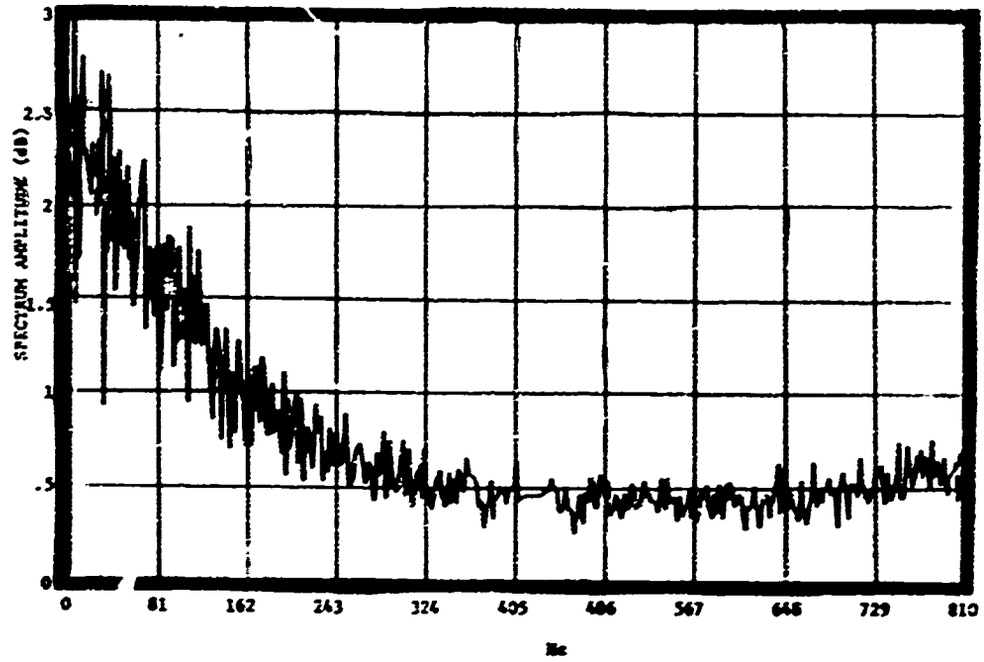

Figure B11. Amplitude of the frequency spectrum of a logarithmic receiver for rain backscatter; 38 mm/hr rain rate, 70 GHz frequency, and VV polarization.

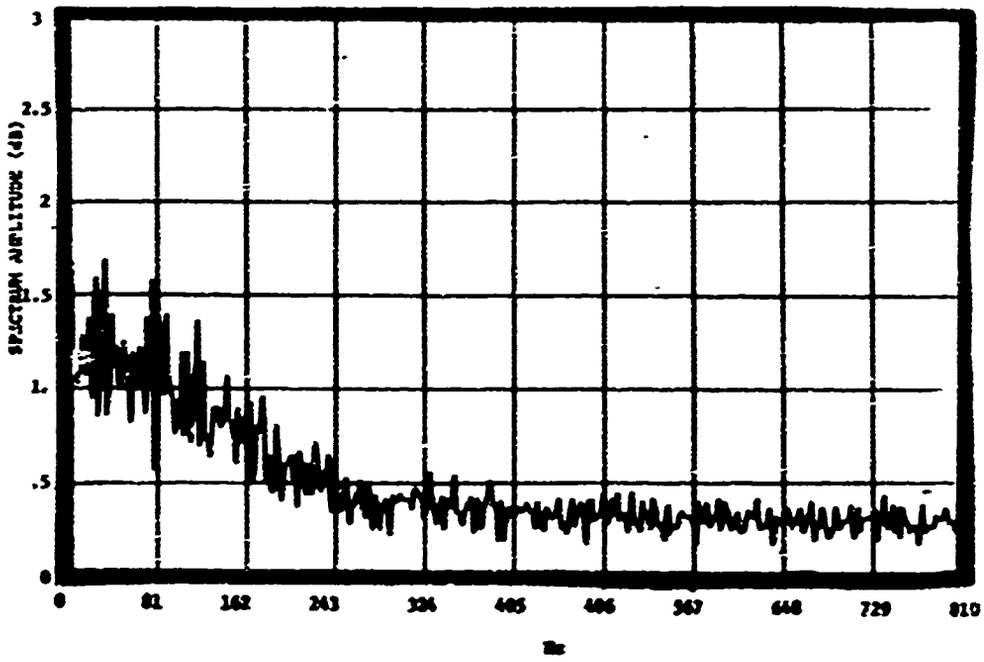

Figure B12. Amplitude of the frequency spectrum of a logarithmic receiver for rain backscatter; 38 mm/hr rain rate, 95 GHz frequency, and VV polarization.

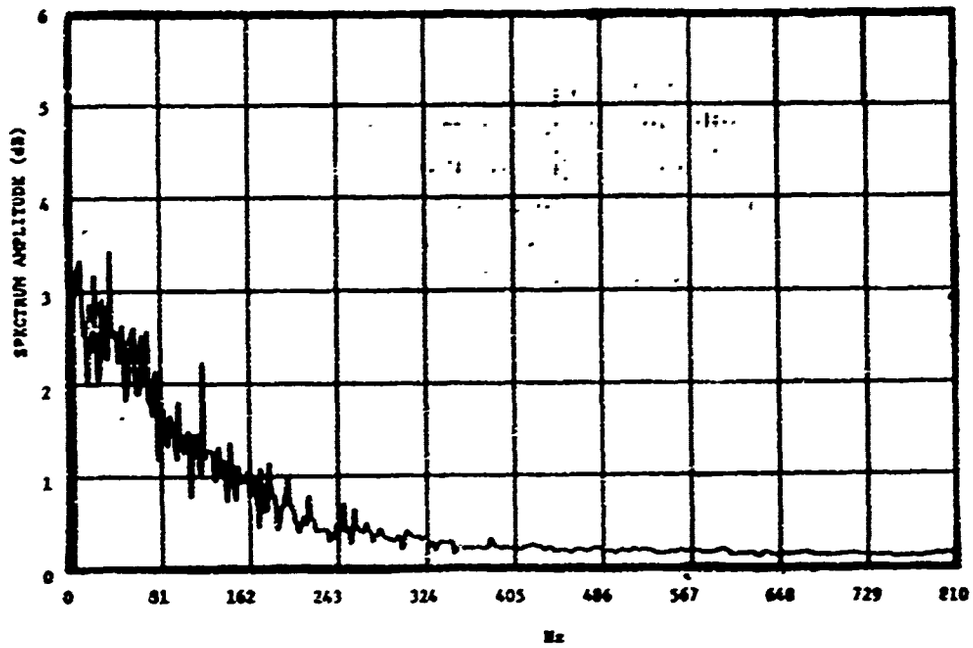

Figure B13. Amplitude of the frequency spectrum of a logarithmic receiver for rain backscatter; 70 mm/hr rain rate, 9.375 GHz frequency, and VV polarization.

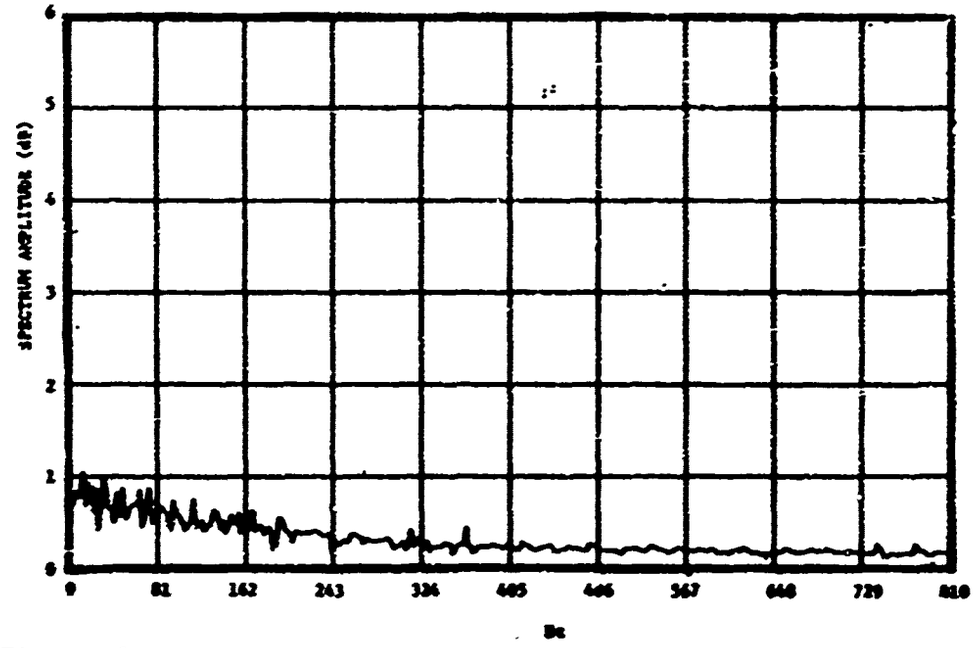

Figure B14. Amplitude of the frequency spectrum of a logarithmic receiver for rain backscatter; 70 mm/hr rain rate, 35 GHz frequency, and VV polarization.

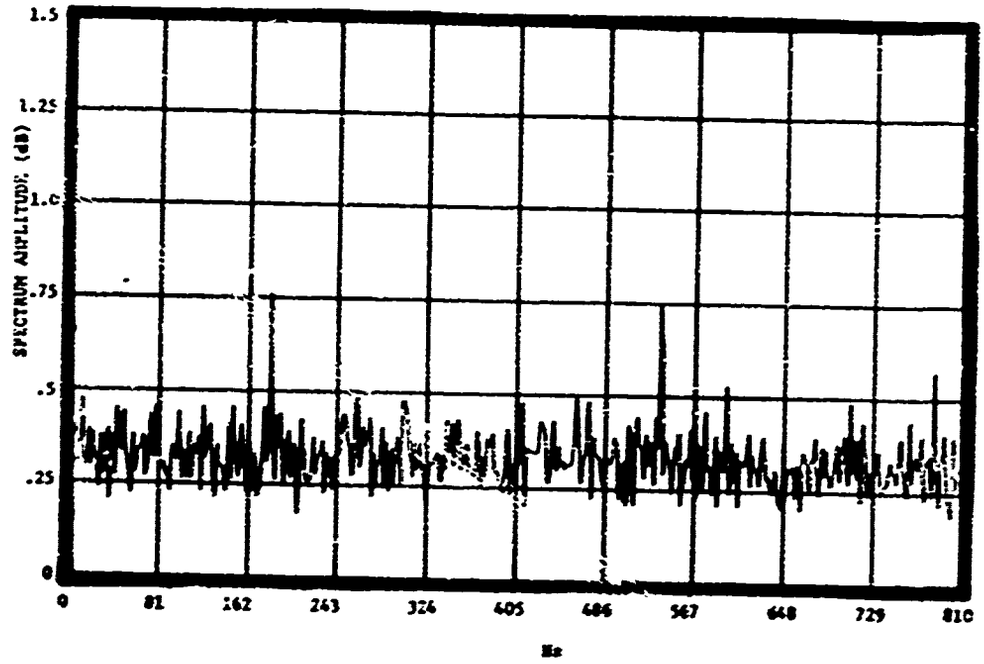

Figure B15. Amplitude of the frequency spectrum of a logarithmic receiver for rain backscatter; 70 mm/hr rain rate, 70 GHz frequency, and VV polarization.

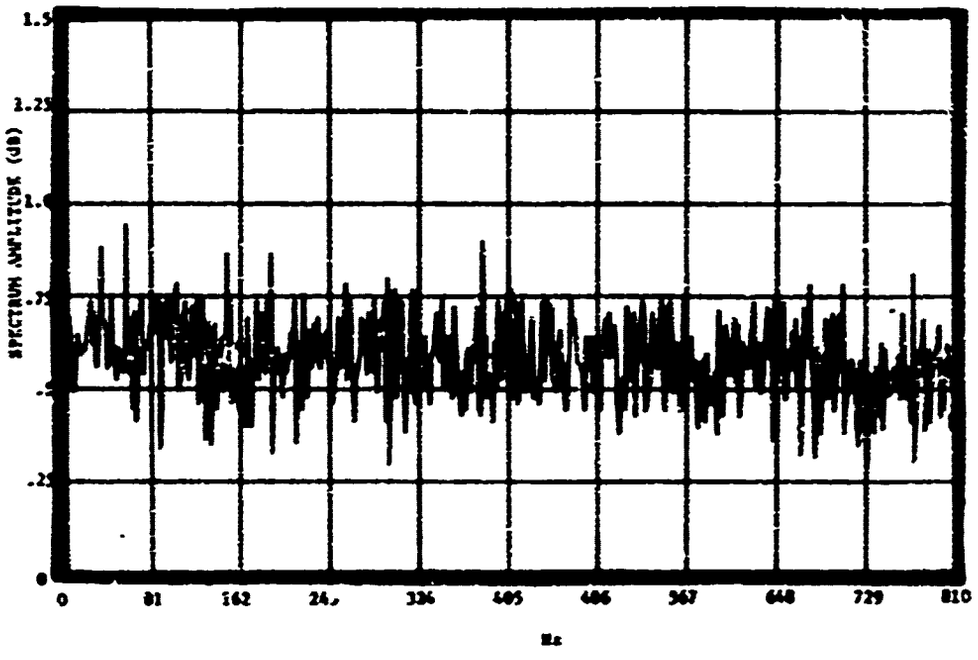

Figure B16. Amplitude of the frequency spectrum of a logarithmic receiver for rain backscatter; 70 mm/hr rain rate, 95 GHz frequency, and VV polarization.

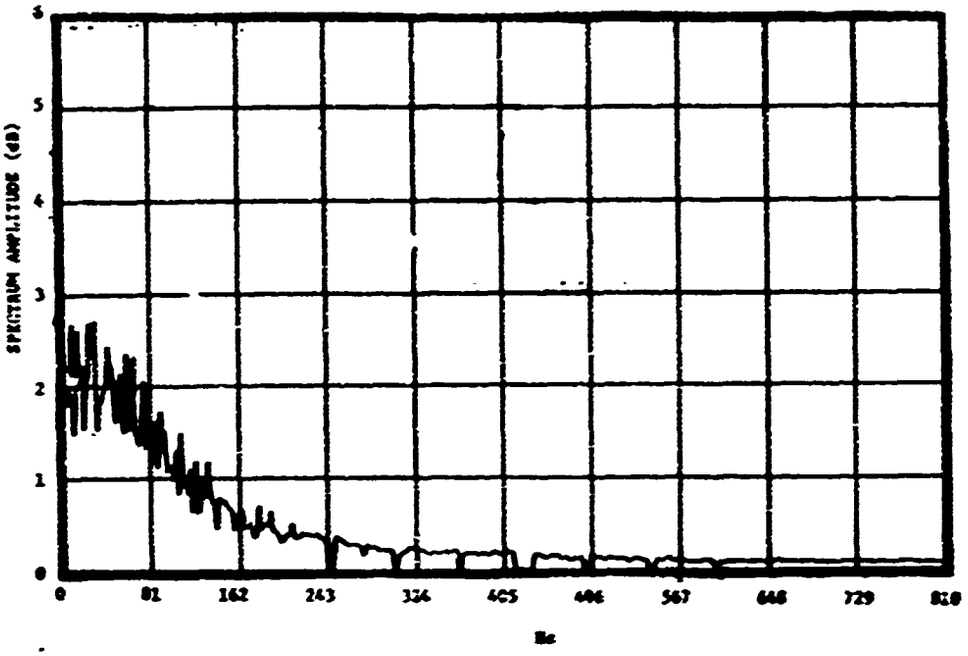

Figure B17. Amplitude of the frequency spectrum of a logarithmic receiver for rain backscatter; 100 mm/hr rain rate, 9.375 GHz frequency, and VV polarization.

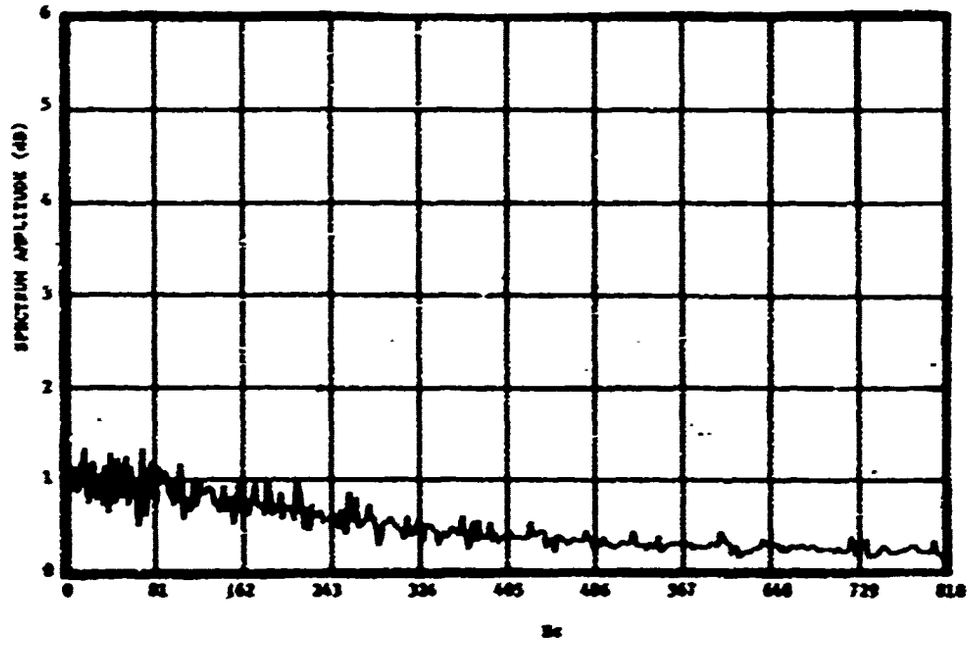

Figure B18. Amplitude of the frequency spectrum of a logarithmic receiver for rain backscatter; 100 mm/hr rain rate, 35 GHz frequency, and VV polarization.

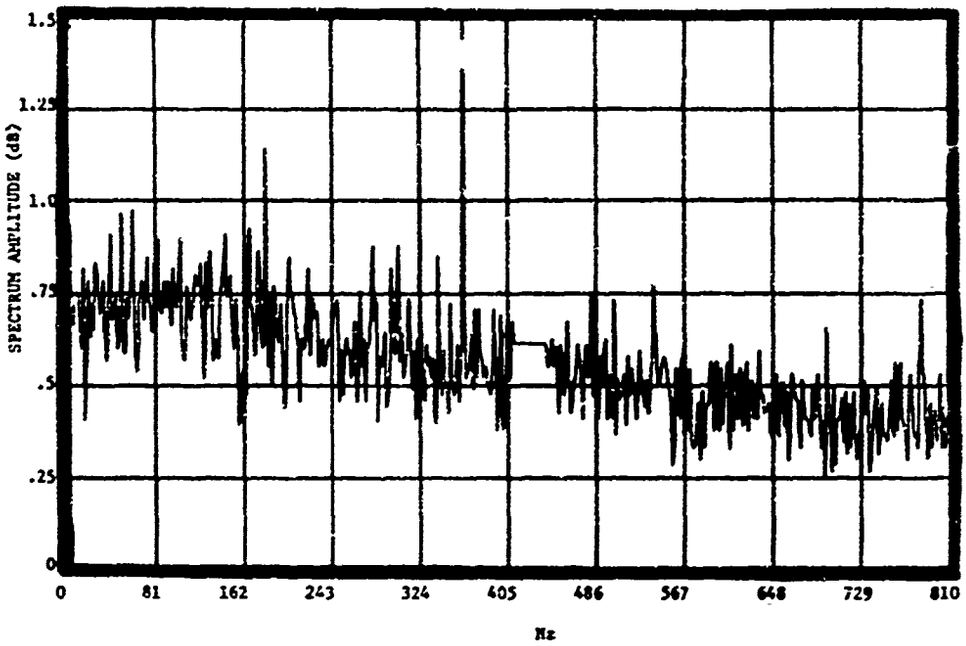

Figure B19. Amplitude of the frequency spectrum of a logarithmic receiver for rain backscatter; 100 mm/hr rain rate, 70 GHz frequency, and VV polarization.

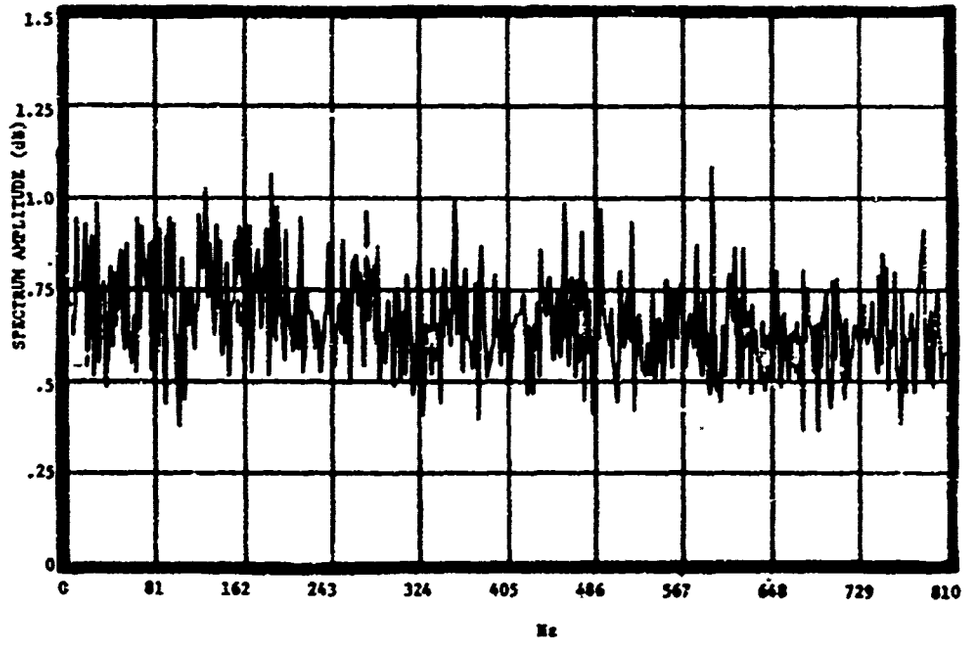

Figure B20. Amplitude of the frequency spectrum of a logarithmic receiver for rain backscatter; 100 mm/hr rain rate, 95 GHz frequency, and VV polarization.

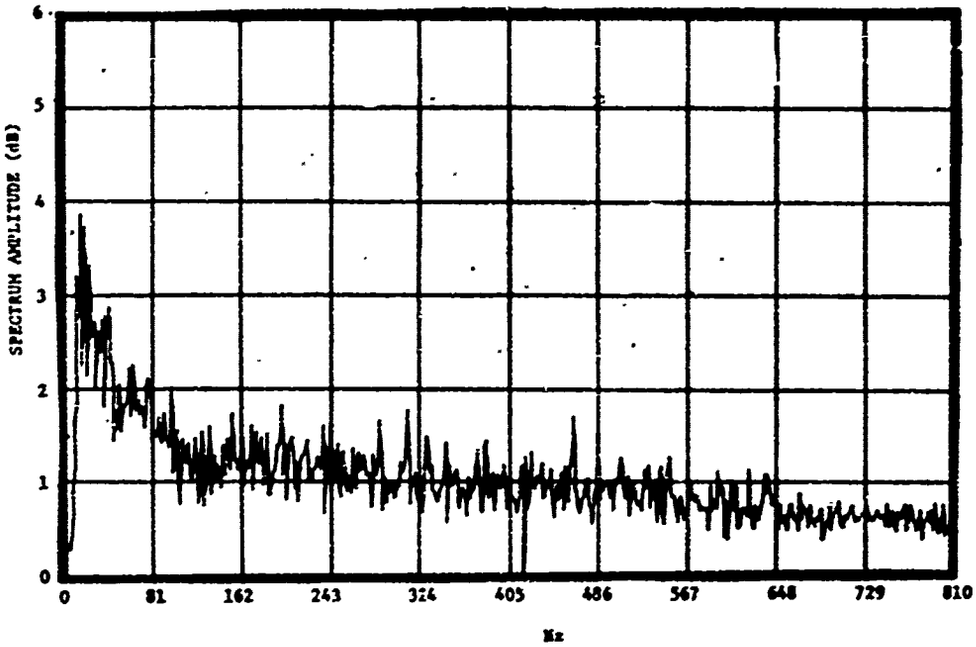

Figure B21. Amplitude of the frequency spectrum of a logarithmic receiver for rain backscatter; 3.1 mm/hr rain rate, 9.375 GHz frequency, and RC polarization.

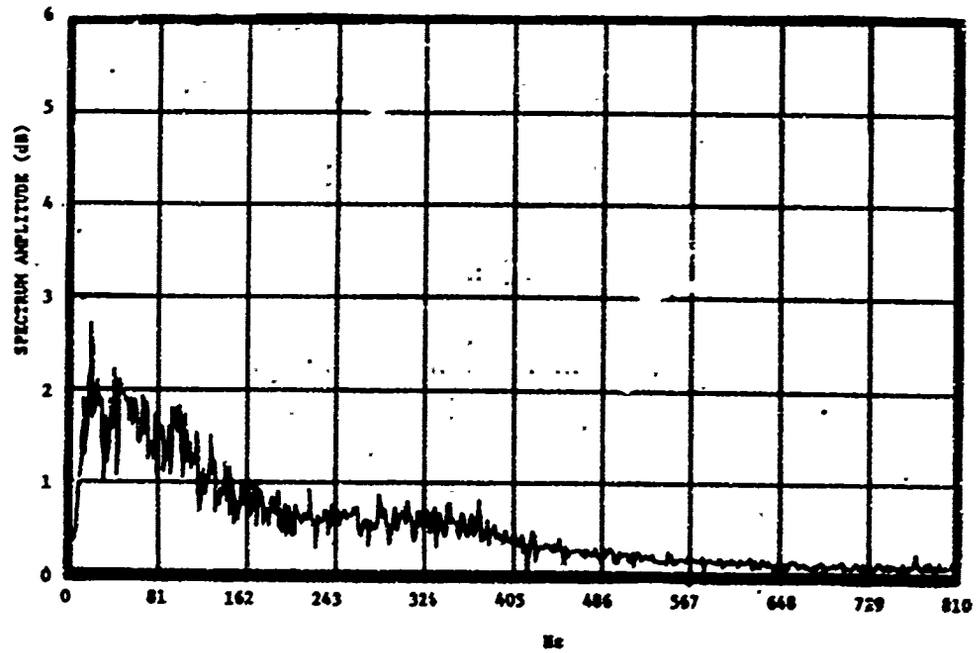

Figure B22. Amplitude of the frequency spectrum of a logarithmic receiver for rain backscatter; 3.1 mm/hr rain rate, 35 GHz frequency, and RC polarization.

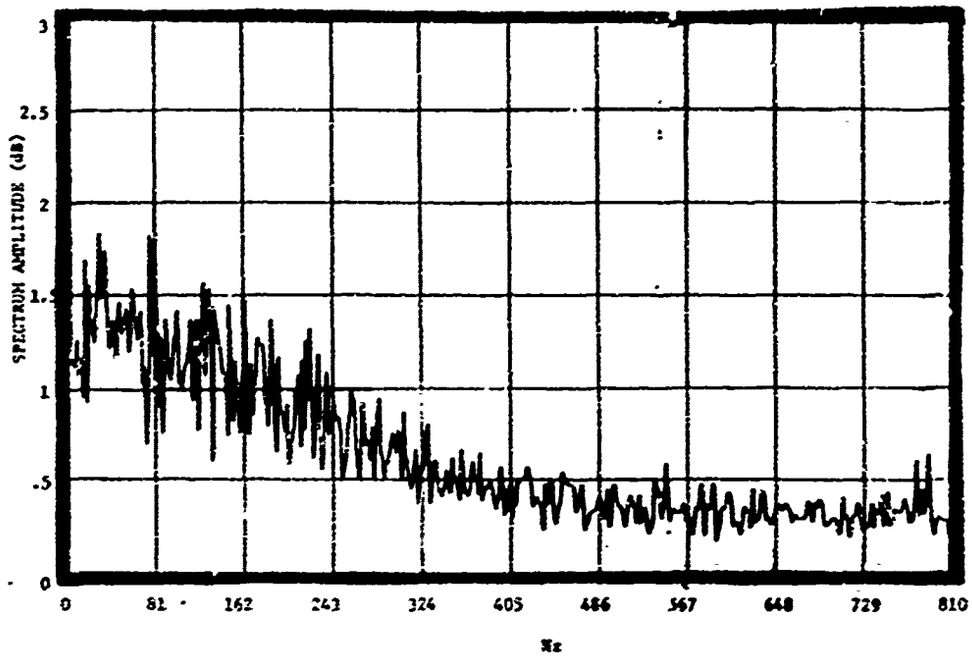

Figure B23. Amplitude of the frequency spectrum of a logarithmic receiver for rain backscatter; 3.1 mm/hr rain rate, 70 GHz frequency, and RC polarization.

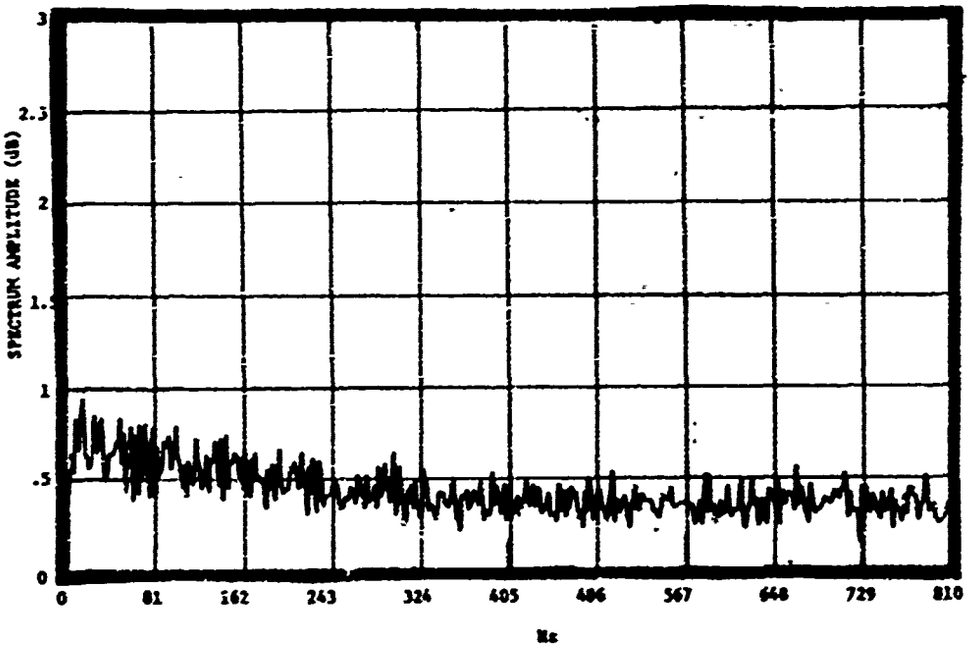

Figure B24. Amplitude of the frequency spectrum of a logarithmic receiver for rain backscatter; 3.1 mm/hr rain rate, 95 GHz frequency, and RC polarization.

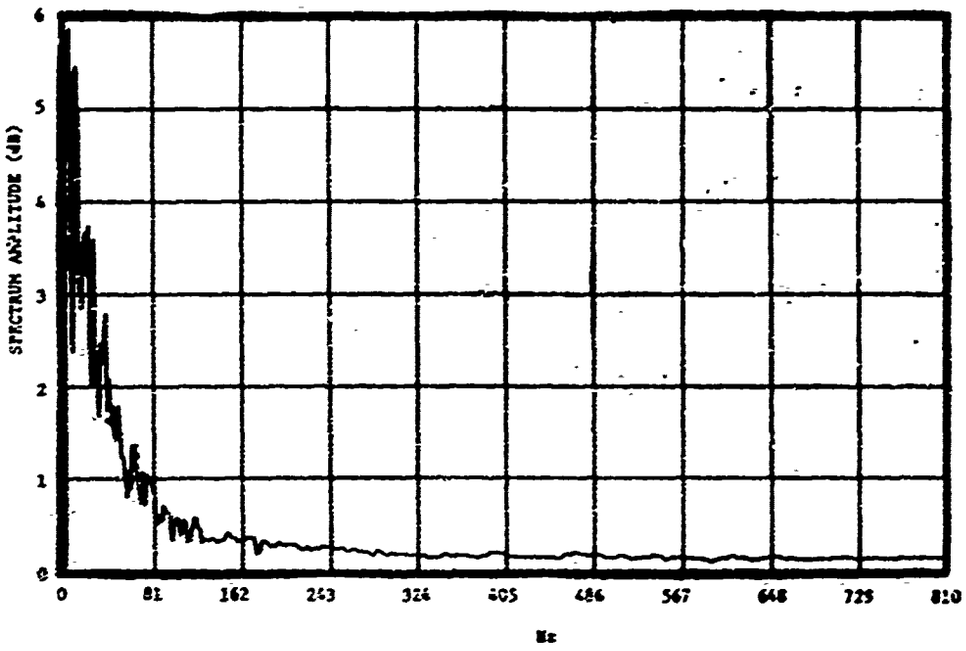

Figure B25. Amplitude of the frequency spectrum of a logarithmic receiver for rain backscatter; 32 mm/hr rain rate, 9.375 GHz frequency, and RC polarization.

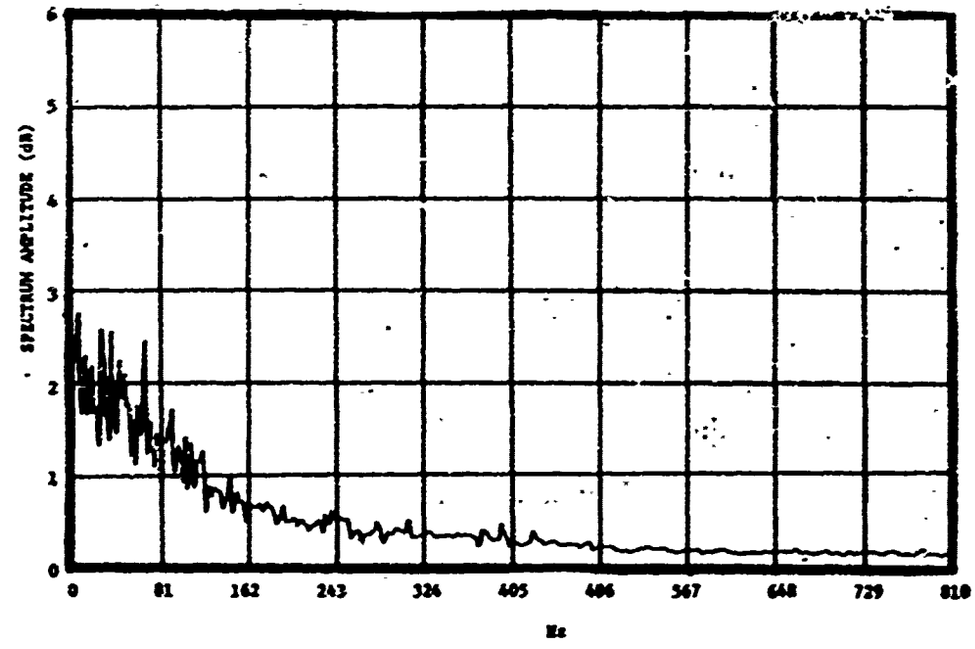

Figure B26. Amplitude of the frequency spectrum of a logarithmic receiver for rain backscatter; 32 mm/hr rain rate, 35 GHz frequency, and RC polarization.

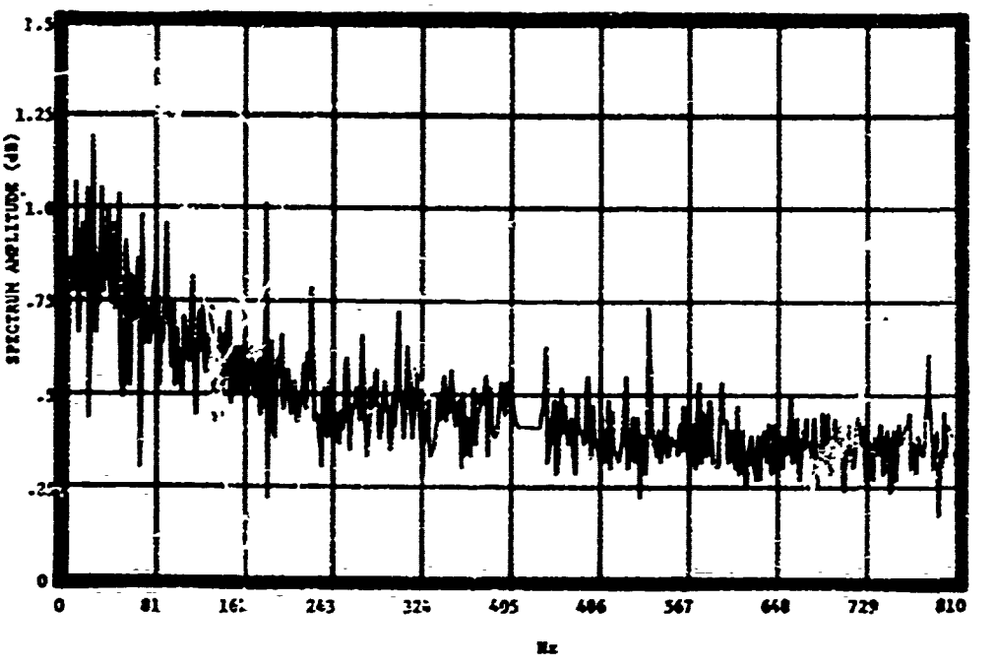

Figure B27. Amplitude of the frequency spectrum of a logarithmic receiver for rain backscatter; 32 mm/hr rain rate, 70 GHz frequency, and RC polarization.

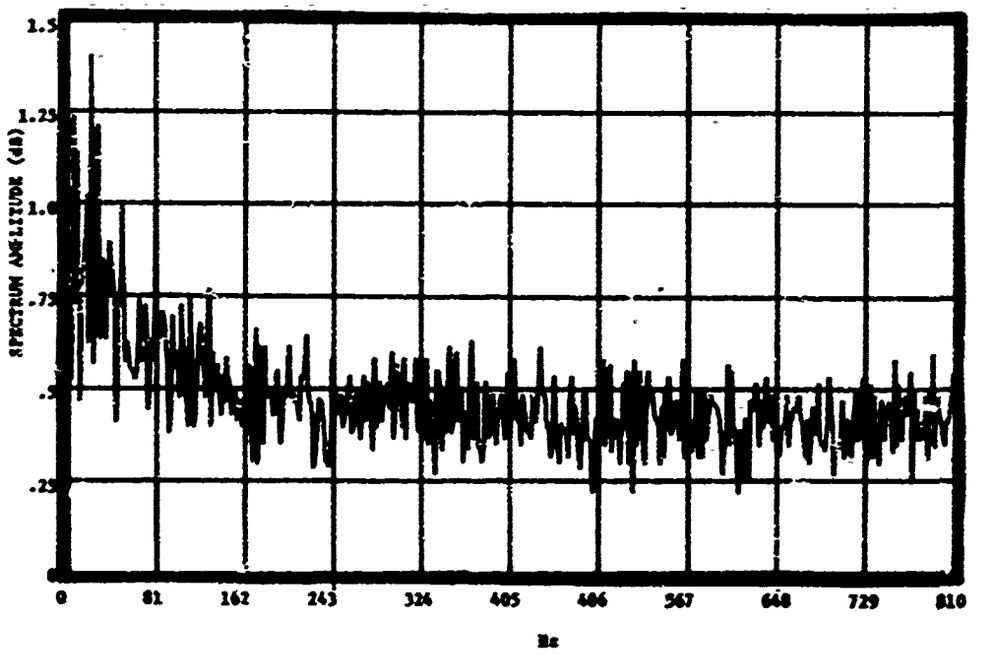

Figure B28. Amplitude of the frequency spectrum of a logarithmic receiver for rain backscatter; 32 mm/hr rain rate, 95 GHz frequency, and RC polarization.

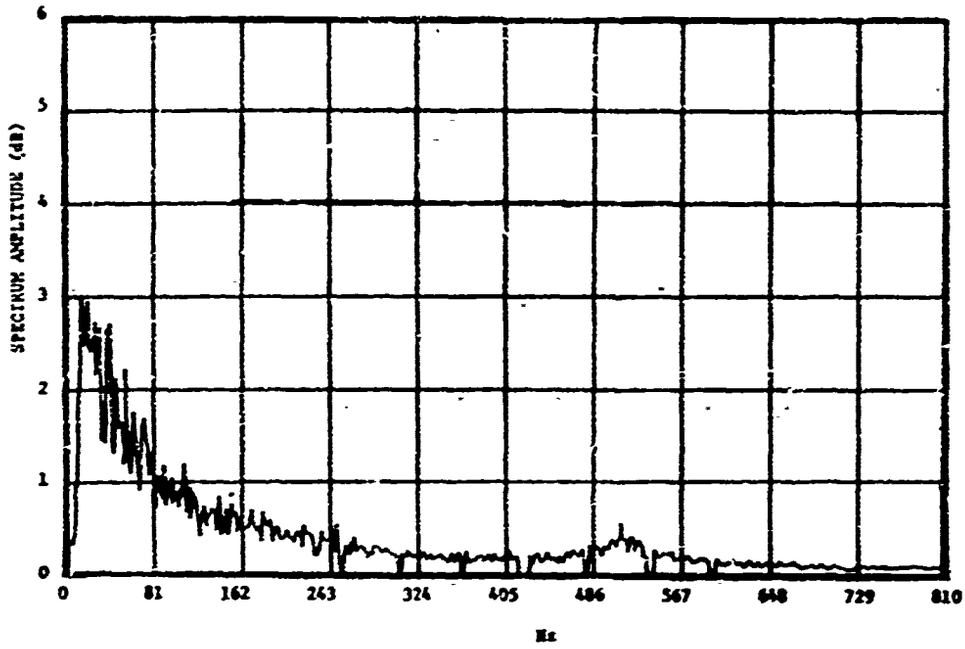

Figure B29. Amplitude of the frequency spectrum of a logarithmic receiver for rain backscatter; 91 mm/hr rain rate, 9.375 GHz frequency, and RC polarization.

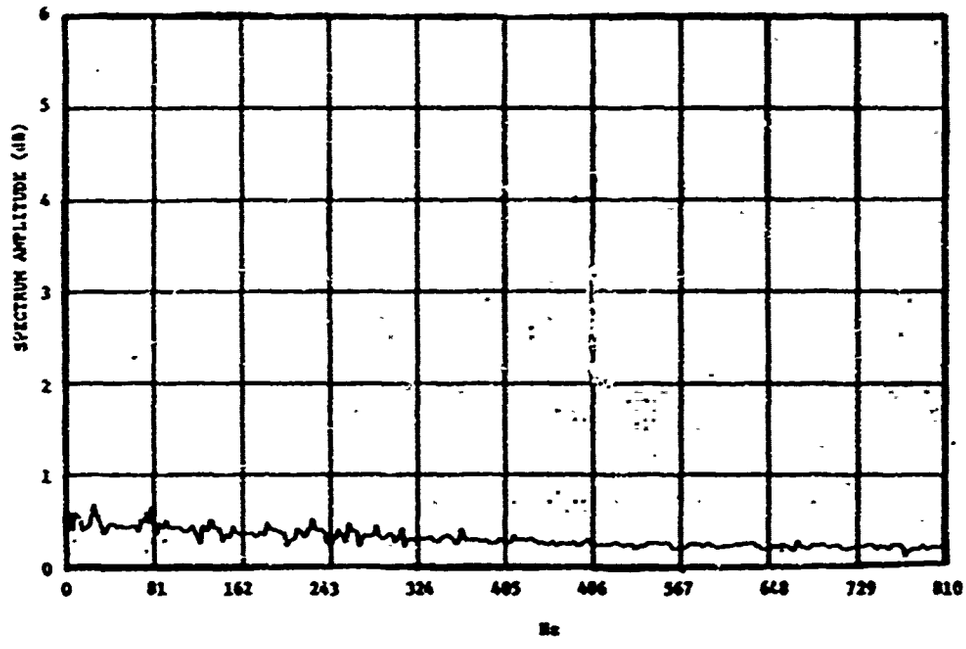

Figure B30. Amplitude of the frequency spectrum of a logarithmic receiver for rain backscatter; 91 mm/hr rain rate, 35 GHz frequency, and RC polarization.

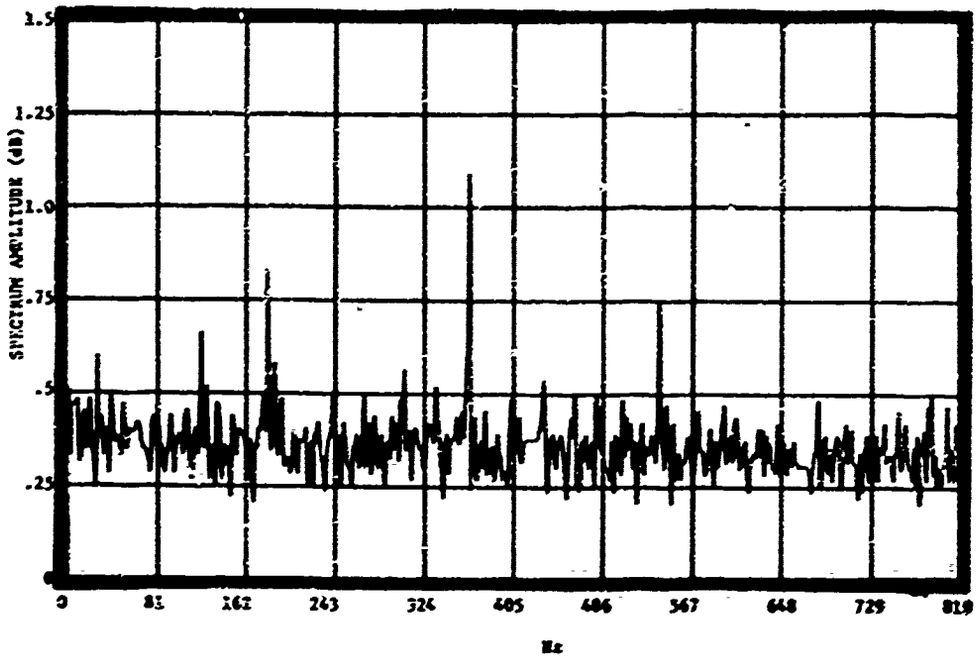

Figure B31. Amplitude of the frequency spectrum of a logarithmic receiver for rain backscatter; 91 mm/hr rain rate, 70 GHz frequency, and RC polarization.

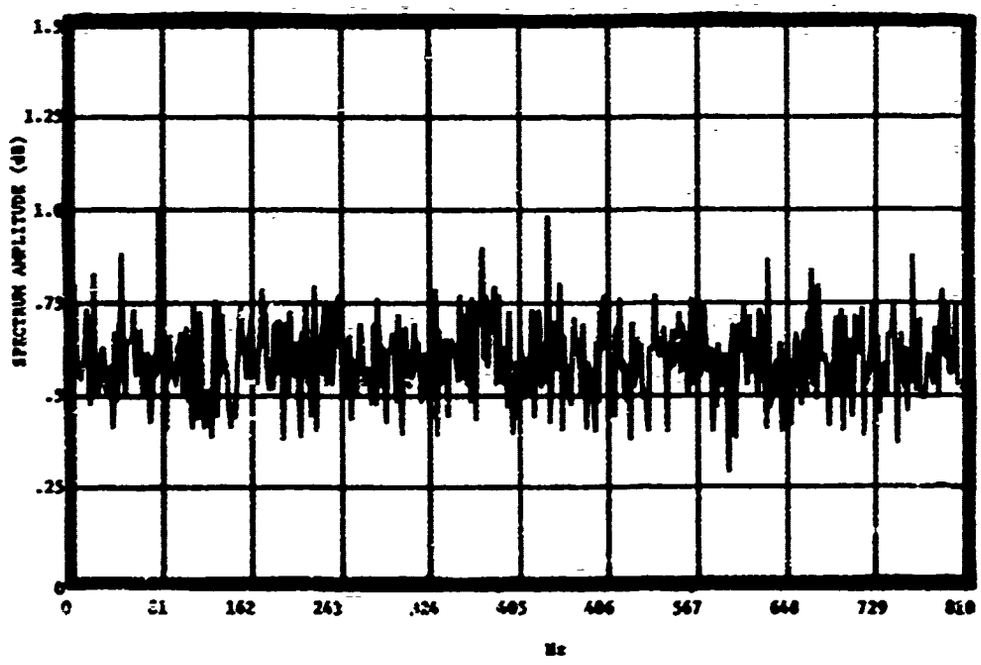

Figure B32. Amplitude of the frequency spectrum of a logarithmic receiver for rain backscatter; 91 mm/hr rain rate, 95 GHz frequency, and RC polarization.